FACULTY OF BIOSCIENCE ENGINEERING

VALIDATION OF *IN VITRO* MODELS OF INTESTINAL EPITHELIUM TO STUDY HOST-MICROBIOTA DIALOGUE IN SHORT BOWEL SYNDROME

Rita Leblans
Student number: 02213282

Promotors: Prof. dr. ir. Tom Van de Wiele, Dr. Ludovica Marinelli
Tutor: Ir. Pieter De Clercq

Master's Dissertation submitted to Ghent University in partial fulfilment of the requirements for the degree of Master of Science in Bioscience Engineering: Cell and Gene Biotechnology

Academic year: 2023 - 2024

UNIVERSITEIT GENT

COPYRIGHT

Ghent, June 7th, 2024

The promotors, Prof. dr. ir. Tom Van de Wiele Dr. Ludovica Marinelli

The tutor, Ir. Pieter De Clercq

The author, Rita Paola Leblans

PREFIX

"Trust your gut." They say.

Indeed, I am glad I chose to start my bio-science engineering education at the University of Antwerp, followed by the cell and gene biotechnology master at Ghent University. Furthermore, choosing a thesis topic from the long list was not easy, but somehow, I am very convinced I made the right choice. This thesis year was more than exploring the actual gut. It was a year full of learning, meeting new people and contributing to research.

First of all, I want to thank Pieter De Clercq and Ludovica Marinelli for guiding me through this year and make me grow in multiple ways. They not only taught me the skills on the field of research, it was also a pleasure working alongside them. They made a great duo, complementing each other. Moreover, I really enjoyed our “Italian group”, so: *Grazie di tutto!*

Next, I would like to express my gratitude to Prof. Dr. Ir. Tom Van de Wiele for giving me this opportunity at CMET and taking his time to give me feedback. Likewise, I would also like to thank the entire CMET team. It was nice that everyone was approachable and willing to help, particularly mentioning the people from the HAM-cluster, who I got to know better during the clean-ups, the HAM meetings and HAM team buildings.

I also got to know some of the other thesis students at CMET, in particular Margot and Merel. It was nice to support each other during this thesis year, whether it was just lunching together in between our lab work, going for a run together or meeting up to grab a drink. The dedication and hard work put into this thesis sometimes felt like climbing mountains, but thanks to this new friendship it was less hard, and we will even climb the beautiful Alpine mountains after graduation.

And last but not least, I want to show my appreciation to my family and friends. My parents for supporting me, giving advice and allowing me to make my own choices. Nonna Lina, my grandmother, for making hectic and stressful days better with her company and by spoiling me with her delicious food. Tante Sandra, zio Angelo and zia Marcella on whom I can always count. And a final thank you to all my friends for all the memories and cherished moments together, which make me forget about the hard days of studying over the past 5 years at university.

I can conclude that trusting my gut led to good decisions, introducing me to amazing people. Now, let’s explore what else I discovered about the gut…

ABSTRACT

Understanding the mechanisms of host-bacteria interactions in health and disease is crucial for developing effective therapeutics. However, the gastrointestinal anatomy, physiology, and interactions between the residing microbiome and different host cell types are highly complex and multifactorial. Therefore, several *in vitro* methodologies are being developed to study this intestinal environment in a mechanistic manner. The aim of this research was to characterize and optimize an *in vitro* Transwell® model of the intestinal epithelium and analyse its response to several stimuli from the digestive tract: bile acids, supernatant from bacterial cultures and live bacteria. The functional characterization of the intestinal epithelium model entailed the analysis of the barrier integrity measured by transepithelial electrical resistance, the permeability measured by the Lucifer Yellow assay, the gene expression of *MUC2* and *ZO1* by quantitative PCR, and the secretion of IL-8 cytokine by enzyme linked immune sorbent assay. Ultimately, this epithelial model was employed to study the impact of human derived complex microbial communities, cultured in an *in vitro* simulator of the human gut that mimicked the conditions of Short Bowel Syndrome. Short Bowel Syndrome, defined by a significant reduction in the absorptive capacity of the intestine due to extensive surgical resection of the small intestine, is characterized by an altered microbial community. An innovative aspect of this research is the integration of multiple cell types and the inclusion of an immune compartment within the *in vitro* model. The results demonstrate that the choice of Transwell® coating agent and goblet cell line influence the properties of the cell model. The host-bacteria interaction experiments demonstrated that several bacterial metabolites modulate epithelial barrier functions. Although multiple complementary readouts are employed, additional experiments are needed in the future to confirm and validate the obtained results, including the gene expression of other tight junction genes, cross-sectional visualisations, and determining the cell ratios post-differentiation.

Key words: *in vitro* Transwell model, intestinal epithelium, host-bacteria interaction, Short Bowel Syndrome

SAMENVATTING

Het begrijpen van de mechanismen die de wisselwerking tussen gastheer en micro-organismen beïnvloeden is essentieel voor het ontwikkelen van werkzame therapeutica. De gastro-intestinale anatomie, fysiologie en interacties tussen microbioom van de gastheer en de epitheel cellen zijn complex. Daarom zijn er verschillende *in vitro* modellen ontwikkeld om de darmen te bestuderen. Het doel van dit onderzoek was om een *in vitro* Transwell® model voor het dunne darm epitheel te karakteriseren en te optimaliseren. Vervolgens werd het model toegepast om de respons van verschillende stimuli te bestuderen: galzuren, supernatans van bacteriën, en levende bacteriën. Dit gebeurde door analyse van de barrière-integriteit gemeten door de Transepitheliaal Elektrische Weerstand, de permeabiliteit gemeten met de Lucifer Yellow assay, de genexpressie van *MUC2* en *ZO1* met kwantitatieve PCR, en de secretie van IL-8 cytokine met enzyme linked immune sorbent assay. Vervolgens werd dit epitheel model gebruikt om de impact te bestuderen van complexe microbiële gemeenschappen van menselijke oorsprong en gecultiveerd in een *in vitro* simulator van het humaan darmstelsel waarbij Short Bowel Syndrome werd nagebootst. Short Bowel Syndrome, een aandoening die wordt gekenmerkt door aanzienlijke vermindering in absorptiecapaciteit van de darmen als gevolg van chirurgische resectie van de dunne darm, wordt gekenmerkt door een aangepaste microbiële gemeenschap. De innovatieve aspecten van dit werk zijn de integratie van meerdere celtypes en het betrekken van een immuun compartiment in het *in vitro* model. De resultaten toonden aan dat de keuze van de Transwell®-coating en de goblet cellijn de eigenschappen van het celmodel beïnvloeden. De experimenten met betrekking tot de interactie tussen gastheer en bacteriën toonden aan dat verschillende bacteriële metabolieten de epitheel barrière kunnen veranderen. Hoewel er meerdere complementaire meetmethoden worden gebruikt, zijn in de toekomst extra experimenten nodig, waaronder de genexpressie van andere tight junction genen, visualisaties van dwarsdoorsneden van het epitheel en het bepalen van de cel ratio's na differentiatie van het model. Hiermee kunnen de verkregen resultaten worden bevestigd en gevalideerd.

Trefwoorden: *in vitro* Transwell model, darmepitheel, interactie tussen gastheer en micro-organismen, Short Bowel Syndrome

INTRODUCTION

Understanding the host-microbiota interaction within the human small intestine is essential to identify novel therapeutic targets. The small intestine is the primary site for nutrient digestion and absorption, processes that can be modulated by gut microbiota. The host microbiota plays a role in metabolic functions, immune system modulation, and in maintaining the integrity of the intestinal barrier. Therefore, it is crucial to preserve the delicate dynamic balance (eubiosis) between host and microbes. Disruptions of this balance (dysbiosis) can lead to a range of health issues, including inflammatory diseases, infections, and metabolic disorders. Hence, a detailed understanding of the cellular mechanisms and the dialogue with gut microbes is essential to develop targeted therapeutic strategies to restore and maintain gut health.

One severe condition highlighting the importance of studying the host-microbiota dialogue is Short Bowel Syndrome (SBS). SBS is a consequence of the extensive loss of small intestinal mass, leading to a significant reduction in the absorptive surface area and resulting in malnutrition along with other complications. Due to the change in the intestinal environment, patients with SBS have drastic alterations in their gut microbiota, which can aggravate the symptoms and hinder recovery.

Despite its crucial role, studying the host-microbiota interactions of the intestine is complex and remains insufficiently described in the literature. This scientific gap is mainly due to the complexity of the intestinal environment and the challenges associated with studying these interactions *in vivo*. Methods such as faecal sampling and colonoscopy provide insights into the composition, function, and dynamics of the microbial communities within the colon. However, these approaches are not directly applicable to the small intestinal microbiota, because the samples are contaminated with colonic microbiota, and the microbial communities in the small intestine differ from those in the colon due to different nutrient availability and luminal conditions.

To address this gap, researchers have developed various *in vitro* models, such as two-dimensional cultures, Transwell systems, three-dimensional organoids and spheroids, and microfluidic devices. These methods reduce the complexity of studying the cellular mechanisms *in vivo* and enable stimulation of the intestinal epithelium under various conditions, including host-bacteria interactions. The methodology of this research involves the use of Transwell co-cultures to investigate the cellular epithelial mechanisms and the host-microbe interactions.

In vitro models need to accurately mimic the *in vivo* environment. Therefore, the first aim of this work is to characterize and optimize an *in vitro* Transwell model for the small intestinal epithelium. More specifically, readouts that characterize the chemical, physical, and immune epithelial barrier are examined. Additionally, the application of these models to study the host-microbe interactions in both health and disease contexts is explored.

The development of the *in vitro* models will be discussed in the subsequent chapters, followed by their application to study host-microbe interactions. The results obtained will be analysed to provide insights into the epithelial and microbial dynamics of the intestine, offering a foundation for future research and therapeutics.

LIST OF ABBREVIATIONS

BA	Bile Acid
DIV	Days In Vitro
ELISA	Enzyme Linked Immune Sorbent Assay
GI	Gastrointestinal
HMI	Host Microbiota Interaction
IEC	Intestinal Epithelial Cells
Ile	Ileum
LY	Lucifer Yellow
PSI	Proximal Small Intestine
qPCR	Quantitative Polymerase Chain Reaction
SBS	Short Bowel Syndrome
SCFA	Short-Chain Fatty Acid
SHIME	Simulator of the Human Intestinal Microbial Ecosystem
SI	Small Intestine
TC	Transverse colon
TEER	Trans Epithelial Electrical Resistances

TABLE OF CONTENTS

CHAPTER 1.
LITERATURE

1.1. The intestinal environment

1.1.1. Anatomy & Physiology

The gastrointestinal (GI) tract (Figure 1) is involved in food ingestion, digestion and nutrient absorption. The ingested food constituents pass through the mouth, esophagus, stomach, small intestine, and large intestine or colon. The small and large intestines, located in the abdomen, form a major part of the gastrointestinal tract and play an important role in the digestion and absorption of nutrients from ingested food [3, 4].

The **small intestine** (SI) is a curved tabular structure with a rich blood supply that constitutes an interface between the external environment and the rest of the body [5-7]. It is the longest organ in the body with an average length of 690.1 ± 93.7 cm and is responsible for approximately 90% of the total nutrient absorption in the digestive tract [2, 8]. The small intestine is divided into three different sections for a sequential and efficient digestion and absorption process: the duodenum, the jejunum and the ileum (Figure 1) [5]. The **duodenum** is the first segment and is connected to the antrum of the stomach. It is the shortest section of the small intestine measuring 20-25 cm on average and is connected to the **jejunum**, that measures approximately 2.5 meters [9]. The third section is the **ileum** measuring around 3 meters and is connected to the colon by the ileocecal valve [10]. Moving from the duodenum to the ileum, there is a gradual reduction in the overall diameter of the small intestine, along with decreased wall thickness [11].

Multiple **gradients of physiological and biochemical parameters** exist along the gastrointestinal tract, such as pH, gas composition and bacterial load. The pH of gastric acid in the stomach ranges between pH 1.0 and pH 2.0 [2, 12]. Upon entry of partially digested food in the duodenum, bicarbonate ions aid in the neutralization of the acidic pH with values ranging from pH 5.7 to pH 6.4 facilitating digestion and additionally protecting the inner lining of the duodenum. Bicarbonate ions also indirectly influence the acidity in the stomach through secretion of hormones that inhibit release of gastric acid, which is called enterogastric reflex [13, 14]. The pH gradually increases along the small intestine and is slightly basic in the ileum [2, 12]. Various gasses, such as oxygen, carbon dioxide, nitrogen and hydrogen exhibit a certain gradient as well [15]. For example, the oxygen tension in human small intestine ranges from 36.0 ± 9.7 mmHg in the mid-ileum to 33.5 ± 11.5 mmHg in the terminal ileum (measured at the serosal surface by intraoperative tissue oximetry) [16]. Due to the differences in nutrient availability, transit time and physio-chemical characteristics, different microbial communities exist along the gastrointestinal tract, including bacterial species, fungi and bacteriophage [17]. Along the small intestine an increase in bacterial density is observed ranging from 10^4-10^5 CFU/mL in the duodenum to 10^7-10^8 CFU/mL in the distal ileum [18]. In section 1.1.4 the microbial communities and host-microbe interaction will be discussed in detail.

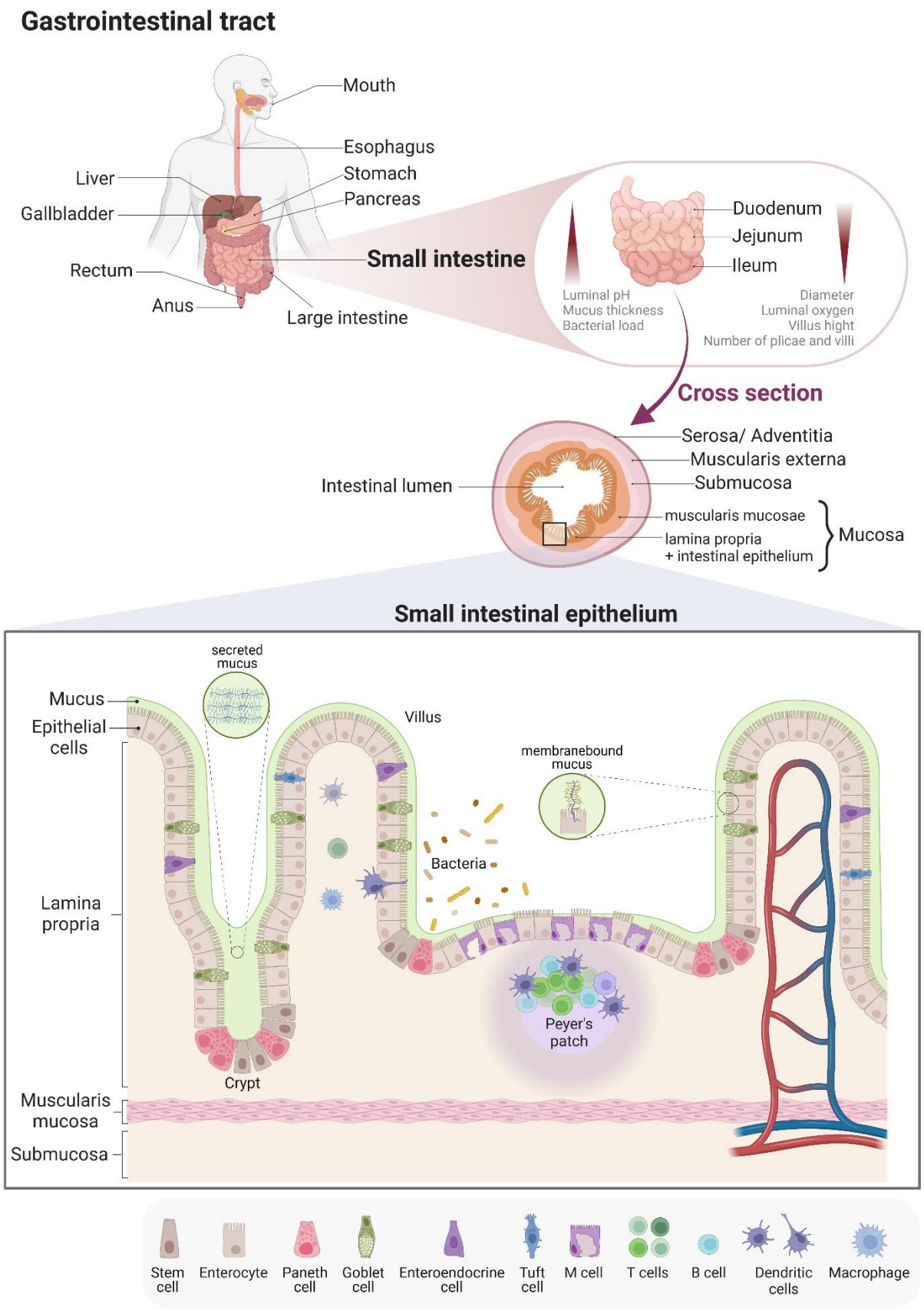

Figure 1: Overview figure of the small intestine created with BioRender. The small intestine is located in the abdomen, is divided into different sections (duodenum, jejunum and ileum) and is composed of different cross-sectional layers (serosa or *adventitia*, *muscularis externa*, submucosa and mucosa). At the bottom of the figure the small intestinal epithelium is visualized illustrating the epithelial structure and the different cell types.

1.1.2. Digestion and absorption of nutrients

Each day eight to ten litres of fluid pass through the gastrointestinal tract, including pancreatic and bile secretions [17, 19]. About 90% of the ingested nutrients are absorbed by the small intestine and the remainder is absorbed in the large intestine. The small intestine mainly absorbs simple carbohydrates and proteins, with a gradual decrease from proximal duodenum to distal ileum. Approximately two litres of fluid reach the colon. Here, water and electrolytes are recovered next to the absorption of microbial fermentation products [3, 4, 17, 19, 20]. Approximately 100 mL of fluid that entered the colon is daily lost through the stools [19].

The process of digestion is initiated in the mouth [21]. At first, food is chewed and mixed with saliva to form a bolus that is swallowed and moves through the oesophagus to the stomach. Here, the bolus is mixed with hydrochloric acid (HCl), protein-digesting proteases and water. In this acid environment, the digestion of proteins begins with the action of pepsin, an enzyme activated by HCl [22]. This semi-fluid mass of partially digested food is now called chyme. Strong peristaltic waves will further digest and mix the stomach content. Subsequently, chyme is transferred to the small intestine where also the pancreatic secretion are reversed [4, 21]. The pancreas secretions, including bicarbonate (HCO_3^-), neutralize the acidic pH of the chyme and activate a range of hydrolytic enzymes, such as proteases, lipases and amylases [23]. These digestive enzymes are delivered to the small intestine where further digestion occurs to enable the absorption of nutrient particles.

Carbohydrates, proteins and lipids are digested and absorbed mainly in the jejunum section of the small intestine [9, 20]. The enzyme amylase, found in the saliva and pancreas, breaks down **carbohydrates** into monosaccharides that can be absorbed by the small intestine [4]. **Proteins** are broken down by pepsin which is activated by the low pH of the stomach [19]. A mixture of intermediate protein moieties, peptides and amino acids is delivered to the duodenum, where pancreatic proenzymes such as trypsinogen, chymotrypsinogen, proelastase and procaboxypeptidase will be activated by mucosal enterokinase into trypsin, chymotrypsin, elastase, and carboxypeptidase. These enzymes further digest proteins into amino acids, dipeptides and tripeptides, which can be absorbed in the small intestine.

The digestion of **lipids** starts in the oral cavity by exposure to lingual lipases [24]. The process continues in the duodenum, where bile and pancreatic juice facilitate the breakdown of lipids into fatty acids and monoglycerides, which can be absorbed in the intestine [25]. Bile contains **bile acids**, which are synthesized in the liver, stored in the gallbladder during fasting and secreted into the duodenum during digestion [25-27]. Different characteristics, such as the conjugation and number of hydroxyl groups, determine the molecule's hydrophobicity and detergent properties [28]. Additionally, bile acids regulate the cholesterol homeostasis, since bile acid synthesis is the major pathway for cholesterol catabolism. Bile acids are synthesized from cholesterol primary in pericentral hepatocytes through a series of sterol ring hydroxylations and side chain oxidation steps [29]. Those bile acids are called **primary bile acids**, whilst bile acids formed by a variety of reactions carried out by gut microbiota are called **secondary bile acids**. Cholic acid (CA) and chenodeoxycholic acid (CDCA) are primary bile acids in humans. They will be converted by microorganisms to secondary bile acids, such as deoxycholic acid (DCA), ursocholic acid (UCA), ursodeoxycholic acid (UDCA) and lithocholic acid (LCA). When the liver secretes bile acids, they are secreted into the small intestine and are reabsorbed in the ileum to then circulate back to the liver, called **enterohepatic circulation** [26]. Only approximately 5% of intestinal bile acids will escape the reabsorption and will end up in the faeces.

Vitamins, minerals and micronutrients are absorbed by the small intestine as well [19]. Many vitamins cannot be synthesized by humans, and therefore need exogenous intake or are synthesized by gut

bacteria. For instance, **Vitamin B_{12}** (cobalamin) which is a water soluble vitamin and obtained from foods of animal origin will be absorbed in the terminal ileum [4, 19]. Fat-soluble vitamins, such as vitamin A, D, E and K are also absorbed in the small intestine. Alongside vitamins, the small intestine is responsible for absorbing **major minerals**, such as calcium, phosphate, iron and magnesium as well as **micronutrients** such as zinc, copper, manganese, cadmium, selenium and chromium [19].

1.1.3. Histology

The small intestinal wall is composed of four layers: the serosa or *adventitia*, *muscularis propria*, submucosa, and mucosa (Figure 1). These play an important role in separating the entrapped digested chyme in the intestinal lumen [2, 4]. The most external layer is the **serosa or *adventitia***, which is a loose and smooth tissue membrane rich in blood vessels and nerves [3, 4]. Moving towards the lumen, the second layer is the ***muscularis externa*** composed of two layers of smooth muscles, *i.e.* the inner circular layer and the outer longitudinal layer. The contraction of this muscle tissue is responsible for the peristaltic movement of the intestine. Peristalsis, a crucial process in the gastrointestinal tract, makes the mechanic and chemical breakdown of food possible throughout the intestine and enables the removal of waste [30]. During peristalsis, the outer longitudinal layer of the *muscularis* contracts, while the inner circular layer relaxes [31]. This regulation of the muscles is assisted by the enteric nervous system [6]. The periodic contraction and relaxation of the small intestinal wall ensures that the intestinal content is agitated, mixed and driven through the intestine [30]. The third layer is the **submucosa**, which is a relatively thin layer, composed of stromal cells and dense network of arteries and lymphatic vessels needed for nutrient absorption. This collagen-rich extracellular matrix also supports the next layer, namely the **mucosa**. This last layer borders the lumen. The principal functions of the mucosa are to ensure absorption and transport of nutrients, keeping the tissue moist and protecting the body from pathogens, toxic compounds and foreign particles [4]. It is further composed of different layers. The inner layer, the **epithelium**, is exposed to the luminal content and supported by the ***lamina propria***, a connective tissue, and the ***muscularis mucosae***, a thin layer of smooth muscle tissue responsible for local movements and mucosa folding.

Small intestinal epithelium

The intestinal epithelium (Figure 1) is a single layer of intestinal epithelial cells (IEC) with a topography organised as finger-like protrusions and pockets, respectively called crypts and *villi* [32]. At the bottom of the crypts, the intestinal epithelium is composed of **stem cells** intercalated by Paneth cells. The stem cells are the progeny of the different cell types present in the intestinal epithelium, including enterocytes, Paneth cells, goblet cells, enteroendocrine cells and tuft cells [4, 11]. The stem cell niche is supported by underlying mesenchymal cells, such as myofibroblasts which secrete essential growth factors [32]. As cells mature, they migrate towards the top of the *villi*, where they eventually undergo apoptosis and are excreted into the intestinal lumen [3, 4]. The intestinal epithelium is the fastest renewing tissue in the human body, where cells are replaced every 4-5 days [4, 11].

At the base of the crypts, the regeneration process starts. Here the $Lgr5^+$ intestinal stem cells generate two symmetric daughter cells [33]. Some daughter cells remain stem cells and others will mature into epithelial cells while migrating upwards towards the top of a villus. The crypts are marked by a population of pyramidal-shaped cells, called **Paneth cells**, that migrate downwards after differentiation and are unique for the small intestinal epithelium [4]. Paneth cells are involved in the secretion of

antimicrobial peptides, proteins, enzymes and growth factors for host defence and immunity [34]. Therefore, Paneth cells are suggested to be involved in maintaining gut homeostasis [35].

Like Paneth cells, microfold cells (**M cells**) are unique to the small intestine [36]. They have a characteristic structure of apical short fold-like invaginations, called microfolds, and a large basolateral pocket enabling close-proximity with lymphocytes. M cells are not evenly distributed along the small intestine, but concentrated above Peyer's patches, lymphoid follicles containing B cells, T cells and mononuclear cells. M cells account for only < 1 % of the epithelium, but they play a role in the transepithelial transport of macromolecules, particles and microorganisms and are crucial for initiating the mucosal immune response by efficient delivery of antigens [37, 38].

Enterocytes, goblet, tuft cells and enteroendocrine cells are differentiated stem cells that migrate and mature towards the top of a villus [4, 39]. **Enterocytes** make up more than 80% of the intestinal epithelial cells (IEC) and are columnar-shaped cells, characterized by a brush border structure formed by *microvilli* on their apical side [4, 36, 40]. This structure increases their absorptive surface. The luminal surface of the small intestine is further enlarged by circular folds, known as plicae circulares, and by *villi* [11]. Together, the *villi* and *microvilli* enhance the small intestinal surface area by 60 to 120 times [41]. Towards the distal part of the small intestine, a decline in the number of plicae and *villi* is observed, as well as a decrease in villus height [11].

The primary function of enterocytes is the absorption of nutrients such as ions, water, sugar, peptides and lipids [4]. Expression of specific cellular receptors on the surface of the epithelium allows the uptake of nutrients available in the lumen [2]. For instance, glucose in the intestinal lumen is mainly taken up by the Na^+/glucose cotransporter (SGLT1). Enterocytes differ in function while maturing and migrating upwards [36, 40]. At the bottom of the villus enterocytes express anti-microbial genes and are more specialized for amino acid transport. Halfway, the enterocytes are mainly transporters for carbohydrates and upper-villus enterocytes account for lipid uptake [37]. Furthermore, it has been discovered that enterocytes cooperate with cells of the intestinal mucosa-associated lymphoid tissue (MALT) and thus are involved in the immune function of the intestinal tract [42].

Goblet cells are exocrine cells, differentiated from the intestinal stem cells, and can be distinguished by their apical accumulation of secretory granules. The proportion of goblet cells increases along the intestine, ranging from 4% in the duodenum to 16% in the terminal colon [43]. Goblet cells are mainly responsible for the synthesis and maintenance of mucus [4, 36, 44]. **Mucus** is a complex, viscous and elastic fluid covering the intestinal epithelium [45]. More than 95% of the mucus is water, which makes it transparent [46, 47]. Additionally, the mucus layer is structured as a skeleton by branched glycoproteins, such as mucins [46, 48]. Mucins are large, long molecules that have a hydrophilic nature and assemble into net-like polymers [46]. More than 20 subtypes of mucins have been identified throughout the human gastrointestinal tract, categorized into membrane bound and secreted mucins, based on their chemical structure and function [48]. **Membrane bound mucins** serve as the protective barrier between the epithelial cell surface and the mucus layer [48]. The most abundant ones present in the small intestine are MUC13 and MUC17 [49]. Conversely, the **secreted mucins** provide protection, lubrication and hydration of the human epithelial tissues to the environment [2]. MUC2 is the most abundant secreted small intestinal gel-forming polymeric mucin, which thus forms the mucus barrier.

Mucus forms a defensive barrier that is not only present in the gastrointestinal tract, but also in the respiratory and reproductive tract [45]. It covers the intestinal epithelium as a coat. The primary functions of mucus involve cleansing and protection [46]. It cleans the surface by washing away bound debris and bacteria. The peristaltic movement in the intestine facilitates the outward flow of mucus fluid away from the host. Overall, the thickness of the mucus layer increases throughout the small

intestine being the thinnest in the duodenum and jejunum, and therefore allows more nutrient absorption in those sections [50]. The small intestinal mucus layer is a single layer and not attached to the epithelium. Small intestinal epithelial regions with M cells have a thinner mucus layer, allowing more efficient contact between the Peyer's patches and the intestinal lumen [37, 38].

In the colon, the mucus layer is even composed of two layers [47]. The double mucus layer consists of a first, inner layer that is 50-200 µm thick and is tightly attached to the epithelium. This layer is assumed free of bacteria, in healthy conditions. The second, outer mucus layer has a less defined outer border and is more loosely attached to the first layer. This loose outer mucus layer is the habitat for the gastrointestinal tract bacteria.

Enteroendocrine cells comprise about 1% of the IEC [36, 51, 52]. They sense luminal contents and stimuli. As a response, they release hormones and multiple regulatory factors such as gastric inhibitory peptide, glucagon-like peptide and vascular intestinal peptide [51, 53]. This way, they control gut motility and regulate the overall digestion, insulin release, and food intake [51, 53]. There are more than 10 subtypes of enteroendocrine cells identified, classified according to the prominent hormone or peptide they produce [52, 53]. Examples of enteroendocrine cell types occurring in the small intestine are: EC cells secreting serotonin; L cells secreting GLP-1 and GLP-2; G cells secreting gastrin; and S cells secreting secretin [54-57].

Tuft cells are a rare population of epithelial cells and are still poorly described [58]. They have a cylindrical shape with thinner basal and apical ends and are located between the crypts and *villi* [59]. The fraction of their occurrence within the epithelial layer is 0.4% [37, 38]. They are epithelial sentinel cells recognizing a variety of luminal cues and initiate immune response. For example, it is known that they play a central role in the initiation of type II immune responses after helminth or bacterial infection [58, 59].

Functions of small intestinal epithelium

All the various intestinal epithelial cell types work together to provide a physical, an immune and a chemical barrier to protect underlying tissues, contributing to homeostasis. On the one hand, individual cells are anchored at their basolateral pole to the basement membrane by hemidesmosomes. On the other hand, neighbouring cells are held together by a narrow continuous belt of **tight junction proteins** such as zonula occludens-1 (ZO-1), occludin and claudins [60]. These tight junction proteins are located more closely towards the brush borders of the cell (Figure 2). The physical barrier is ensured by those intracellular junction proteins, excluding passage of most intestinal luminal bacteria, noxious substances and enzymes. However, the lateral spaces between cells allow paracellular transport. This paracellular transport across the tight junction can occur via the pore pathway or the leaky pathway [61, 62]. Both pathways are differentially regulated by immune signalling and have distinct size- and charge-selectivity. Thus, there is a delicate balance between paracellular permeability and tight junctions since the flux of pathogenic luminal materials needs to prevent and contemporaneously allow nutrient and water absorption [62]. For example, the reabsorption of bile acids occurs via transcellular passive or active mechanisms [29]. Paracellular transport is not possible because the bile acid molecule is too large and less hydrophilic to pass through the tight junctions of the intestinal epithelium.

Another line of defence is the immune barrier. The intestinal immune system is composed of an innate and an adaptive component [63]. The innate system includes innate lymphoid cells, macrophages, and some of the intestinal epithelial cells such as goblet cells, Paneth cells and M cells; dendritic cells link the innate and adaptive immune system; whereas the Peyer's patches and the nearby M cells play a role in the adaptive immune system [63, 64].

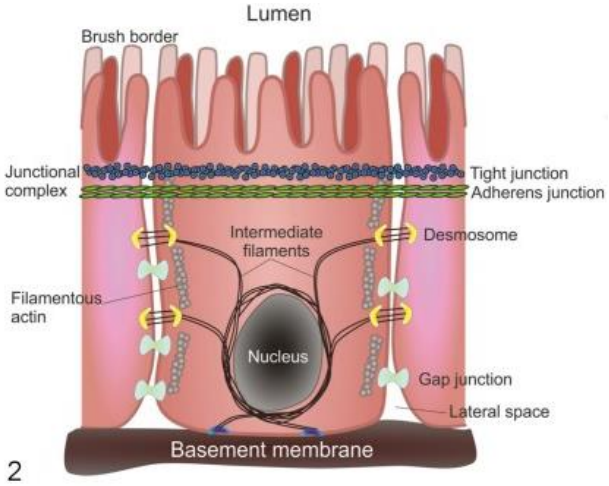

Figure 2: Figure from *Williams et al. (2015)* illustrating the tight junctions of intestinal epithelial cells, functioning as the epithelial barrier function.

Pattern recognition receptors (PRRs) on macrophages and dendritic cells initiate rapid inflammatory responses mediated by the secretion of cytokines and chemokines [65]. PRRs are classified in different families, including Toll-like receptors (TLRs), RIG-I-like receptors (RLRs), NOD-like receptors (NLRs), and DNA receptors (cytosolic sensors for DNA) [66]. PRRs are membrane-bound receptors binding to pathogen-associated molecular patterns (PAMPs) and are either expressed on the cell surface or associated with intracellular vesicles. Once PRRs recognize microbial specific PAMPs, a signalling-cascade transduction will be initiated [67]. The M cells, located nearby the Peyer's patches, capture antigens from the intestinal lumen. By transcytosis those antigens are transferred to a dendritic cell or macrophage [63, 68]. Depending on the surrounding signals it results in a pro- or anti-inflammatory response. For example, interleukine-1 (IL-1) and tumour necrosis factor (TNF) are proinflammatory cytokines and interleukin-10 (IL-10) is an anti-inflammatory cytokine [69, 70].

As mentioned in section 1.1.3, goblet cells are specialized for the secretion of mucus. As some bacteria can degrade the mucus layer by secreting mucinases and proteases, the continuous production and secretion of mucus is crucial to preserve the intestinal homeostasis and contribute to the immune barrier [71].

An important feature of the intestinal immune system is that it can function independently of the immune system in the rest of the body [72]. Dendritic cells usually do not go further than the mesenteric lymph nodes that drain the intestinal tissues and B and T cells will keep surveying the intestine instead of entering the normal traffic pattern of circulating lymphocytes. To conclude, the small intestine's physical, chemical and immune barrier work together to prevent pathogen infections and the uptake of toxic compounds, while allowing nutrient absorption [73].

1.1.4. Intestinal microbiota and host-microbe interaction

Human intestinal microbiota landscaping

The gut is the most densely populated habitat for microorganisms in the human body, with an estimated microbial biomass of 0.15 kg cell dry weight [74]. The intestinal microbiota include bacterial species but also non-bacterial species such as fungi, archaea, and bacteriophages [17]. However, for the aim of this research work, the focus of this thesis will be on the bacterial fraction of the human intestinal microbiota.

Most studies on gut microbiota rely on faecal samples, which primarily reflect the microbiota of the colon. It has been shown human faecal microbiota can be categorized according to the community composition, also termed **enterotypes** [74, 75]. The four predominant European enterotypes in the human gut, based on the abundance patterns, are: Faecalibacterium, Bacteroides, Prevotella, and Clostridiales [76]. Yet, the microbiome of a person is dynamic and thus the enterotype is not a static feature.

The distribution and variety of gut microbes are unique to each individual [77]. Ethnicity, sex, age and health status all contribute to the **inter-individual variability**. Additionally, the microbiome shows **intra-individual differences**, is dynamic and evolves through the individual's lifespan. It rapidly changes in early childhood, stabilizes in adults and changes significantly with the aging process in old age [78, 79]. Moreover, factors as mode of birth, infant feeding, lifestyle, medication, the host genetics and environmental factors influence the microorganisms of the intestine [77]. For example, Rothschild *et al. (2018)* reported that more than 20% of the inter-person microbiome variability is caused by environmental factors such as diet and lifestyle [80]. Compared to a more traditional diet, the Western diet is high in fat and simple carbohydrates but low in fibres and microbiota-accessible carbohydrates [81]. *Sonnenburg et al. (2016)* shows that microbiota-accessible carbohydrates are crucial for shaping the microbial ecosystem, since a diet low in microbiota-accessible carbohydrates results in lower taxa abundance [82].

Studying the microbiota of the small intestine is challenging, because it is poorly accessible compared to the colon [18]. Invasive techniques are needed such as esophagoduodenogastroscopy or nasoduodenal catheters. Some studies also sampled the ileal-mucosa during colonoscopy, intestinal resection, small-bowel transplantation or from death victims. By colonoscopy the terminal ileum is reached by passing through the anus and colon which means that the sample is contaminated with faecal and colon microbes[2]. Similarly but less pronounced, enteroscopy sampling results in contamination from the oral compartment and the stomach.

The small intestinal bacterial community is mostly constituted by the main phyla: Firmicutes, Proteobacteria, Bacteroidetes, Fusobacteria, and Actinobacteria (recently respectively renamed as Bacillota, Pseudomonadota, Bacteroidota, Fusobacteriota, and Actinomycetota) [2]. However, due to the difference in structural and physio-chemical parameters along the small intestinal segments, differences exist in bacterial composition and abundance. The bacterial genera found along the different sections of the small intestine, including luminal and mucosal bacteria, are listed as follows (Reviewed in *Delbaere and Rogiers et al. (2023)*):

- **Duodenum**: *Carnobacteriaceae*, *Gemella*, *Gemellaceae*, *Lactobacillaceae*, *Streptococcaceae*, *Streptococcus*, *Veillonellaceae*, *Veillonella*, *Enterobacteriaceae*, *Escherichia–Shigella*, *Haemophilus*, *Pasteurellaceae*, *Prevotella*, *Rothia*, *Fusobacterium*, *Faecalibacterium*, *Lactobacillus*

- **Jejunum**: *Carnobacteriaceae*, *Clostridiaceae*, *Gemella*, *Lactobacillaceae*, *Streptococcaceae*, *Streptococcus*, *Veillonellaceae*, *Veillonella*, *Enterobacteriaceae*, *Escherichia*, *Pasteurellaceae*, *Pseudomonas*, *Prevotella*, *Rothia*, *Fusobacterium*, *Clostridium IX*, *Clostridium XI*, *Lactobacilli*, *Actinobacillus*, *Bradyrhizobiaceae*, *Enterococcus*, *Haemophilus*, *Klebsiella*, *Pseudomonadaceae*, *Proteobacteria*, *Bacteroidetes*, *Prevotellaceae*, *Actinomyces*, *Rothia*, *Fusobacteria*
- **Proximal ileum**: *Clostridium I*, *Streptococcus*, *Veillonella*, *Enterococcus*, *Oxalobacter*, *Streptococcaceae*, *Veillonellaceae*, *Veillonella*, *Comamonadaceae*, *Escherichia*, *Haemophilus*, *Pseudomonadaceae*, *Bacteroides*, *Micrococcaceae*
- **Terminal ileum**: *Clostridium XIVa*, *Clostridium IV*, *Clostridium IX*, *Clostridium XIVb*, *Granulicatella*, *Lachnospiraceae*, *Ruminocacceae*, *Streptococcus*, *Veillonellaceae*, *Acinetobacter*, *Aeromonadaceae*, *Cupriavidus*, *Enterobacteriaceae*, *Escherichia*, *Bacteroidaceae*, *Bacteroidetes*, *Bacteroides*, *Actinomyces*, *Rothia*, *Cetobacterium*, *Fusobacterium*, *Verrucomicrobiaceae*, *TM7(G-1)*

Host-microbe interactions in the small intestine

The gut microbiota affects the energy homeostasis of the host by fermenting energy-yielding nutrients, especially complex carbohydrates, which are present in the lumen and the microbiota need for their own energy supply [77]. In fact, 5-10% of the energy needs of a human are produced by those microbiota [83]. To a lesser extent they also ferment proteins monosaccharides and amino acids.

When digesting dietary fibers, certain anaerobic gut bacteria such as Firmicutes species, including *Lactobacillaceae*, *Ruminococcaceae* and *Lachnospiraceae*, produce short-chain fatty acids (SCFAs). These organic acids have a carbon chain composed of less than six carbons [84-87]. The most prevalent ones in the intestine are acetate (C2), propionate (C3) and butyrate (C4) at total concentration of approximately 13 mM in the terminal ileum [88, 89]. SCFA can be absorbed by passive diffusion [86]. However, the uptake is enhanced by transporters such as the monocarboxylate transporter 1 and the sodium-coupled monocarboxylate transporter.

SCFAs modulate different processes such as cell proliferation, cell differentiation, mucus production, hormone secretion and immune response of the intestine [90, 91]. Both anti-inflammatory effect of acetate and propionate, and the proinflammatory effect of butyrate on innate immune system cells have been observed [92]. Moreover, SCFAs can enter the blood circulation and migrate to other organs [93, 94]. Therefore, SCFAs have a regulatory effect outside the gastrointestinal tract as well. For example, SCFAs can bind to G-protein-coupled receptors (GPCRs) such as GPR41 and GPR43, which are present among others in adipose tissue, immune cells, and the peripheral nervous system [93].

Next to SCFAs, also bile acids have shown to regulate homeostasis. In the small intestinal lumen the bile acid concentration averages 10 mM [95, 96]. Primary bile acids that are not reabsorbed can serve as substrates for microbial metabolism, resulting in the conversion of primary bile acids to secondary bile acids [77, 97]. Microbes can transform the primary bile acids into secondary bile acids. The major biotransformations of primary bile acids include: hydrolysis of conjugated bile acids to free bile acids and glycine or taurine by bile salt hydrolase (BSH); 7α-dehydroxylation of cholic acid (CA), and chenodeoxycholic acid (CDCA) yielding deoxycholic acid (DCA) and lithocholic acid (LCA), respectively; bile acids 7β-dehydroxylation of ursodeoxycholic acid (UDCA) yielding LCA [98]. Both primary as secondary bile acids have their metabolic functions by binding to cellular receptors such as farnesoid X receptor (FXR), vitamin D receptor (VDR), TGR5 and pregnane X receptor (PXR) [77].

There is still much to elucidate in the host-bacteria crosstalk. Therefore, it is challenging to define a healthy microbial composition in relation to the host's metabolic activity [77]. However, gut microbial communities from healthy individuals are characterized by a high taxa diversity, high microbial gene richness and stable microbiome functional cores [99]. When the balance in host-microbe interactions is disrupted, it can lead to significant alterations of composition and functionality of the gut's microbiome. Indeed, dysbiosis is observed in conditions such as inflammatory bowel disease (IBD) and irritable bowel syndrome (IBS) [100, 101]. IBD is one of the most studied human conditions linked to the gut microbiota and comprises both Crohn's disease and ulcerative colitis [102]. The dysbiosis manifests as a decrease in microbial diversity and an overrepresentation of certain bacteria, such as members of the Gammaproteobacteria class [102]. The altered microbiota can stimulate the immune system excessively, leading to chronic inflammation and damage to the intestinal mucosa. Moreover, bacteria that produce short chain fatty acids (SCFAs), which have anti-inflammatory properties, are often depleted in IBD patients, further increasing inflammation.

The direct causal relationship between dysbiosis and a disease is difficult to identify since the host-bacteria dialogue is a two-way interaction. This can also be illustrated by the example of the Short Bowel Syndrome (SBS). When the intestinal environment is disrupted, by resection, the microbial communities of the more distal intestinal sections are exposed to a higher load of nutrients.

Host-microbe interaction in disease: Short Bowel Syndrome

Short Bowel Syndrome (SBS) is a condition, resulting from the extensive loss of small intestinal mass either due to genetic defects at birth or following surgical resection of the small intestine leading to nutrient malabsorption [20, 103]. In Europe, the prevalence of SBS is estimated at 1-9 cases per 100 000 inhabitants [104]. This estimation includes patients with extensive intestinal resection due to vascular disease, congenital defects, or underlying disease, leading to the loss of absorptive intestinal surface [103, 105, 106]. SBS can be classified based on anatomical, pathophysiological and postoperative evolution criteria [2]. The gastrointestinal anatomy after resection is crucial to evaluate to be able to address the physiological impact and the specific nutritional requirements of the SBS patient. Based on **pathophysiology**, patients can be divided into two groups, namely SBS with colon in continuity and SBS without colon in continuity [107]. Based on **anatomical criteria** three classes can be distinguished (Table 1) [2, 103, 107]:

- **SBS type I**, resulted from end-jejunostomy and characterized by the complete removal of ileum, ileocecal valve and colon. The remaining part of the jejunum is directly anastomosed to the skin.
- **SBS type II** is the result of a jejuno-colonic anastomosis, characterized by a removal of ileum and ileocecal valve but the remnant jejunum is in continuity with part of the colon.
- **SBS type III** is derived from jejuno-ileal anastomosis and characterized by the preservation of the ileocecal valve and the colon in continuity.

On average, the small intestine of an adult measures 600 cm and a single meal needs about five hours to be processed through the entire length of the small intestine [2, 20, 106]. In normal conditions, the majority of nutrients are absorbed in the first 100 cm of the jejunum [106]. In adults, SBS is defined by a residual small intestine shorter than 200 cm [2, 106]. Due to the reduced absorptive surface, SBS patients suffer from **intestinal failure**, defined as the reduction in functioning gut mass below the minimal amount necessary for adequate digestion and adsorption of food to maintain health and

growth [106, 108]. Thus, patients with intestinal failure have impaired nutrient absorption, known as **malabsorption**, and need nutritional supplementation to maintain health and growth [109].

At **physiological level** three phases are recognized after surgery: (i) an acute intestinal failure phase lasting for three to four weeks; (ii) an adaptation phase and (iii) a chronic SBS phase [103]. The intestinal **adaptation phase** occurs weeks to months after resection, lasting for one to two years and is characterized by spontaneous morphological changes of the remnant intestine [110]. There is intestinal dilatation, increased area and length of the *villi*, expanded number of goblet cells and elevated intestinal epithelial sodium permeability [2].

In terms of the luminal environment, due to the shortened length of the intestine of SBS patients high oxygen levels are described in the remnant colon (when present), which is unfavourable for anaerobic bacteria to grow [110, 111]. Moreover, in SBS patients the rapid transit time, the pH, the disruption of the enterohepatic circulation of bile acids, and the amount of undigested nutrients strongly affect the luminal environment. As a consequence, SBS patients have a different composition in gut microbiota compared to healthy humans having an intact gastrointestinal tract [110]. In particular, a relative decrease in bacterial richness and in butyrate-producers, such as *Blautia*, *Dorea*, *Lachnospira Anaerostipes*, *Fusicatenibacter Roseburia*, *Pseudobutyrivibrio Flavonifractor* and *Faecalibacterium Bacteroides* has been noticed for SBS type II and type III [2]. A relative increase is seen for the genus *Lactobacillus* for SBS type III. In addition, there is a disruption in the composition of the faecal and colonic mucosa microbiota [110]. Lower bacterial diversity and higher prevalence of lactobacilli lead to lower SCFAs production and higher lactate production [112]. This higher lactate production, combined with the reduced absorptive capacity can lead to its accumulation. In particular, accumulation of D-lactate in humans may lead to life-threatening D-lactic acidosis [113].

Table 1: Table from *Delbaere, Roegiers et al. (2023)* representing the anatomical classification of SBS and its characteristics.

Surgical procedure	Type I SBS End-jejunostomy	Type II SBS Jejuno–colic anastomosis	Type III SBS Jejuno–ileal anastomosis
		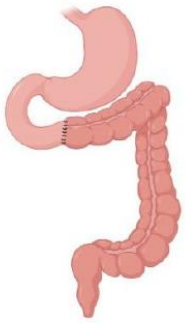	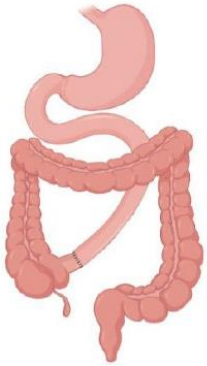
Preservation of ileocecal valve	No	No	Yes
Preservation of colon	No	Partial	Complete

1.2. Mimicking the small intestinal environment

The small intestine is a complex environment to model due to the number of intertwined parameters related to both host and microbiota, including nutrient availability, microbial diversity, immune responses and metabolite production. A variety of different approaches to study the small intestine exist and can be categorized in four groups: *in vivo*, *ex vivo*, *in vitro* and *in silico*. In the subsequent sections those models will be discussed, summarized in Figure 3, together with their advantages and drawbacks, with the main focus on the *in vitro* models.

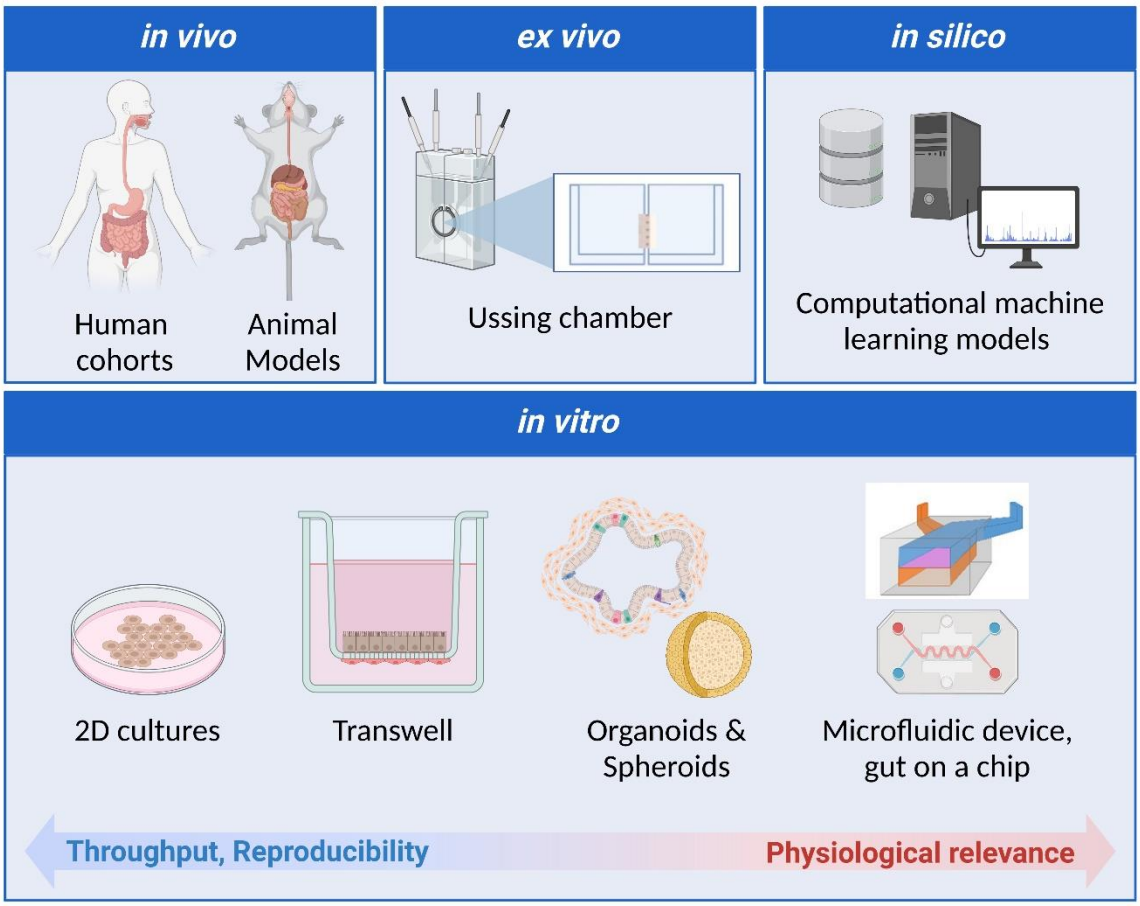

Figure 3: Overview figure for models mimicking the small intestine discussed in this chapter. This figure is inspired by Figure 2 from *Delbaere, Roegiers et al. (2023)* and Figure 1 from *Jung and Kim (2022)* [1, 2]. Figure created in BioRender.com

1.2.1. *In vivo*

To study the intestinal environment, *in vivo* approaches can be used, either through **human cohort** studies or **animal models**. Yet, invasiveness of some procedures as well as the inter-individual variability in human cohort limit the applicability for *in vivo* intestinal epithelial studies and host-microbiota research. In this context, rodents and especially murine models are a good choice for intestinal simulation, as their intestine is comparable in terms of physiology and partially in morphology to the human intestine [1]. The use of laboratory animals, instead of human cohorts, allows a controlled genetic background, controlled diet, and controlled environmental conditions [114, 115]. Moreover, there are more ethical constraints for humans and non-human primates than for rodents, even if both have ethical limitations. Besides the ethical aspect, *in vivo* models are expensive and time-consuming.

Even though the gastrointestinal tract of rodents is comparable to humans, there are differences in diet, overall gene expression, physiology, anatomy, and microbiome composition [116]. Rodents are coprophagous and have a larger cecum relative to their total gastrointestinal tract, which has an impact on the composition and proportion of microbial species through the intestine [1, 117]. Also, there is a difference in pH: the human small intestine has a pH of 6.0 – 8.0 during fasting and 5.0 – 6.5 when it is fed, while it is respectively 5.0 and 4.8 for mouse, and 4.5 – 7.5 and 3.8 – 5.0 for rat [38]. Other differences in regard to the physiology are the difference in volume and surface area of the intestine, as well as mucus thickness [116, 118]. These inter-species differences may complicate the extrapolation to humans. To better understand the underlying cell mechanisms, a more simplified model with reduced complexity and more controlled environment is needed. Therefore, *ex vivo*, *in vitro*, and *in silico* models are often employed.

1.2.2. *Ex vivo*

Ex vivo approaches take advantage of organs or tissues harvested from *in vivo* conditions and are maintained in a controlled environment for research outside an organism [1, 119]. This type of model can be used for predictions in clinical trials because it fully simulates the *in vivo* state of the intestine and at the same time the tissues can be treated or stimulated in a controlled environment. Nevertheless, the model can only be maintained for limited amount of time and advanced techniques or procedures are required for successful cultivation and prolonged survival [1]. Just like *in vivo* models, there are ethical constraints for the applicability of *ex vivo* approaches.

One of the main reasons for limited survival of the *ex vivo* tissues is the physiological change and change in nutrient supply compared to the natural state [120]. For example, the lack of blood supply can cause ischemic damage.

One example of *ex vivo* approaches to study intestinal physiology is the **Ussing chamber**, named after Hans Ussing who first developed this type of model. In particular, the Ussing chamber has been used to study the intestinal permeability across epithelial tissues and host-bacteria interactions [119, 121]. For example, *Hecht et al. (1999)* used the Ussing chamber to study the effect of pathogenic *Escherichia coli* on the intestinal epithelium [122]. They discovered that *E. coli* increases the Cl^- secretion. This brings scientifically relevant information using an *ex vivo* model.

1.2.3. *In vitro*

In vitro models mimicking the human small intestine play a crucial role in scientific research for several reasons. Firstly, species differ in anatomy and physiology of their small intestine [123]. Secondly, the small intestine is highly intertwined and complex, making it challenging to study *in vivo*. *In vitro* models offer a reductionist approach, allowing researchers to dissect and analyse individual components of the intestine's function in a controlled environment. Third, accessing the small intestine *in vivo* poses significant challenges: collecting intestinal mucosal and aspirates requires invasive procedures such as colonoscopy or enteroscopy, not possible to be performed in healthy individuals. Faecal samples can be an alternative to analyse the colon microbiota, however these samples do not give a representative picture of the microbial community of the small intestine [124, 125].

Overall, small intestinal *in vitro* models offer a non-invasive tool for advancing our understanding of intestinal biology, intestinal host-microbiota interaction, and disease mechanisms. *In vitro* models can provide predictive results, but the translatability of the results to humans is only justified once a substantial *in vitro – in vivo* correlation is established [38].

Different types of *in vitro* models have been used for stimulating the small intestine. Most are cell-based methods, but also non-cell-based methods exist. For cell-based approaches, different cell types are currently used to study the intestinal epithelium. Firstly, **primary cells** or human small intestinal epithelial-like cells, derived from human induced pluripotent stem cells (**hiPSCs**), can be used in *in vitro* models [3, 126]. Next, diverse **immortalized cell lines** derived from tumoral and healthy tissues of animals or humans can be used to mimic the intestinal environment [38]. Typically, enterocyte-like cell lines are used in combination with other cell lines to add mucus secreting and/or immune response function to the model [1, 38]. Examples of cell lines commonly used to model the intestinal epithelium, and relevant for this thesis, are described in more detail below:

- **Caco-2 cells** commonly used to simulate the intestinal epithelial barrier [38, 127]. Caco-2 cells are isolated from human colon adenocarcinoma but they can spontaneously differentiate and polarize into enterocyte-like cells of the small intestine. The Caco-2 cells resemble enterocyte cells because they develop apical *microvilli*, form tight junctions with adjacent cells and express diverse enzymes, such as disaccharidase and peptidase, typically expressed by intestinal cells [38, 128].
- **T84 cells** are, like Caco-2 cells, derived from human colorectal adenocarcinoma and differentiate spontaneously into enterocyte-like cells [129]. In contrast to Caco-2 that originates from a primary tumour and expresses more genes typically expressed by the small intestinal enterocytes, T84 originates from lung metastasis and typically expresses more colonocyte-specific genes [129, 130].
- **HT29** is an immortalized intestinal cell line derived from human colon adenocarcinoma [131]. **HT29-methotrexate (HT29-MTX)** cell line is isolated from HT29 to derive a homogenous population of polarized goblet cells that secrete mucins [38, 132, 133].
- Another mucin secreting cell line is **LS-174T**, which originates from a human Caucasian colon adenocarcinoma [134]. This cell line produces significant amounts of secretory mucin thereby resembling goblet cells.
- To include endocrine-like cells in a model to study the intestinal epithelium, **NCI-H716** can be used [135]. NCI-H716 is derived from human Caucasian colorectal adenocarcinoma.
- To include the innate immune system, the **THP-1** cell line, derived from human monocytic leukemia and having a spherical single-cell morphology, can be differentiated into macrophage cells [136].

- Finally, **CCD-18Co** is a cell line derived from human colon, and can enhance a more connective tissue [137, 138].

It is difficult to create a representative *in vitro* model that is able to fully capture the intestinal environment. In summary, the model should contain diverse cell types that together comprise the intestinal functions, include the complex 3D structure of the intestine, generate mechanical cues as in the intestine, and include the interaction of the epithelial cells and the immune system [8, 139]. General accepted cell-based models include: 2D cultures, Transwell®-based models, organoids, microfluidic-based systems and organoids [1, 38]. In the following paragraphs these models will be explained in more detail.

2D co-culture model

Two-dimensional (2D) cultures are mostly composed of a cell monolayer by growing the cells on multi-well plates or on inserts. 2D cultures can be monocultures or co-cultures with multiple cell types. The main advantages compared to more complex models, such as spheroids and organoids, are: a better reproducibility, less labour intensive, higher throughput, and lower cost. On the other hand, 2D models do not recapitulate the intestinal architecture: there is no interaction with the cells on the opposite site of the mucosa and the oxygen and metabolite gradients are not present [140-142].

Transwell® model

2D models can for example grow on a Transwell®. **Transwell®-base systems** (Figure 4) are often used to study the permeability of the intestinal epithelium [1, 38]. The Transwell system is composed of an insert that separates the culture vessel in an apical and basolateral compartment. This dual set-up corresponds with the intestinal lumen and submucosa [38]. The Transwell insert has a porous membrane, with a thickness of 10 µm, that allows the diffusion of substances between both compartments. There are different types of membranes, such as a polyester membrane, polycarbonate membrane or collagen-coated polytetrafluoroethylene membrane [143]. Also, the pore size can vary depending on the different applications. For permeability studies on cell lines usually a pore size between 0.4 - 3.0 µm is used [38, 143]. For cell invasion, chemotaxis and motility studies a pore size larger than 3.0 µm is generally more suitable [143].

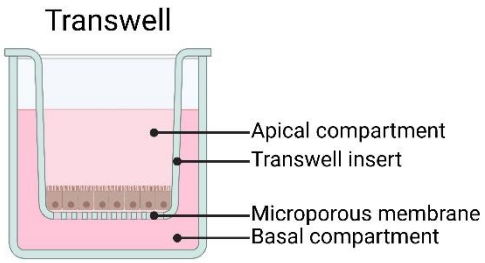

Figure 4: Set-up of a Transwell-based system. Figure made with BioRender.com.

Monocultures or co-cultures containing multiple cell lines (usually two or three different cell lines) are seeded on the apical side of the Transwell [38, 144, 145]. Recently, *Gautier et al. (2022)* generated for the first time a quadricellular Transwell model [146]. Their model was made of Caco-2, HT29-MTX, M cells, and enteroendocrine cells (NCI-H716). Creating a culture model with even more cell lines could be interesting to simulate the *in vivo* situation even better, although there are functional and practical limitations, such as the increased complexity of the system and the challenges in maintaining the viability and functionality of the multiple cell types during culturing.

Intestinal 3D models: Organoids & Spheroids

Three-dimensional (3D) cell models give an added value to *in vitro* models because they simulate better the architecture of the intestinal epithelium [38]. A current method to mimic the small intestinal natural microenvironment in a Transwell is the use of scaffolds on the apical side to obtain the 3D structure [38, 147]. Scaffolds can be fabricated in different manners and made of different materials [8]. Collagen is often used, but polymeric scaffolds, nanofibers, L-pNIPAM hydrogel and Matrigel could be used as well [38]. *Castello et al. (2014)* studied that using scaffolds for reconstructing the surface topography with accurately sized intestinal *villi* will enable cellular differentiation along the *villi* axis similar to the native intestine [147].

Spheroids and **organoids** are 3D models that can be used to study the intestine. They are 3D spherical shaped aggregations of cells, with enhanced cell-cell and cell-extra-cellular matrix interactions [148]. The difference between spheroids and organoids is the cellular source and protocol for establishment [149]. Spheroids are simpler 3D structures derived from tumour cells, hepatocytes, or embryoid bodies [150]. They do not require a scaffold to form 3D structures and the cells stick together by their natural adhesive properties. Organoids are more complex clusters of organ-specific cells growing into microscopic versions of parent organs [150]. The formation of organoids requires a certain scaffolding extracellular environment, such as Matrigel or Collagen. Spheroids and organoids are suitable to overcome the limitations of 2D monolayer culture models because they replicate the main features of the intestinal architecture. Although, 3D models are more challenging to establish and maintain in culture [149]. Moreover, stimulating organoids or spheroids with compounds or bacteria is more complicated than 2D models, considering that the luminal side is not facing the outside of the model.

Intestinal organoids, or the so called “mini guts” or “enteroids”, are self-organized 3D structures of (small) intestinal cells originated from stem cells residing in the base of the crypts [8]. The stem cells can be differentiated into mature intestinal epithelial cells, resulting in an architecture recapitulating crypts and *villi* structures. However, as the luminal side is not facing outwards, stimulating organoids or spheroids with compounds or bacteria is more complicated than 2D models [151, 152]. In fact, the lumen is only accessible by microinjection or disruption of the organoid polarization [153]. Nonetheless, *Roodsant et al. (2020)* used proximal and distal small intestinal organoids to generate 2D monolayers [153, 154]. *Wright et al. (2023)* described and characterized a novel 96-well human gut organoid-derived monolayer system [153, 154]. Here, organoids are broken into single cells and seeded onto semi-permeable Transwells to generate 2D cultures. This way the 3D model can be manipulated and stimulated in 2D.

Modelling intestinal host-microbiota interaction

To mimic the intestinal environment for studying host-microbe interactions, a proper understanding of the resident microbial ecology is essential. However, for the small intestine, this proves to be more challenging due to poor accessibility compared to the colon [18]. Invasive techniques are needed such as esophagoduodenogastroscopy or nasoduodenal catheters. Some studies also sampled the *ileal mucosa* during colonoscopy, intestinal resection, small-intestinal transplantation or from death victims. By colonoscopy the terminal ileum is reached passing through the anus and colon which means that the sample is contaminated with faecal and colon microbes [2]. Although less pronounced, eneteroscopy sampling includes contamination as well, but from the oral compartment and the stomach. For these reasons, *in vitro* models such as the **SHIME** (Simulator of the Human Intestinal Microbial Ecosystem) can be used to study the intestinal microbiota. The SHIME consists of multiple compartments dynamically simulating human gut [155].

The host-microbiota interaction can be studied using different *in vitro* models. In 2D models and **Transwell models**, host-microbe interactions can be studied by adding microorganisms at the apical side which corresponds to the *in vivo* representation [1]. However, those models are static. To overcome the static behaviour, microfluidics-based systems have been developed [38]. **Microfluidic devices**, such as gut-on-a-chip and human-microbial cross talk (HuMiX), are able to simulate the 3D topology, dynamic environment and gut microbiome of the (small) intestine [38]. Thus, this type of *in vitro* model mimics even more the *in vivo* situation of the intestine. Figure 5 from *Marrero et al. (2021)* illustrates the set-up of such microfluidic models [156].

Gut-on-a-chip is generally composed of a porous membrane that supports a monolayer of intestinal epithelium cells and separates two compartments, mimicking the lumen and blood circulation of the intestine [38, 157]. Hence, compared to the above mentioned 2D and 3D approaches, gut-on-a-chip includes microfluidic channels where the medium can flow through [157]. Additionally, the peristaltic movement of the intestine can be simulated by, for example, cyclic suction of tubes connected to vacuum chambers using a computer-controlled FX5K tension instrument, which is able to elongate the porous membrane [157]. An intestinal microbe, *Lactobacillus rhamnosus GG* has been co-cultured in this type of model on the luminal surface of the cultured intestinal epithelium.

HuMiX is another microfluidic device that facilitates host-microbe studies [38, 158]. This device is built up of three co-laminar microchannels: one for microbial culture, one for epithelial cell culture and one for medium perfusion. The main advantages of the HuMix model are that cells and microbes can be cultured simultaneously and that the oxygen concentration and transepithelial electrical resistance (TEER) can be measured in real-time.

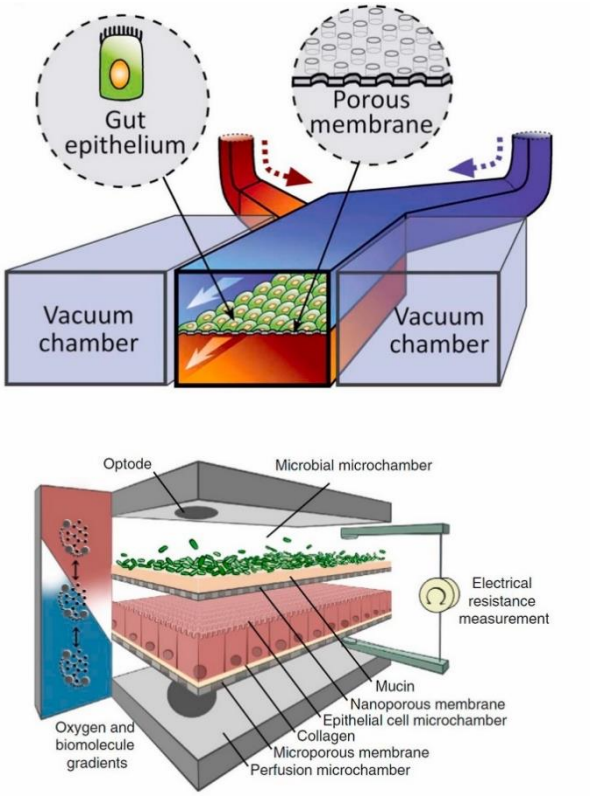

Figure 5: Part of a figure originating from *Marrero et al. (2021)* showing the built up of microfluidic based systems. On top the composition of gut-on-a-chip is shown and below the HuMiX model.

Marzorati et al. (2014) developed an innovative *in vitro* model called the **Host-Microbiota Interaction (HMI) module** to study the host-microbe interaction in the gastrointestinal tract [159]. The setup of an HMI module is shown in Figure 6. It is composed of two compartments and this in parallel in order to perform the experiments in duplicate. The upper compartment represents the lumen of the gastrointestinal tract containing mixed microbiota from the SHIME. The lower compartment contains enterocytes, simulating the host. Those compartments are separated by a double layer that consists of a mucus layer on top of a semipermeable polyamide membrane. The HMI module offers three advantages compared to other available *in vitro* models. Firstly, it makes it possible to simulate the bacterial adhesion to the gut wall and at the same time the indirect effect on human cell lines. Secondly, the HMI module makes it feasible to perform experiments up to 48 hours with a complex

microbial community representing the *in vivo* composition. Thirdly, it is possible to couple the HMI to the SHIME, which is a continuous, reactor-based simulator of the human gastrointestinal tract.

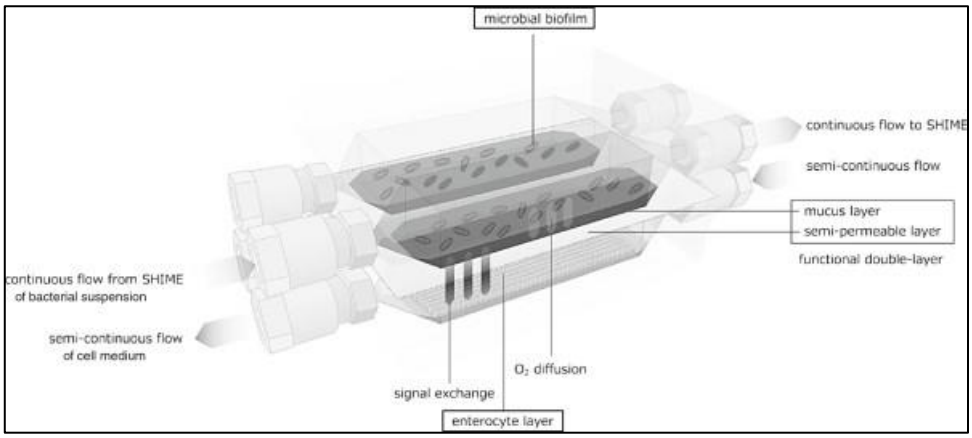

Figure 6: A scheme of the Host-Microbiota Interaction (HMI) module developed by *Marzorati et al. (2014)*.

In conclusion, *in vitro* models, ranging from traditional two-dimensional cultures to more advanced systems like Transwell setups, three-dimensional organoids and spheroids, as well as microfluidic devices, present a valuable reductional approach for investigating the cellular mechanisms of the intestinal epithelium. Compared to *in vivo* and *ex vivo* methods, these *in vitro* models offer controlled environments and higher throughput for studying specific aspects of intestinal physiology and pathology. However, it is crucial to recognize the inherent trade-off between representability and feasibility in designing laboratory setups. Therefore, to address the intricate interplay of numerous parameters within the intestine, *in silico* methods often complement *in vitro* approaches.

1.2.4. *In silico*

In silico modelling is the development of computer models for pharmacologic or physiologic processes [160]. Both benefits of *in vivo* and *in vitro* are combined in *in silico* models. In theory, researchers can add unlimited parameters to the system to obtain a model representing the whole organism. Moreover, *in silico* allows the control of the computational parameters and machine learning can identify trends and patterns. In contrast to *in vivo* and *ex vivo* models, the ethical aspect of *in silico* is only related to the data usage. However, it has to be considered that in silico models are dependent on *in vivo* and/ or *in vitro* datasets. Moreover, to construct a model, assumptions need to be made. In general, in silico models are used for screening and prediction.

Some *in silico* models for the small intestine already exist. For example, Du et al. (2016) created a virtual model that mainly focused on the electrophysiology and motility of the small intestine [161].

1.3. Objectives

To study small intestinal Host-Microbiota-Interactions (HMI), *in vitro* models are essential. *In vivo* models are physiologically more relevant, but have their ethical considerations. Also, *in vitro* models can validate the intestinal anatomical, genetic and microbial differences between human and mice. In addition, *in vitro* approaches can be used to study more specifically the cellular mechanisms, which is more difficult *in vivo* due to the higher complexity of the organisms. *In vitro* models, ranging from traditional two-dimensional cultures to more advanced systems like Transwell setups, three-dimensional organoids and spheroids, as well as microfluidic devices, are already been used to investigate the cellular mechanisms of the intestinal epithelium and HMI. Transwell® models for the colon are been studied in the hosting laboratory and are already better described in the literature [130, 145]. In contrast, *in vitro* models for the small intestinal epithelium including multiple cell lines have not yet well been characterized in the literature. To address this gap, this thesis aims at optimizing and characterizing a Transwell *in vitro* model to study the small intestinal epithelium and to describe mechanisms of host-microbe interaction (HMI). As such, this work aimed to enhance the understanding and application of the intestinal *in vitro* model by mainly analysing the barrier integrity, permeability, gene expression of *ZO1* and the gene expression of *MUC2*.

The primary research question for the characterization and optimization of the Transwell *in vitro* model is: How do different coating agents, different goblet cell types (HT29-MTX-E12 or LS174T), and the addition of an immune compartment affect the barrier functions of the *in vitro* model? The main research question regarding the host-microbiota dialogue is: What are the effects of bile acids, bacterial supernatant, and the live bacterium *Clostridium leptum* on epithelial functions?

CHAPTER 2.
MATERIALS AND METHODS

2.1. Cell lines and cell maintenance

Cell passaging was performed when cells reached a confluency of proximately 70-80%. For the adherent cell lines, PBS -/- (Thermo Fisher Scientific) was used to wash the cells. To detach the cells, incubation with filter sterilized trypsin-EDTA (Sigma-Aldrich) at 37°C and 10% CO_2 for approximately 3-5 minutes was performed. The trypsin-EDTA was inactivated by adding three times more serum-supplemented cell medium.

The used **cell lines** were grown at 37°C, 10% CO_2 and 90% relative humidity.

Caco-2 (Sigma, cat n° 86010202-1VL) and HT29-MTX-E12 (Sigma, cat n° 86010202-1VL) were cultured in Dulbecco's Modified Eagle Medium (DMEM, Gibco, Thermo Fisher Scientific). LS174T (CLS-cell lines service Germany, cat n° 300392) and CCD18CO (ATCC® CRL-1459™) were cultured in Minimal Essential Medium (MEM, Gibco, Thermo Fisher Scientific). NCI-H716 (ATCC® CCL-251™) and THP1 (Sigma, cat n° 88081201-1VL) were cultured in Roswell Park Memorial Institute medium (RPMI 1640, Gibco, Thermo Fisher Scientific). The T84 cell line (CLS-cell lines service Germany, cat n° 300354) was cultured in Dulbecco's Modified Eagle Medium/ Nutrient Mixture F 12 (DMEM/F 12, Gibco, Thermo Fisher Scientific). DMEM was supplemented with heat inactivated Foetal Bovine Serum (FBS premium grade, Avator VWR), Non-essential amino acid solution (Gibco, Thermo Fisher Scientific), and Penicillin-Streptomycin-Amphotericin B (P/S/A, Merck). MEM, DMEM/F12, and RPMI- 1640 were supplemented with heat inactivated Foetal Bovine Serum (FBS premium grade, Avator VWR), and Penicillin-Streptomycin-Amphotericin B (P/S/A, Merck). FBS was heat inactivated by incubation at 56 °C for 30 minutes. Each 2-3 days the medium of the cell cultures was renewed.

Primovert inverted **light microscope** (Carl Zeiss Microscopy Gottingen, Germany) was used to regularly check the cell cultures, to check if the cells detached and to image the morphology of the epithelium over time. Pictures were acquired with a Lumenera INFINITY 1 camera and processed with ImageJ. For the differentiation of the THP-1 into macrophages, **IncuCyte®** Live-Cell Analysis System (Sartorius) was used for live imaging and images were acquired and processed with the built-in software (Sartorius).

Absence of **mycoplasma contamination** on the cell cultures was regularly confirmed using MycoAlert® Mycoplasma Detection Kit (Lonza). The mycoplasma assay was regularly conducted and especially before using the cells in an experiment or prior to freezing the cells.

For **cell counting**, Trypan Blue Stain (0.4%, Gibco) was used to distinguish live and dead cells, counted using a Neubauer hemocytometer.

2.2. *In vitro* epithelial co-culture models

2.2.1. *In vitro* model set-up: membrane coating and cell seeding

To establish the cell models, **Transwell®** Permeable Supports, Polycarbonate (PC) Membrane from Corning Incorporated Costar® (2 Alfred Rd., Kennebunk, ME 04043, USA) were used. Collagen type I (solution from rat tail, Merck) with a stock concentration of 3.3 mg/mL was diluted in PBS +/+ to a final concentration of 6 µg/cm^2 to coat Transwells insert membranes (Corning) for 2 hours at 37°C, 10% CO_2 and 90% relative humidity. After incubation, the Transwell inserts were washed twice with PBS -/- and immediately used for cell seeding.

Instead of collagen, in some models Matrigel was used. Matrigel (Matrigel®, Basement Membrane Matrix, Corning®) with a stock concentration of 9.8 mg/mL was diluted in PBS +/+ to coat the wells with a concentration of 25 µg/cm².

To establish the **intestinal epithelium layer**, the cells were harvested by trypsinisation, counted and then seeded on the apical side of the Transwell, as detailed below and visualized in Figure 7:

i. For the **double co-culture cell model**, Caco-2 cell line in combination with either LS174T or HT29-MTX-E12 was used with respective seeding ratio of 90:10.
ii. For the **triple co-culture small intestinal model** Caco-2, LS174T or HT29-MTX-E12 and NCI-H716 cell lines were used with respective seeding ratio of 89:10:1.
iii. For the **triple co-culture colon model** T84, LS174T and NCI-H716 cell lines were used with respective seeding ratio of 79:20:1.

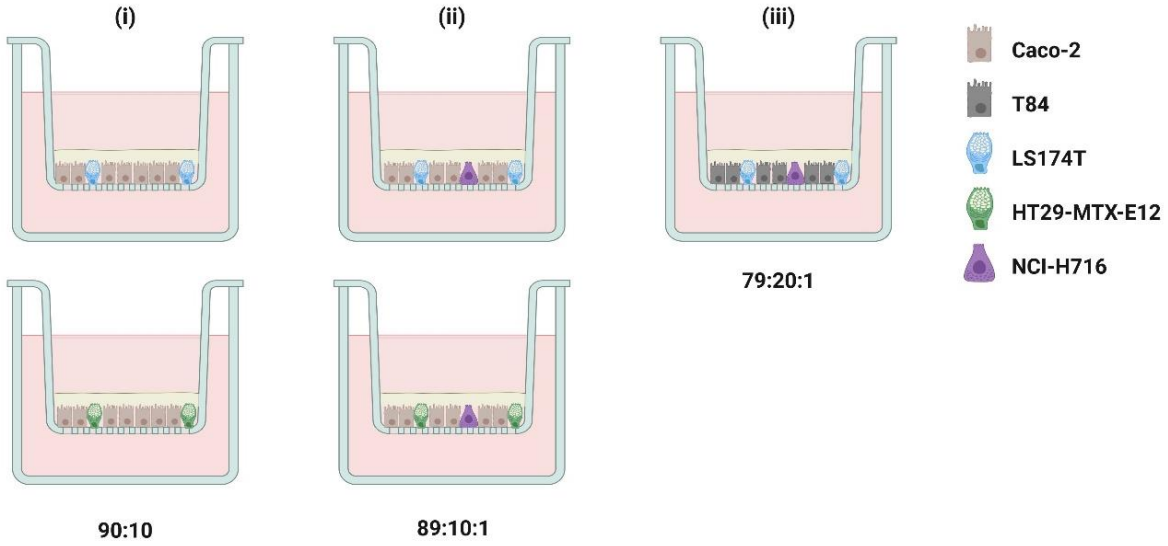

Figure 7: Visualisation of the double and triple models for the small intestine and colon with their respective seeding ratios for the enterocyte-, goblet-, and endocrine-like cells. The models are: (i) double co-culture small intestinal models, (ii) triple co-culture small intestinal models, and (iii) triple co-culture colon model. Figure created in BioRender.com.

The total amount of cells seeded and the working volume were determined based on the area of the Transwell insert used, as listed in Table 2.

Table 2: Total amount of apical seeded cells and used volumes for the different Transwell formats.

Transwell Insert Format	Insert diameter (mm)	Approx. Surface area (cm^2)	Total amount of seeded cells (cells/ well)	Working Volume Well (mL)	Working Volume insert (mL)
24-well	6.5	0.33	$52 \cdot 10^3$	0.5	0.1
12-well	12	1.12	$175 \cdot 10^3$	1.5	0.5
6-well	24	4.67	$750 \cdot 10^3$	3.0	1.5

For some models an additional **fibroblast cell layer** was added (Figure 8A). In this case the CCD-18CO cell line was used and seeded on the collagen coated inserts at first. For a 12-well Transwell 175.000 fibroblast cells/ well were seeded. The fibroblast grew for 4 days on the Transwell whereafter the epithelial cell layer of Caco-2:LS174T:NCI-H716 in ratio of 89:10:1 was seeded. In another set-up, the cultured CCD-18CO cells' supernatant was collected and used together with DMEM medium (ratio 50:50) to culture a triple model of Caco-2:LS174T:NCI H716 in ratio of 89:10:1 (Figure 8B).

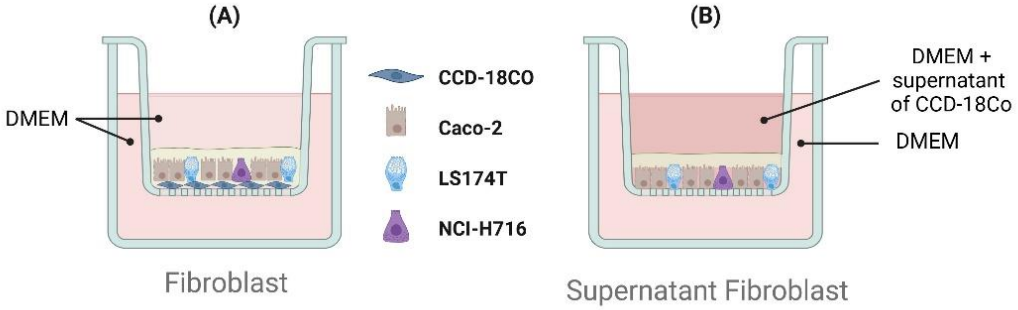

Figure 8: Visualization of (A) setup with an additional fibroblast layer, and (B) setup using the fibroblasts' supernatant to culture triple small intestinal models. Figure created with BioRender.com.

Including the **immune compartment**, **THP-1** cells were seeded at the basal side of the Transwell insert with a seeding density of 15.000 cells/cm^2 (Figure 9A). Then, the cells were differentiated to macrophages by incubating the cells in 100nM phorbol myristate acetate (PMA, Sigma-Aldrich) for 24 hours.

In a next experiment, different PMA concentrations (ranging from 10 to 150nM), were tested in the lab. Moreover, macrophages were added to Transwell monocultures of LS174T, Caco-2, and HT29-MTX-E12 cells at different timepoints. According to those experiments a new concentration and differentiation period was chosen based on visualizing the adherence and morphological changes. PMA concentration of 150nM was used to differentiate the THP-1 cells seeded at the bottom of a well-plate during an incubation period of 48 hours followed by 48 hours of resting period in medium deprived of PMA. Finally, the macrophages were added to a triple small intestinal Transwell model (Figure 9B) and this setup was used in the model for *Clostridium leptum* stimulation.

Figure 9: Visualization of two set-ups for the inclusion of macrophages in the triple model. (A) THP 1 cells are seeded at the basal side of a Transwell insert. (B) THP-1 cells are seeded at the bottom of a well-plate. Figure created with BioRender.com.

Supplemented DMEM medium was used both on the apical and basal side of the Transwell, unless otherwise specified. The Transwell models were maintained by refreshing the medium every 2 to 3 days for a total period of 19-22 days until **differentiation**, unless otherwise specified. Each week after seeding the cell morphology (imaging), epithelial integrity (trans-epithelial electrical resistance, TEER) and permeability (lucifer yellow assay) were monitored, as described in chapter 2.3. As well, both apical and basal compartments' supernatant was sampled throughout the differentiation period. The collected medium was preserved in 2mL centrifuge tubes at -20°C and later on the secreted cytokines and hormones were analysed by ELISA (Enzyme Linked Immune Sorbent Assay).

After differentiation and stimulation, the cell models were either lysed for RNA extraction and gene expression quantification. As well, apical and basal supernatants were collected and stored at -20°C for cytokine quantification.

2.2.2. Stimulation of the cell models with bile acids

Tauroursodeoxycholic acid (TUDCA, Merck Life Science) and Lithocholic acid (LCA, Merck Life Science) at a final concentration of 25µM were used to stimulate triple co-culture small intestinal models (in results section 3.3.2). The stock solution of TUDCA (18.8 mg/µL in DMSO, Merck Life Science) and LCA (28.8 mg/mL in DMSO) was diluted with DMEM.

2.2.3. Stimulation of cell models with bacterial samples

The cell models were stimulated either with bacterial supernatants (in results section 3.3.1 and 3.3.4) and live bacteria (in results section 3.3.3).

For the stimulation with **bacterial supernatants**, complex microbial communities from different compartments and time points of a SHIME (Simulator of Human Intestinal Microbial Ecosystem) were used. First, the bacterial load of each SHIME sample was quantified for each collection moment using Accuri C6+ flow cytometer (BD, Erembodegem, Belgium). To determine the live and dead bacterial fraction, samples were stained with SYBR Green I (1000× diluted, Invitrogen, Carlsbad, USA)/propidium iodide (4 µM final concentration, Sigma-Aldrich, Merelbeke, Belgium) (SGPI) staining solution for 20 minutes at 37°C in the dark. Cell count registration and analysis was performed using the BD Accuri C6 Plus software (BD, Erembodegem, Belgium). Then, each samples was centrifuged for 10 minutes at

5000*g*, filtered with a sterile 0.2 µm membrane filter and stored at -20°C until use. For host-microbe interaction (HMI) assay, each sample was gently defrosted in the fridge and diluted in DMEM medium, to the desired final concentration. The dilution was determined based on the bacterial load of the original SHIME sample, at the moment of the collection.

For the proximal small intestine (PSI) and Ileum (Ile) supernatant, the samples were diluted to an equivalent final bacterial concentration of 10^5 and 10^6, respectively. For the transverse colon (TC) supernatant, the final concentration was equivalent to 10^7 live bacterial load. The SHIME medium (composition can be found in Table 5 of appendix) was centrifuged, sterile filtered and diluted with the same dilution factor of the most concentrated sample; and served as negative control.

For the stimulation with l**ive bacteria**, cultures of *Clostridium leptum* were used.

Briefly, *C. leptum* (DSM 753) was cultured for 48 hours in the DSMZ 104c medium (with strain specific modification, as recommended by DSMZ), prior to cell stimulation. Cell concentration was determined by flow cytometry prior to the experiment. Recommended culturing medium by DSMZ was used (DSM 104c: with strain specific modifications for DSM 753, see Appendix Table 4 for media composition).

For cell stimulation with live bacteria, an **artificial mucus layer** was added to provide additional protection to the epithelial layer. The artificial mucus layer (shown in Figure *10*D) for microbe coincubation was prepared by adding 250µL of a 0.8% agar (Carl Roth, Karlsruhe, Germany) and 5% porcine mucin type II-solution (Sigma-Aldrich, Overijse, Belgium) in dH_2O. NaOH was added until a neutral pH was obtained. Consequently, the solution was poured onto a Transwell polycarbonate filters with 0.4µm pores (1.12cm² diameter, Greiner). Once solidified, the artificial mucus layer was stored in the fridge until one day before the experiment. Then, together with the cell model a pre-incubation step overnight was included in microaerophilic conditions (O_2 = 9.7%) to allow the cell model to adapt to the **microaerophilic conditions** needed for the bacteria-cell co-incubation.

On the day of the experiment, the live bacterial concentration of the *C. leptum* cultures was determined by flow cytometry. For this, a serial dilution was made of the culture in filtered PBS (Thermofisher Scientific) followed by a Syber Green (Thermofisher Scientific) and propidium iodide (Thermofisher Scientific) staining (1%) for 20 min at 37°C. Then gating was performed to determine the viable population. For this a heat-killed control was included (95°C for 20 min). Finally, the sample was diluted to a total bacterial load of 10^6 bacteria. The same bacterial medium was used to dilute the sample.

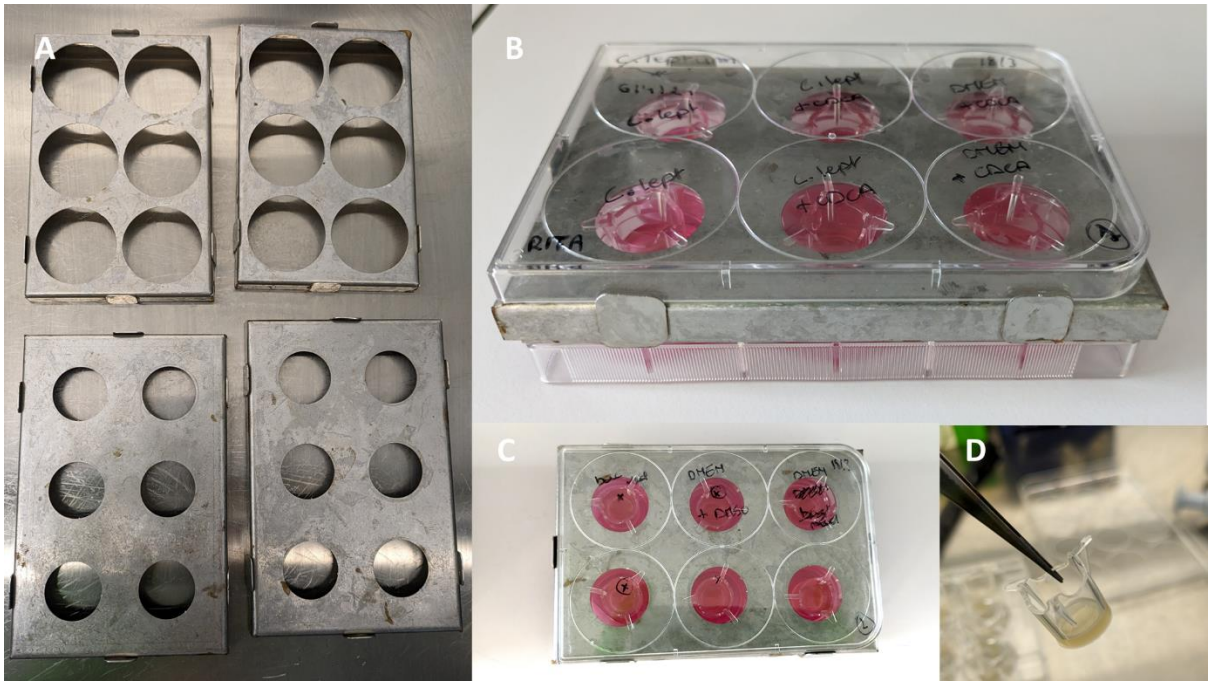

Figure 10: Set-up of the experiment for stimulation with live bacteria (*C. leptum*). (A) Shows the metal scaffolds for the extra Transwell, serving as the bacterial compartment. (B) and (C) show the complete set-up of the Transwells using the scaffolds. (D) shows the artificial mucus layer.

2.3. Characterization of the *in vitro* model

The cell models differentiated for 19 to 22 days. At the beginning (DIV6-8), the middle (DIV13-15) and the end (DIV19-22) of the differentiation period the barrier integrity and permeability was assessed. As well, supernatant of both apical and basal compartment was collected to analyse the secreted cytokines and hormones.

After differentiation and stimulation, the cell models were either lysed to assess the gene expression, or cryopreserved and histochemically stained to look at the cross section of the epithelial layer. The latter was not part of this thesis' framework.

2.3.1. Assessing epithelial barrier integrity

Transepithelial Electrical Resistance (TEER) is a quantitative method to measure barrier integrity of cell culture monolayers. The electrical resistance (R) is measured in Ohms (Ω) by Millicell® ERS probes (EMD Millipore Corporation, Burlington MA 01803, MERSSTX01). The basolateral electrode touches the bottom of the well and the apical electrode is placed in the apical side of the Transwell, without touching the layer of cells.

Before usage and to prevent cross-contamination between different conditions, the electrode was placed in 70% ethanol for 2-5 minutes and let air-dry.

To calculate the reported TEER values, the surface area of the Transwell insert ($A_{transwell}$ in cm^2) is taken into account. $R_{measured}$ and R_{blank} are respectively the resistances measured of a Transwell cell model and a Transwell with only medium and no cells. R_{tissue} (in Ω) and the reported TEER value ($TEER_{reported}$ in cm^2) are calculated by the following formulas, as explained in *Srinivasan et al. (2015)* [162]:

$$R_{tissue} = R_{measured} - R_{blank} \; [=] \; \Omega$$

$$TEER_{reported} = R_{tissue} \cdot A_{transwell} \; [=] \; \Omega \cdot cm^2$$

2.3.2. Evaluation of the epithelial permeability

Lucifer yellow CH dilithium salt (LY) is a small and hydrophilic molecule (452 Da) able to cross the cellular membranes and barriers, used for assessing the passive paracellular transport across a cell layer. Knowing that this compound gets excited at wavelengths of 430nm and the emission spectra can be measured at wavelengths of 540nm, the permeability coefficient of the cell model can be obtained.

The Lucifer Yellow stock solution (100mM in DMSO, Merck) was diluted in DMEM culture medium to achieve a final concentration of 100µM. For each assay a standard curve was prepared in a black 96-well microplate (Greiner Bio-One) by setting up a 2-fold serial dilution from 100µM to 2µM, including a blank which is only DMEM. The diluted Lucifer Yellow solution (100µM) was added to the apical side of the Transwell. After 2 hours of incubation at 37°C and 10% CO_2, 100 µL of apical and basal medium of the Transwell was transferred to the black 96-well plate to measure the fluorescence of the samples. The standard series were incubated at the same conditions, to prevent bias resulting from temperature differences.

The fluorescence measurements were conducted using a microplate reader Tecan Infinite 200 PRO (Tecan Austria GmbH). The excitation and emission were respectively measured at 430nm and 540nm. Greiner 96 Flat Black plates are used and some specific settings were used, namely a shaking step of 5 seconds, 6 flashes and optimal gain.

The apparent permeability apical to basal $\left(P_{app,\,A-B}\right)$ was calculated using the following formula [163]:

$$P_{app,\,A-B} = \frac{Q}{\Delta t} \cdot \frac{1}{A \cdot C_0} [=] \frac{cm}{s}$$

where Q is the absolute amount of Lucifer Yellow present in the basal compartment in µmol, calculated based on the generated standard curve; the Δt represents the incubation time in seconds; C_0 is the Lucifer Yellow concentration added to the wells (100µM) and A is the surface area of the Transwell insert in cm².

2.3.3. Quantification of secreted cytokines

Human IL-8 Uncoated ELISA kit (Invitrogen-88-8086, ThermoFisher Scientific) was used for quantitative detection of secreted human IL-8 cytokine in apical and basal media collected from the co-culture Transwell models, following the manufacturer's guidelines. ELISA/ELISPOT Diluent from the kit was used to diluted the samples 1:10. The samples were incubated overnight at 4°C before adding the Detection Antibody.

Human GLP1 (Glucagon Like Peptide 1) Sandwich ELISA Kit (AssayGenie, HUFI00805) was used for the quantitative detection of GLP-1 in supernatant samples of co-culture Transwell models, following the manufacturer's guidelines.

2.4. Quantification of gene expression

Quantitative reverse transcription polymerase chain reaction (qRT-PCR) was performed to analyse the gene expression of cell cultures and co-culture models.

Firstly, **RNA was extracted** using the NucleoSpin® RNA Plus kit (Macherey-Nagel GmbH & Co. KG). The RNA yield was determined with DS-11+ Quantification Spectrophotometer (DeNovix). Subsequently, the **DNA digestion** was performed using DNase I, RNase-free (ThermoFisher Scientific), following the manufacturer's instruction. The DNase-treated RNA was then use for **cDNA synthesis** using the Reverse Transcriptase Core kit (Eurogentec) and using a Thermal Cycler (Bio-Rad), following the manufacturer's protocol.

For the quantification of gene expression, qPCRs reaction mix consists of 10µL Power Track™ SYBR Green Master Mix, 200-500nM forward primer, 300-500mM reverse primer, 100ng-100fg DNA sample and PCR water up to a total of 20µL reaction mix per well. The **qRT-PCR** was conducted using QuantStudio™ 3 Real-Time PCR System (Applied Biosystems) with the following thermal cycling program: 20-30 seconds at 95°C for initial polymerase activation and DNA denaturation, followed by 35-40 cycles of amplification with denaturation during 15 seconds at 95°C, and annealing during 60 seconds at 60 °C. The melt curve analysis was performed as follow: 65°C-95°C with 0.5°C increment 2-5 seconds per step.

Gene expression of human *MUC-2*, *ZO-1* was performed using the primers listed in Table 3. All primers were validated for an amplification efficiency of approximately 100%. Human actine-beta (*ACT*β*)* and *GAPDH* were included as housekeeping genes. For each sample, technical triplicates and duplicates were analysed for the gene of interests and housekeeping genes, respectively. Additionally, a non-template control for each gene was added.

Table 3: Primer sequences for gene expression quantification by qRT-PCR (Eurogentec).

Genes	**Forward Primer sequence 5'-3'**	**Reverse Primer sequence 3'-5'**
MUC2	CAG-CAC-CGA-TTG-CTG-AGT-TG	GCT-GGT-CAT-CTC-AAT-GGC-AG
GAPDH	GGA-GTC-CAC-TGG-CGT-CTT-CAC	GAG-GCA-TTG-CTG-ATG-ATC-TTG-AGG
*ACT*β	CTG-GAA-CGG-TGA-AGG-TGA-CA	AAG-GGA-CTT-CCT-GTA-ACA-ATG-CA
ZO1	CGG-TCC-TCT-GAG-CCT-GTA-AG	GGA-TCT-ACA-TGC-GAC-GAC-AA

The obtained mean Ct (cycle threshold) values of the QuantStudio™ are used to calculate the ΔCT and ΔΔCT values. The ΔCT is the normalisation of the Ct value on the Ct value of the housekeeping gene(s) and is calculated using the following formula:

$$\Delta\mathrm{CT} = Ct_{gene\ of\ interest} - Ct_{housekeeping\ genes}$$

where $Ct_{gene\ of\ interest}$ is the mean Ct value of the technical replicates of the gene of interest of the qPCR run. $Ct_{housekeeping\ gene(s)}$ is the geometric mean of the Ct value of the housekeeping genes of analysed on the same qPCR run.

When a certain treatment is compared to the blank/ control condition, then the relative gene expression is calculated using the $2^{-\Delta\Delta CT}$ method [164]. $\Delta\Delta CT$ is calculated as follows:

$$\Delta\Delta CT = \Delta CT_{treatment} - \Delta CT_{control}$$

The ΔΔCT value enables the assessment of gene expression relative to the control condition. The $\Delta CT_{treatment}$ is the difference in Ct value between the gene of interest in the treated condition and the housekeeping genes in the same treated condition. The $\Delta CT_{control}$ is the difference in Ct value between the gene of interest in the control condition and the housekeeping genes in the control condition.

If $2^{-\Delta\Delta CT} > 1$ then the gene in the treated condition is expressed more than the gene in the control condition. And the opposite is true for $2^{-\Delta\Delta CT} < 1$.

2.5. Statistics

Statistics were applied in this work to test the technical reproducibility of the following measurements: (i) the barrier integrity assessed by TEER, (ii) the permeability analysed by Lucifer Yellow assay, and (iii) the gene expression evaluated by qPCR. The null hypothesis considered no difference in variance. The Shapiro-Wilk test was used to check for normality of the residuals and Levene's test to examine the homogeneity of variances across different groups. These tests were performed in RStudio using the following packages: readxl, car, and dplyr.

2.6. Integration of A.I. tools

For this work, available Artificial Intelligence (AI) tools, such as ChatGPT and Copilot, were used (i) to enhance and correct R.studio code, (ii) for correcting and improving grammar and vocabulary of the text, and (iii) to have a preliminary search of available scientific articles.

CHAPTER 3.
RESULTS

This chapter first discusses the optimization and characterisation of the *in vitro* cell models, followed by their application to study Host-Microbiota-Interaction (HMI) in both health and disease conditions.

The optimization and characterisation cover the optimization of different membrane coating approaches, the comparison of different goblet-like cell lines, and the inclusion of macrophages-like and fibroblast cell lines to the *in vitro* model. The HMI applications involve the analysis of the barrier integrity, permeability, *ZO-1* gene expression, and *MUC2* gene expression when: (i) testing the effect of complex microbial communities related to health and disease (Short Bowel Syndrome); (ii) assessing the stimulation with secondary bile acids; and (iii) studying the host-bile-bacteria dialogue through the stimulation of the cell model with a known bacterium, *Clostridium leptum*, producing bile acids.

3.1. Technical reproducibility of the used methods

This section aims to verify the technical reproducibility of the experiments of barrier integrity, permeability and qPCR as an additional control for interpretation throughout the results of this work. The technical reproducibility of the performed assays between experiments was statistically checked. The null hypothesis considered no difference in variance.

For the barrier integrity, the TEER values did not show a significant difference in variance ($p = 0.6154$) testing 8 technical replicates over 3 different timepoints. Neither the Lucifer Yellow assay showed a significant difference in variance ($p = 0.2349$) testing the apparent permeability (P_{app}) of 8 technical replicates over 3 different timepoints. Likewise, the technical reproducibility of the q-RT-PCR was confirmed ($p = 0.3338$) by testing the difference in variance of the CT values of 3 technical replicates over 8 different conditions.

3.2. Optimization & Characterization of the cell models

3.2.1. Difference in collagen coating

Different collagen coating conditions were tested to assess the effect on the epithelial cell layer, in particular on the barrier integrity and permeability measuring respectively the Trans Epithelial Electrical Resistances (TEER) and the fluorescence intensity of the Lucifer Yellow (LY) assay. Two conditions were tested before seeding the cells on the Transwell insert membrane: incubation of collagen coating at 4°C overnight and at room temperature overnight. The triple cell model (Caco-2:LS174T:NCI-H716 with ratio 89:10:1) differentiated during 21 days (DIV21 = 21 days *in vitro*) and at three timepoints the barrier integrity and permeability was analysed (Figure 11).

Comparing the barrier integrity at the beginning of the differentiation period (DIV7), the 4°C model shows a higher TEER than the room temperature model: respectively 282.54 ± 85.35 Ω·cm² and 81.84 ± 50.20 Ω·cm². At the end of the differentiation period (DIV21) there is only a minor difference in TEER value, namely 90.15 ± 12.09 Ω·cm² for the 4°C model and 109.67 ± 19.14 Ω·cm² for the room temperature model. Thus, the collagen coating has more impact at the beginning then at the end of differentiation of the epithelial cell layer. Although, the technical variability is rather high, so more biological replicates are needed to confirm this data.

Coherently, by comparing both collagen incubations at the start and end point of the differentiation period of the cell layer, the difference in apparent permeability apical to basal (P_{app} AB) is lower at DIV21 than DIV7. For DIV7 the P_{app} AB of the 4°C model is (46.98 ± 67.14)·10^{-7} cm/s, while at room temperature it is (305.01 ± 249.59)·10^{-7} cm/s. At DIV21 the P_{app} AB values are (33.80 ± 3.46)·10^{-7} cm/s and (122.87 ± 159.54)·10^{-7} for 4°C and room temperature respectively.

For the next cell models it was opted to perform the collagen incubation at 37°C for 2 hours, which is comparable to the conditions at room temperature over night, but with reduced temperature fluctuations.

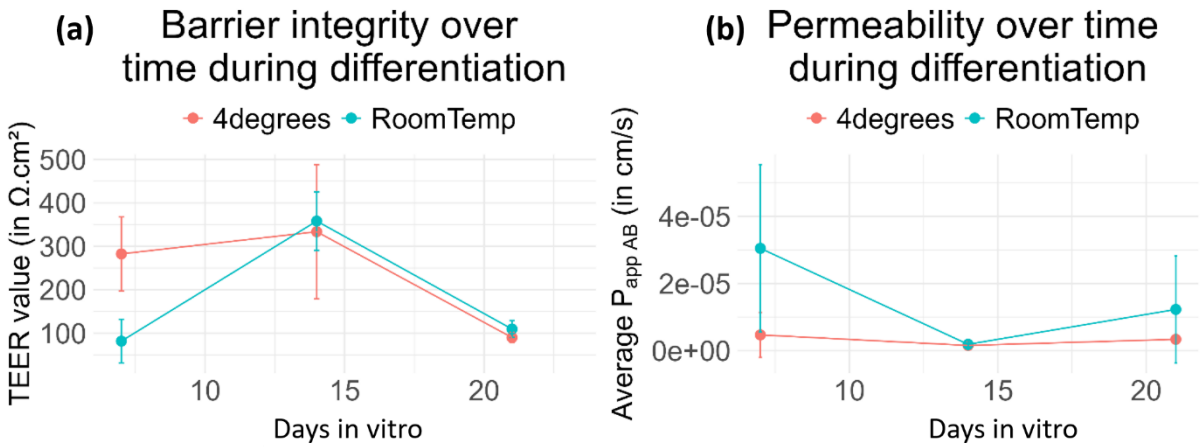

Figure 11: The barrier integrity (a) and permeability (b) of triple cell models over a differentiation period of 21 days. Two collagen coating conditions are compared: incubation over night at 4°C (red) and incubation over night at room temperature (blue). The error bars represent the technical variability (n = 3).

3.2.2. Comparing goblet-like cell lines: HT19-MTX-E12 and LS174T

HT29-MTX-E12 and LS174T are both goblet-like cell lines used in intestinal epithelium *in vitro* models [145, 165]. The difference in morphology of triple models, using either HT29-MTX-E12 or LS174T as goblet-like cells, is shown on the microscopic images of Figure 12. The evolution over time during differentiation is shown for both cell type models, with each two technical replicates. The images show that the models with HT29-MTX-E12 grow as a structured monolayer, while the LS174T model forms dome-like structures (indicated by arrows on Figure 12).

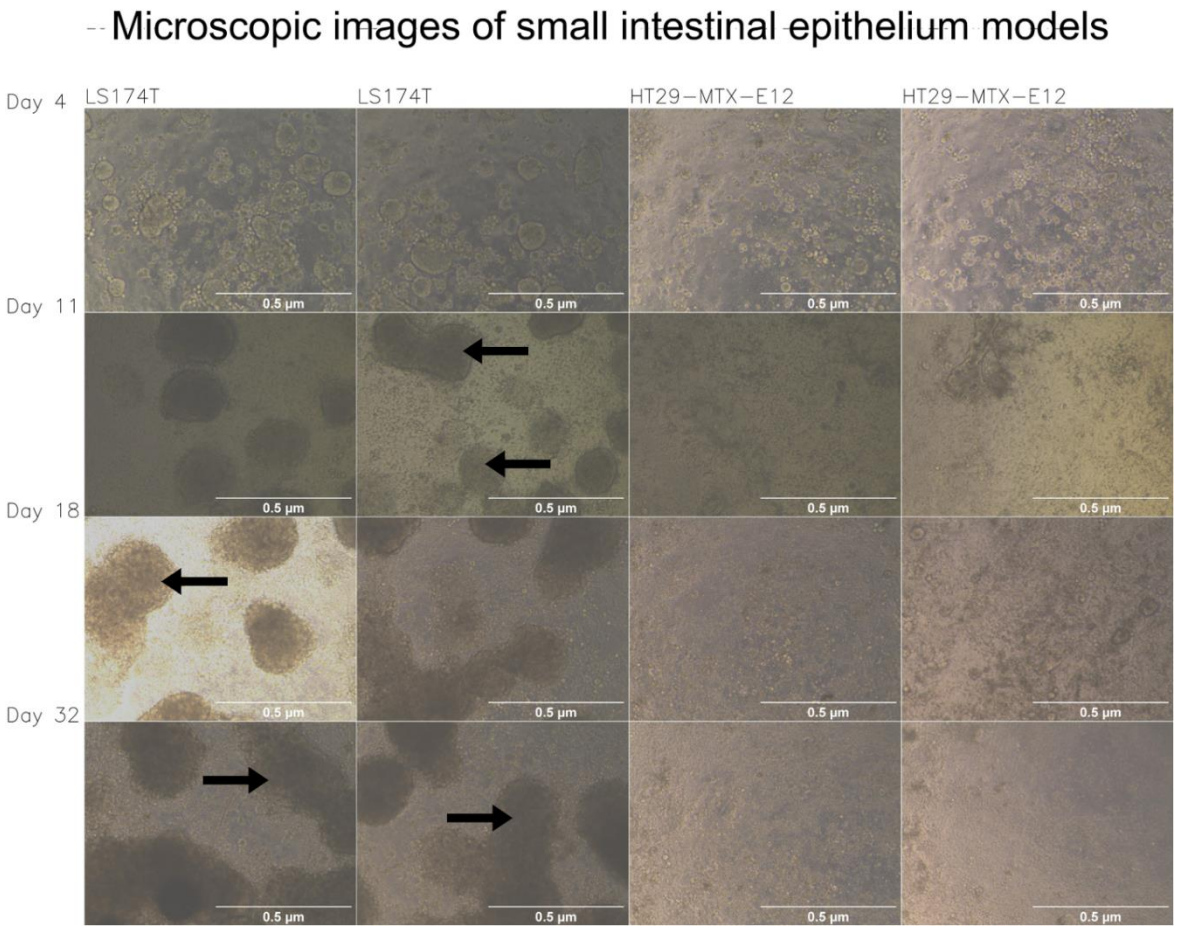

Figure 12: Light microscopy images showing the morphology of a triple small intestinal model (Caco-2:goblet:NCI-H176 with seeding ratio 89:10:1). Either HT29-MTX-E12 or LS174T cells were used as goblet-like cells, over a differentiation period of 32 days in technical duplicate (n = 2). Arrows indicate the dome structures of the triple model including LS174T cells.

The *MUC2* gene expression and *ZO1* gene expression for a double cell model, including Caco-2 and either one of the goblet-like cell lines (seeding ratio 90:10), was analysed by qPCR after 21 days of differentiation. Figure 13a shows the ΔCT value for *MUC2* relative to the housekeeping genes. The model including HT29-MTX-E12 shows a higher ΔCT value for *MUC2*, hence the *MUC2* expression in this experimental condition is lower than what is observed for a similar small intestinal cell model including LS174T. In contrast, Figure 13b indicates that the *ZO1* expression is higher for the model including HT29-MTX-E12, but with a less substantial difference.

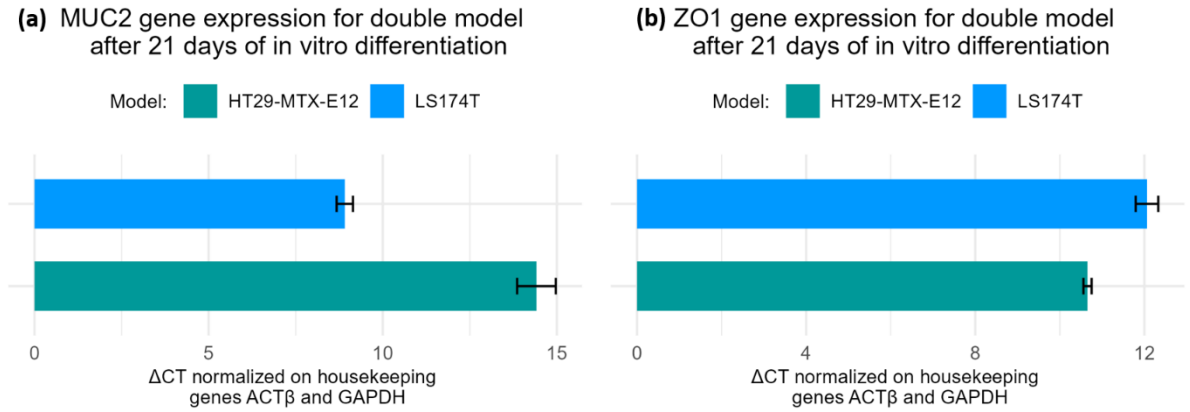

Figure 13*:* The gene expression of (a) *MUC2* and (b) *ZO1* for model of Caco2 and either HT29-MTX-E12 or LS174T with seeding ratio 90:10. The ΔCT values represent the gene expression of the cell models after 21 days of differentiation. The error bars show the technical variability (n = 2).

The double model shown in Figure 13 was further adapted to include NCI-H716 as enteroendocrine-like cells. These triple cell models are seeded in ratio of 89:10:1 for respectively Caco-2, goblet-like cells and NCI-H716. The barrier integrity, permeability, IL-8 secretion, *MUC2* gene expression and *ZO1* gene expression was characterized for multiple triple cell models, either with LS174T or HT29-MTX-E12 as goblet-like cell line. The results of those triple small intestinal models are shown in Figure 14, and Figure 15.

In Figure 14c the barrier integrity of a triple model with **LS174T** as goblet-like cell line is shown for two biological replicates. Both replicates show a similar decreasing trend, but with other TEER values. For the first biological replicate (orange), the barrier integrity decreases from (110.80 ± 1.75) Ω·cm² at the beginning of the differentiation period, to (72.44 ± 2.10)Ω·cm² at the middle and (56.43 ± 0.23)Ω·cm² at the end. For the second biological replicate (green) the barrier integrity starts at a similar value of (98.27 ± 18.85)Ω·cm² at the beginning of the differentiation period, but decreases to (17.79 ± 1.76)Ω·cm² at the middle and even to (6.27 ± 1.73)Ω·cm² at the end.

Coherently, the permeability for this triple models with LS174T increase over time for both biological replicates (Figure 14d). At the beginning and middle of the differentiation period, the average P_{app} AB is similar for both replicates, namely at the beginning $(22.93 \pm 1.75)\cdot 10^{-7}$ cm/s for replicate 1 and $(55.64 \pm 46.23)\cdot 10^{-7}$ cm/s for replicate 2; and at the middle of the differentiation period $(50.87 \pm 1.07)\cdot 10^{-7}$ for replicate 1 and $(60.15 \pm 22.77)\cdot 10^{-7}$ cm/s for replicate 2. At the end of the differentiation period the second biological replicate (green) shows a higher P_{app} AB of $(179.89 \pm 33.23)\cdot 10^{-7}$ cm/s compared to $(71.13 \pm 2.42)\cdot 10^{-7}$ cm/s for the first biological replicate (orange). This difference in permeability between the biological replicates at the end of the differentiation period is in line with the difference in barrier integrity.

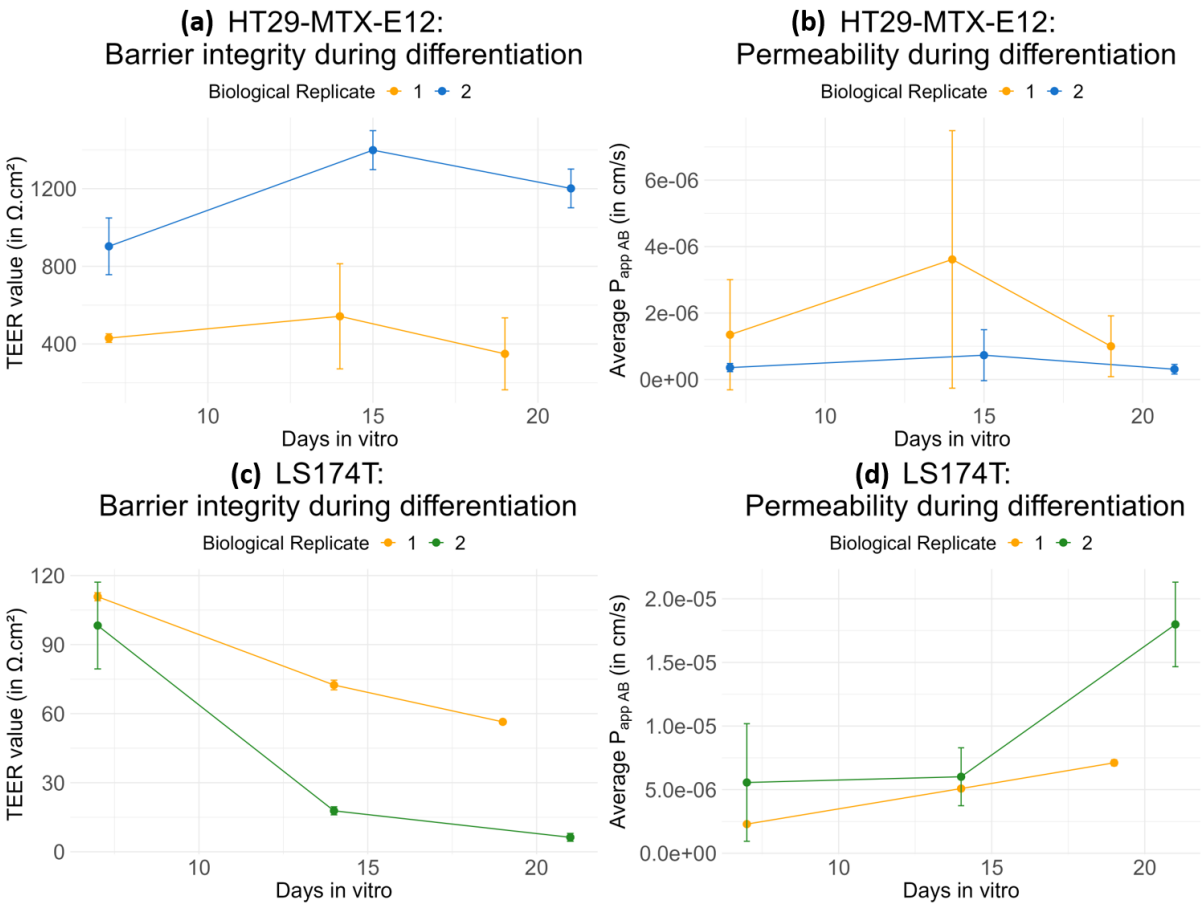

Figure 14: The barrier integrity (a and c) and permeability (b and d) during differentiation of small intestinal triple models, with either HT29-MTX-E12 (a and b) or LS174T (c and d) as goblet-like cells. The error bars represent the standard deviations of the technical replicates of the wells (n = 2, n = 8 and n = 10 for the orange, green, and blue datapoints respectively).

Overall, the triple models with **HT29-MTX-E12** as goblet-like cells, shown in Figure 14a and Figure 14b, display a higher technical variability for both the barrier integrity and permeability compared to the previously discussed triple model with LS174T cells. The biological replicates of the HT29-MTX-E12 models show a similar progress over time, namely an increase followed by a decrease for both the barrier integrity as the permeability.

The barrier integrity of the first biological replicate (orange) evolves from (429.99 ± 22.17) Ω·cm² at the beginning, to (542.36 ± 270.91)Ω·cm² at the middle, and (348.89 ± 185.39) Ω·cm² at the end of the differentiation period. The second biological replicate (blue) has the same progress but has higher TEER values: at the beginning a value of (903.06 ± 146.14)Ω·cm², increases at the middle of the period up to (1398.67 ± 100.33)Ω·cm² and then decreases to (1201.36 ± 99.78)Ω·cm² at the end.

The permeability at the beginning and end of the differentiation period remains similar for the HT29-MTX-E12 model for both biological replicates: biological replicate 1 (orange) starts at $(13.473 \pm 16.58)\cdot10^{-7}$ cm/s on DIV7, and ends at $(10.00 \pm 9.15)\cdot10^{-7}$ cm/s on DIV21; biological replicate 2 (blue) starts at $(3.59 \pm 1.24)\cdot10^{-7}$ cm/s on DIV7 and ends at $(3.09 \pm 1.45)\cdot10^{-7}$ cm/s on DIV21. This is different from the LS174T models for which the permeability keeps increasing during the 21 days of differentiation, and for which the P_{app} AB values already starts at a higher value on DIV7.

The **relative gene expression** levels of *MUC2* and *ZO1* of cell models including either HT29-MTX-E12 or LS174T cell line was measured by qPCR. The ΔCT values, relative to the housekeeping genes *ACT*β and *GAPDH*, are visualized in Figure 15.

Figure 15a shows the gene expression level of a triple model with LS174T for *MUC2* and *ZO1* after 22 days of differentiation. The gene expression of *MUC2* has a ΔCT value of 10.86 ± 0.17 and for *ZO1* a value of 12.33 ± 0.12, which means that there is slightly more *MUC2* expression than *ZO1.* Figure 15b shows the gene expression level of a triple model with HT29-MTX-E12 for *MUC2* and *ZO1* after 31 days of differentiation. The gene expression of *MUC2* has a ΔCT value of 15.40 ± 0.48 and for *ZO1* a value of 8.87 ± 0.30, which means there is more *ZO1* expression than *MUC2*.

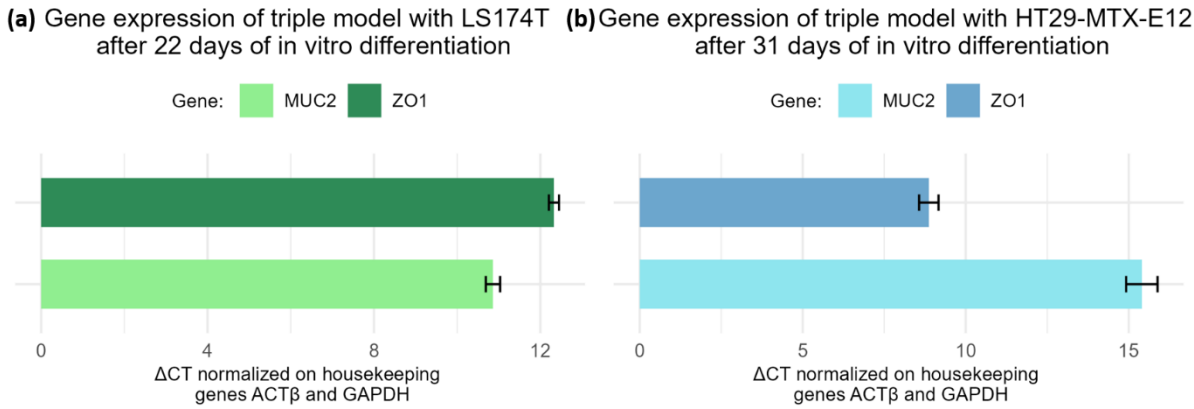

Figure 15: The gene expression of *MUC2* and *ZO1* for triple models with either (a) LS174T or (b) HT29-MTX-E12 as goblet-like cells. The ΔCT values represent the gene expression of the cell models after 21 days for the LS174T model and after 31 days for the HT29-MTX-E12 model. The error bars show the technical variability (n = 2).

3.2.3. Inclusion of an immune compartment

To increase the relevance of the cell model for host-bacteria interaction studies, the addition of **THP-1 cells, seeded at the basal side of the Transwell insert,** was investigated to simulate the immune compartment of the *in vivo* situation (Figure 9A).

The modulation of barrier integrity by the macrophage differentiation through PMA stimulation and of their activation through LPS polarization is shown in Figure 16a and Figure 16b for either a triple cell model with HT29-MTX-E12 as goblet-like cells or LS174T. For PMA stimulation also the secretion of IL-8 cytokine at the apical and basal compartment was analysed (Figure 16c and Figure 16d).

The barrier integrity increased when THP-1 cells were differentiated into macrophages (Figure 16a), and decrease when the macrophages were activated (Figure 16b), for both cell models. However, the HT29-MTX-E12 model showed a higher increase upon PMA stimulation than the model with LS174T: (59.42 ± 26.17)% compared to (13.16 ± 8.28)%. A similar decrease for both model types was observed upon LPS polarization, but with a higher variability for the HT29-MTX-E12 model: decrease of (13.75 ± 63.56)% for HT29-MTX-E12 and (13.83 ± 6.73)% for LS174T.

For both model types, the secretion of IL-8 cytokine decreased after the stimulation of PMA in both the apical and basal compartments. In the apical compartment the decrease is similar for both model types: (55.09 ± 4.59)% for HT29-MTX-E12 and (62.42 ± 5.17)% for LS174T model. At the basal compartment, the HT29-MTX-E12 model displays a higher decrease of (79.50 ± 3.38)% in secreted IL-8 cytokine, compared to (54.20 ± 12.69)% for the LS174T model.

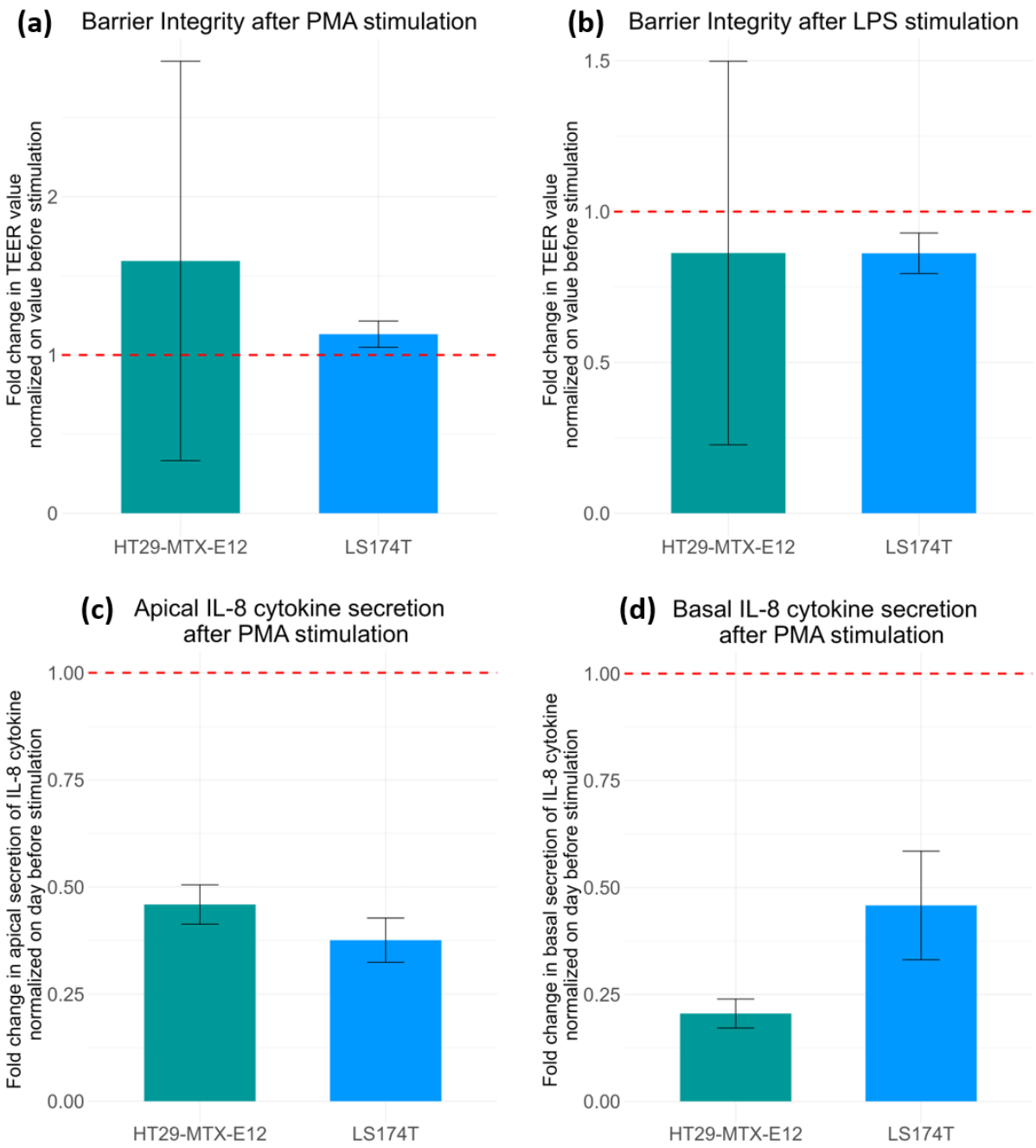

Figure 16: The difference in effect of stimulating a triple cell model with either HT29-MTX-E12 cells or LS174T upon stimulation of THP-1 cells with PMA to differentiate them into macrophages and the macrophage activation by LPS polarization. The measurements are normalized on the measurements of the day before stimulation. The error bars represent the technical variability (n = 2).

The **IL-8 cytokine secretion** of cell models including THP-1 cells and either HT29-MTX-E12 or LS174T cell lines was quantified by ELISA, both in the apical as the basal compartment of the Transwell. Figure **17** shows the box plots for the apical and basal secretion. At the apical compartment, an increase in IL-8 cytokine secretion is observed overtime in both cell models with higher concentrations measured for the one including LS174T cells: at DIV7 of differentiation (648.12 ± 163.37)pg/mL for HT29-MTX-E12 and (1074.04 ± NA)pg/mL for LS174T; at DIV14 (243.63 ± 90.38)pg/mL for HT29-MTX-E12 and (917.12 ± 161.19)pg/mL for LS174T; and at DIV20 (3449.55 ± 270.32)pg/mL for HT29-MTX-E12 and (7253.36 ± 385.99)pg/mL for LS174T.

At the basal compartment the IL-8 cytokine secretion is in the same order for HT29-MTX-E12 and LS174T at DIV7 and DIV14, namely (261.92 ± 136.84)pg/mL and (219.09 ± 163.55)pg/mL for HT29-MTX-E12 and (231.61 ± NA)pg/mL and (219.09 ± 163.55)pg/mL for LS174T. Yet, at DIV20 there is almost twice as much secretion of IL-8 cytokines quantified in the model with HT29-MTX-E12 than LS174T cells: (5890.51 ± 681.94)pg/mL compared to (3156.28 ± 503.09)pg/mL.

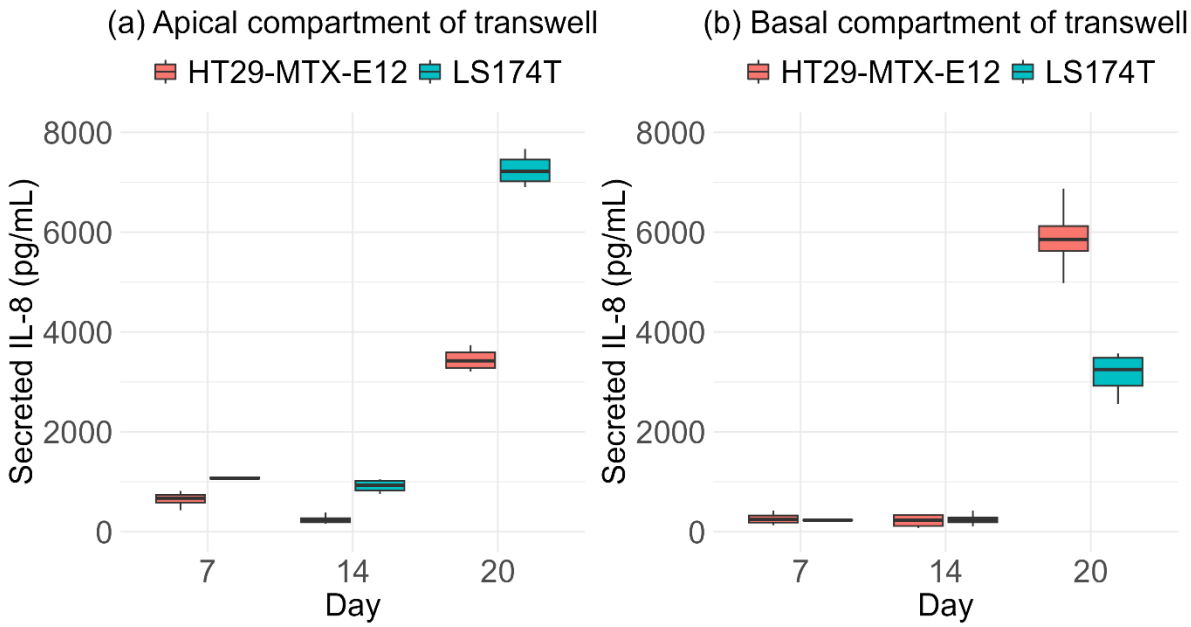

Figure 17: Secreted IL-8 cytokines from the (a) apical and (b) basal compartments of the triple co-culture models including either HT29-MTX-E12 (red) or LS174T (blue) cell lines as model for goblet cells, quantified by ELISA assay. Error bars indicate the technical variability between the Transwells (n = 2).

A next experiment incorporated **THP-1 cells, seeded at the bottom of the well-plate** instead of at the basal side of the Transwell insert (Figure 9B), were differentiated into macrophages following the protocol described in the material and methods chapter. The differentiated THP-1 cells were added to a triple model including Caco2, HT29-MTX-E12 and NCI-H716 cells, on day 21. Figure 18 shows no evident change in barrier integrity, while the average permeability doubles by adding the macrophages to the cell model. The average TEER value was 1201.36 ± 99.78 Ω·cm² before adding the macrophages and 1156.06 ± 139.08 Ω·cm² after addition of the macrophages. Yet, the average permeability showed a drastic increase after the macrophage differentiation: it doubled from $(3.09 \pm 1.45) \cdot 10^{-7}$ cm/s to $(6.60 \pm 3.57) \cdot 10^{-7}$ cm/s.

After those barrier integrity and permeability measurements, the cell model with the macrophages was successfully cultured for additional ten days and the macrophage heterogeneity was monitored using the incucyte (Figure 19).

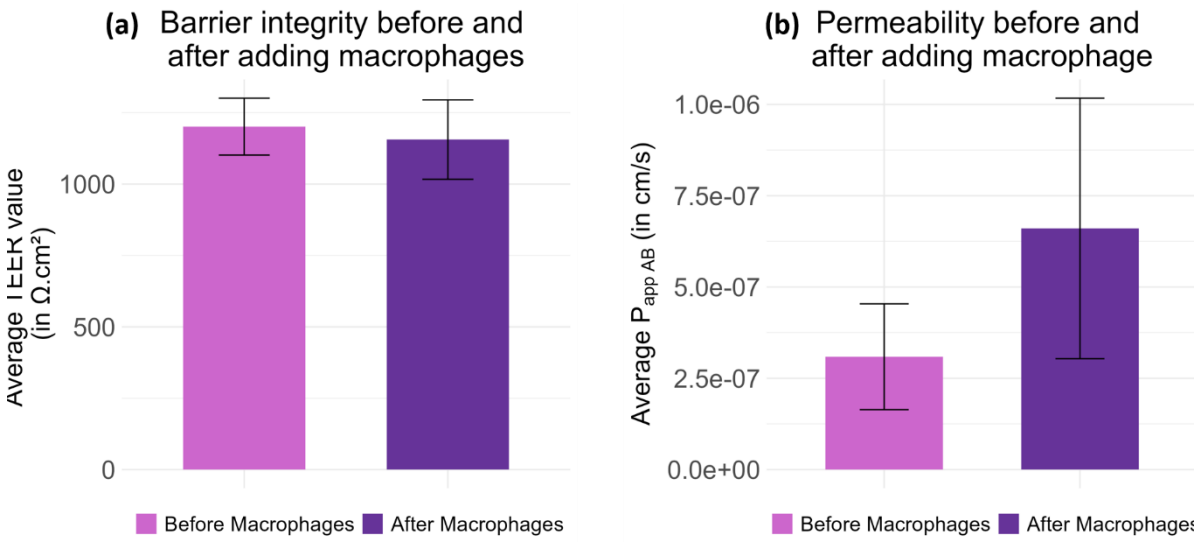

Figure 18: The barrier integrity (a) and permeability (b) before and after the addition of macrophages to a small intestinal model with HT29-MTX-E12 as goblet-like cell line. The error bars represent the technical variability of the wells (n = 10).

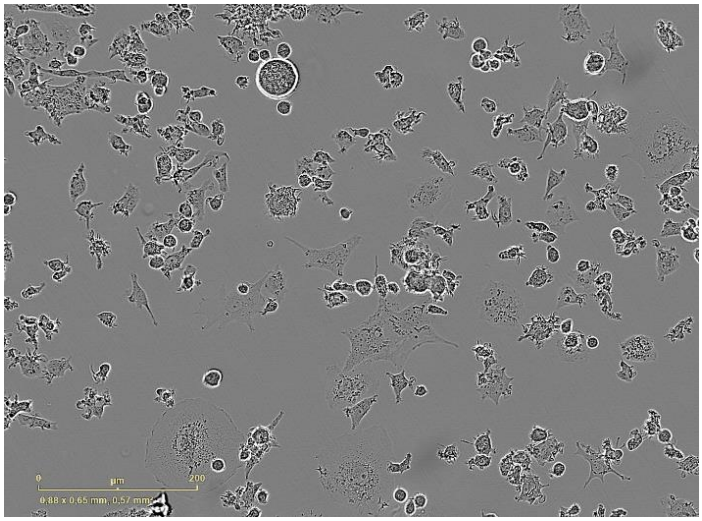

Figure 19: Representative incucyte image of the heterogeneity of macrophages. THP-1 cells, seeded at the bottom of a well, were stimulated with PMA and differentiated for 2 days before adding to the triple model.

3.2.4. Addition of fibroblast cells and evaluation of NCI-H716 adherence

The use of Matrigel coating compared to the previously described collagen was tested to check the impact on the barrier integrity, permeability and adherence capacity of NCI-H716 cells [166]. Additionally, the impact on cell adherence was tested, by the addition of either fibroblast cell line (CCD-18Co) or fibroblast supernatant cells.

In Figure 20 four different conditions of small intestinal models are represented: (i) Transwell coating with collagen and the addition of fibroblast cell layer ("Fibroblast"); (ii) Transwell coating with collagen and using the fibroblasts' supernatants as culture medium ("Supernatant Fibroblast"); (iii) Transwell coating with Matrigel ("Matrigel"); and (iv) Transwell coating with collagen ("DMEM") served as control.

The **barrier integrity** of the DMEM, Matrigel and Supernatant Fibroblast models has the same descending trend over the differentiation period of 21 days (Figure 20a). The Fibroblast model shows a more stable barrier integrity over time, with only a variation of approximately 10% over time, and almost no difference in barrier integrity comparing the first and last measurement: 166.60 ± 5.15 Ω·cm² and 163.52 ± 3.96 Ω·cm². Compared to the Fibroblast model, at the beginning of differentiation, the other 3 conditions have an higher average TEER value: 918.12 ± 59.79 Ω·cm² for DMEM, 512.40 ± 8.71 Ω·cm² for Matrigel and 948.08 ± 16.63 Ω·cm² for Supernatant Fibroblast. At DIV22 of differentiation, the TEER value drops more than 60% to respectively (310.52 ± 25.74) Ω·cm², 191.52 ± 7.92 Ω·cm² and 308.28 ± 4.36 Ω·cm². Even if the same decreasing trend for the fold change in TEER value is observed, at all timepoints the TEER value (in Ω·cm²) was twice as high for the collagen coated condition compared to the Matrigel coated condition.

Figure 20b displays the **permeability** for the four conditions. By rescaling the y-axis Figure 20c provides a clearer view of the evolution during differentiation for "DMEM" and "Fibroblast". In this rescaled graph it is visible that the permeability of the Fibroblast model slightly increases during the differentiation of 22 days: $(45.71 \pm 1.86)\cdot10^{-7}$ cm/s at the beginning, $(61.34 \pm 3.07)\cdot10^{-7}$ cm/s at the middle, and $(68.06 \pm 5.54)\cdot10^{-7}$ cm/s at the end. The DMEM model also shows a gradual increase: $(3.57 \pm 0.23)\cdot10^{-7}$ cm/s at the beginning, $(7.68 \pm 0.38)\cdot10^{-7}$ cm/s at the middle and $(15.95 \pm 0.02)\cdot10^{-7}$ cm/s at the end of the differentiation period. The Matrigel and Supernatant Fibroblast show a similar trend. At the beginning and the middle of the differentiation period the P_{app} AB remains stable, whilst it increases substantially at the end. The permeability of the Matrigel condition starts at $(7.10 \pm 0.10)\cdot10^{-7}$ cm/s, is $(17.59 \pm 0.82)\cdot10^{-7}$ cm/s at the middle and notably increases to a level of $(1333.24 \pm 58.66)\cdot10^{-7}$ cm/s at the end. Similarly, the Supernatant Fibroblast starts at $(4.71 \pm 1.41)\cdot10^{-7}$ cm/s, is $(7.78 \pm 0.63)\cdot10^{-7}$ cm/s at the middle, and increase to $(1302.93 \pm 8.21)\cdot10^{-7}$ cm/s at the end.

The secretion of **glucagon-like peptide-1 (GLP-1)** was assessed for these 4 conditions (DMEM, Fibroblast, Matrigel and Supernatant Fibroblast). However, the detection limit of the GLP-1 ELISA kit was not sensitive enough for our models. Therefore, no data about the GLP-1 secretion was obtained.

In addition, Figure 21 shows the difference in adherence of NCI-H716 cells between wells coated with collagen and Matrigel. The adherence of the cells seeded on the collagen coated well (Figure 21 B) is comparable to the uncoated wells (Figure 21A), whilst the Matrigel coating (Figure 21C) displays apparent more adherence of NCI-H716.

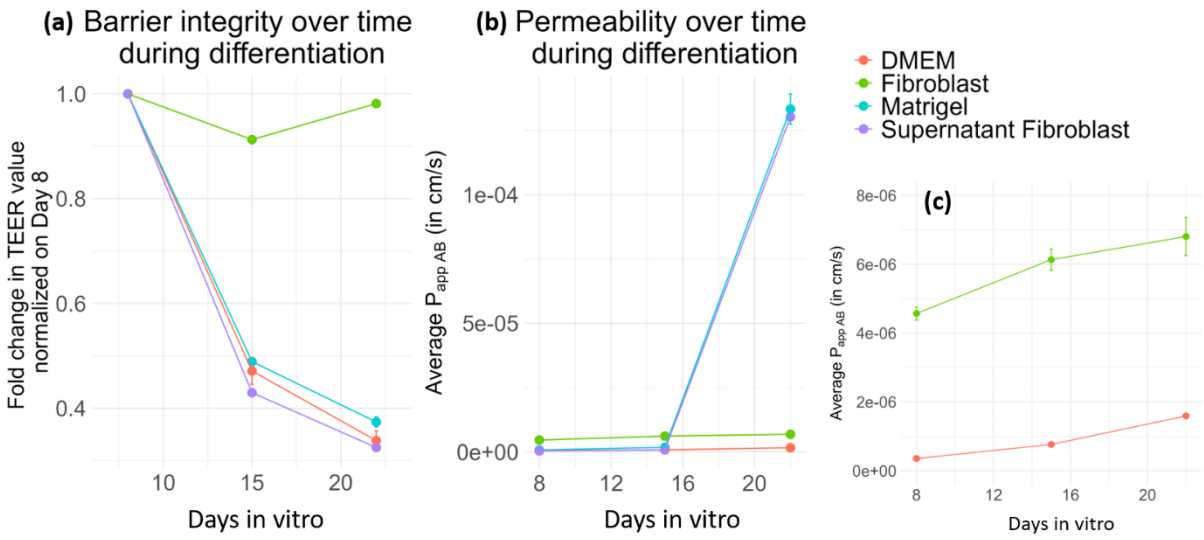

Figure 20: The barrier integrity (a) and permeability (b) of small intestinal models over a differentiation period of 21 days. Plot (c) is the same as (b) but with a zoomed y-axis. This figure compares the addition of a fibroblast cell layer (green), using the supernatant of fibroblasts (purple) and coating with Matrigel (blue) to the control with DMEM and collagen coating (orange). The barrier integrity plot datapoints are normalized on the TEER value of day 8. The error bars represent the technical replicates (n = 2).

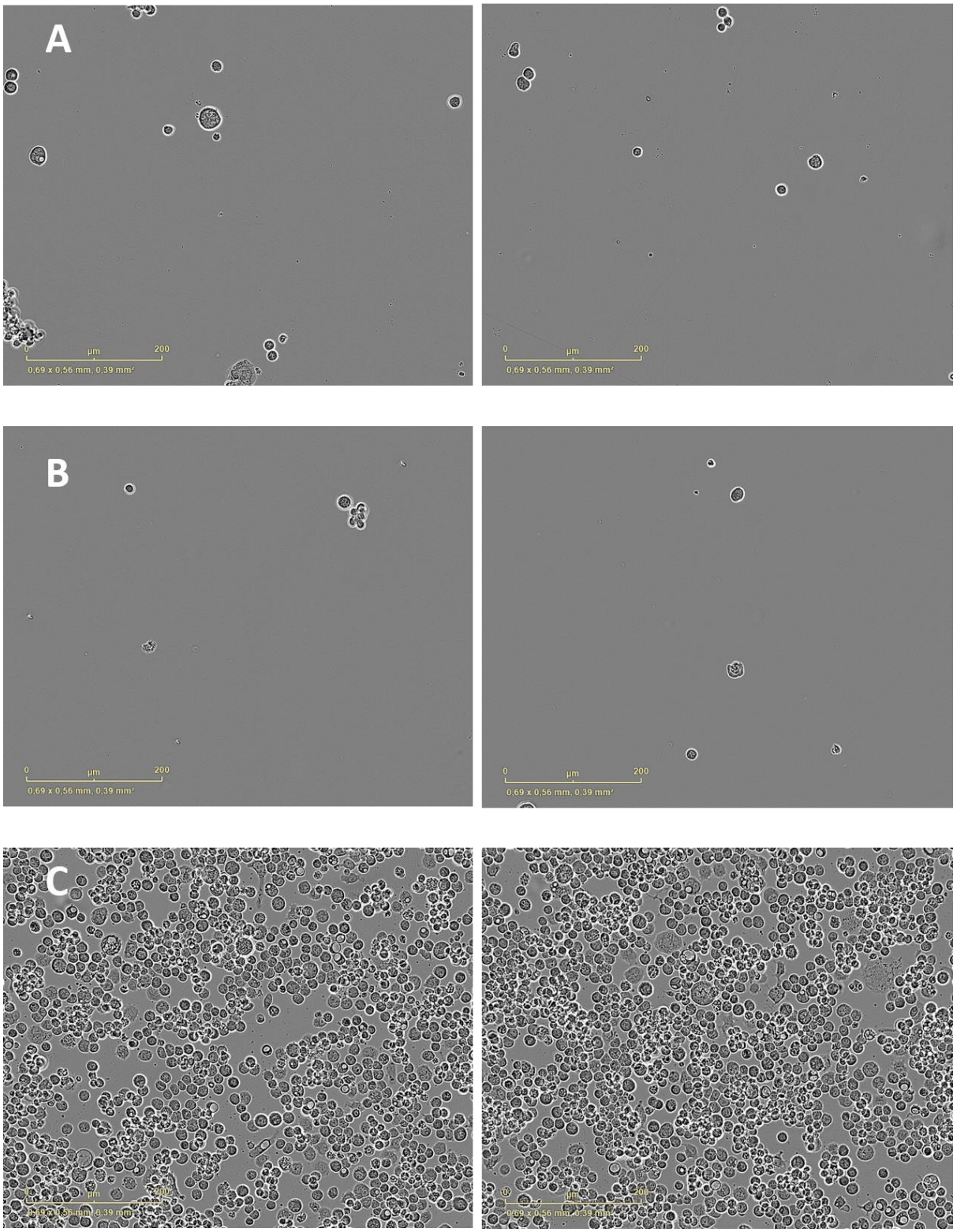

Figure 21: Incucyte images showing the adherence of NCI H716 cell line on (A) uncoated wells (control), (B) wells coated with collagen, and (C) wells coated with Matrigel.

3.2.5. Colon model

In vitro Transwell models for the colon epithelium are already well characterized and described in the literature (and made the object of previous and current projects in the hosting laboratory) [130, 145]. A colon model composed of T84, LS174T and NCI-H716 cell lines (respective seeding ratio of 79:20:1) will be used to investigate the altered host-bacteria interaction of a specific condition, called Short Bowel Syndrome (SBS). For these experiments, 3 biological replicates of a colon triple cell models were cultured over a differentiation period of 21 days. The characterization of those biological replicates is described in this section.

Figure 23a shows the barrier integrity and Figure 23b the permeability of the 3 biological replicates of colon models. The biological replicates follow the same descending trend for the barrier integrity. However, the TEER value of biological replicate 2 increases on day 21 compared to day 14, while the others have a decrease in TEER value. For the permeability, biological replicate 3 shows an increasing trend, while the others increase followed by a decrease.

The gene expression levels of *MUC2* and *ZO1* for three biological replicates of colon models after 22 days of differentiation are shown in **Figure 22**. The average ΔCT for *MUC2* is 12.07 ± 0.14 and for *ZO1* is 14.44 ± 1.29. The biological variability for *ZO1* expression is thus higher than for *MUC2*.

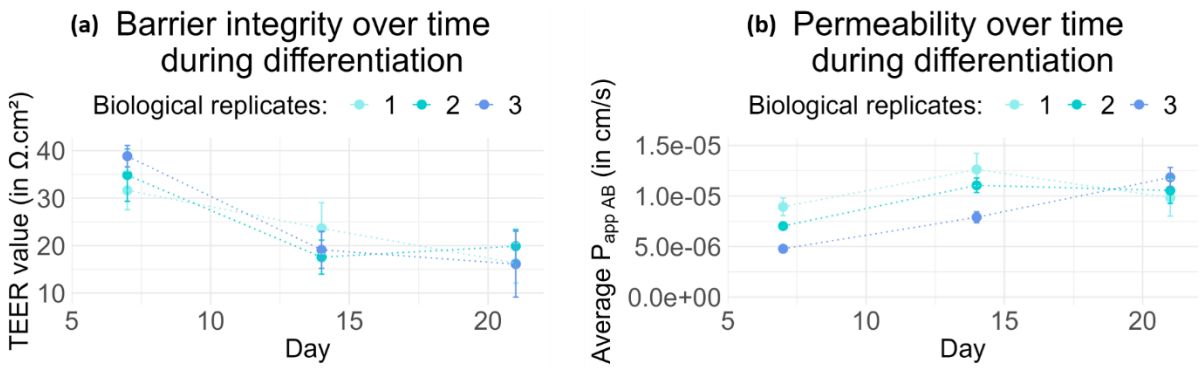

Figure 23: The barrier integrity (a) and permeability (b) of 3 biological replicates of colon models during a differentiation period of 21 days is shown. The error bars show the technical variability (n = 8).

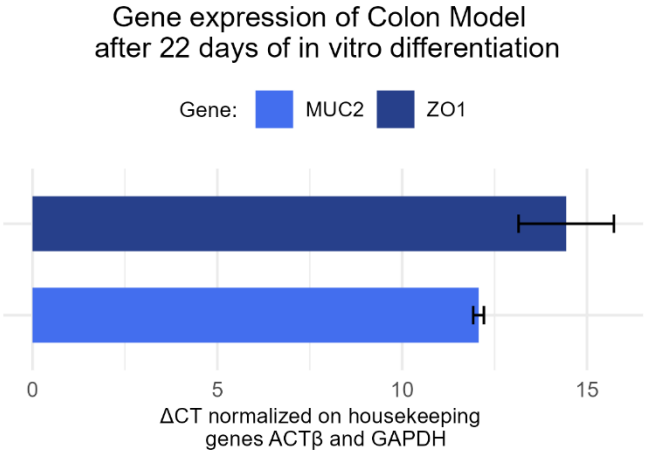

Figure 22: The gene expression levels of *MUC2* and *ZO1* for colon models after 22 days of differentiation. The error bars indicate the biological variability (n = 3).

3.3. Application for Host-Microbiota Interaction (HMI)

3.3.1. Health: pre-SBS bacterial supernatant samples of the small intestine

First, the small intestinal epithelium model was applied to study the host-bacteria interaction in healthy condition. For this purpose, the cell model was stimulated with **supernatant samples of a SHIME run**. SHIME is an acronym for Simulator of the Human Intestinal Microbial Ecosystem. This *in vitro* system mimics the human gastrointestinal tract, including the host-microbiota interactions. The microbiota was derived from *in vivo* faecal samples of human donors. To investigate the impact of bacterial metabolites on the intestinal epithelium, filtered supernatant of the SHIME was used.

In this context, the impact of the SHIME samples on the Proximal Small Intestine (PSI), and Ileum (Ile) was assessed by an incubation of 24 hours. The barrier integrity, permeability, *MUC2* gene expression and *ZO1* gene expression upon stimulation will be assessed (Figure 24 and Figure 25) on a **triple small intestinal model (Caco-2:LS174T:NCI-H716)**.

Compared to the control cell model without any stimulation (Figure 24a), the SHIME medium increased the barrier integrity only for (4.76 ± 0.06)%. Proximal Small Intestine (PSI) and Ileum (Ile) condition decreased the barrier integrity in the order of respectively (9.05 ± 0.43)% and (7.14 ± 0.43)%. Those small changes in barrier integrity are not considered as biologically relevant.

Figure 24b shows a decrease of (15.69 ± 1.61)% in permeability for the SHIME medium compared to the non-stimulated control condition. Taking this decreasing effect of the SHIME medium into account, an increase in permeability of (39.05 ± 3.93)% and (32.19 ± 6.14)% was seen for respectively the PSI and Ile condition.

On the one hand, the SHIME medium induces a decrease in *ZO1* gene expression (Figure 25b). Considering this decrease by the SHIME medium, the bacterial supernatant of the PSI and Ile increased the *ZO1* gene expression by (250 ± 45)% and (60 ± 9)%, respectively.

On the other hand, stimulation with SHIME medium did not induce a change in gene expression for *MUC2* (Figure 25a). Thus, the PSI and Ile microbial supernatant increased the gene expression for respectively (356 ± 61)% and (249 ± 44)%. Although, the technical variability for the PSI condition is considerable high.

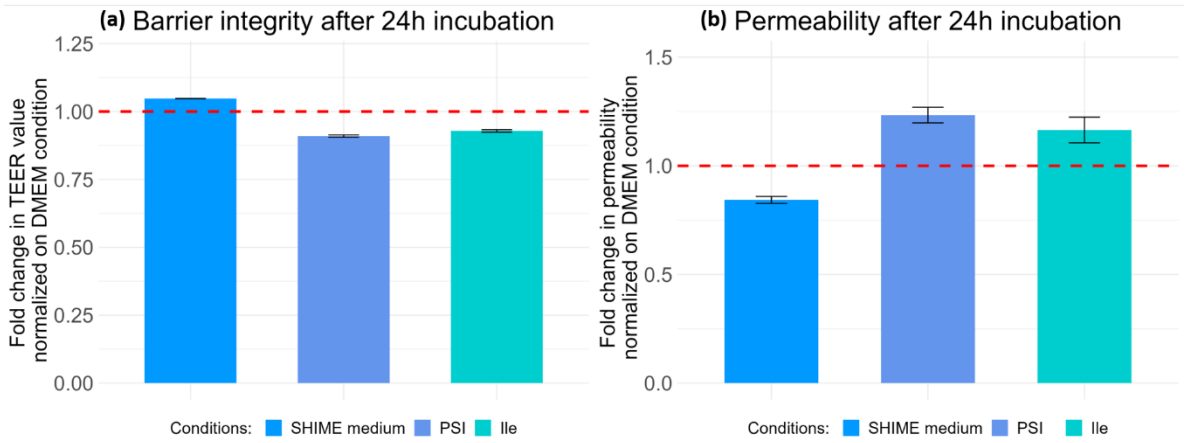

Figure 24: The barrier integrity (a) and permeability (b) of a small intestinal model upon stimulation with complex mixture of microbial supernatant for 24 hours. The conditions are normalized on the control cell model without any stimulation. SHIME medium refers to the medium used during the SHIME run. PSI refers to the proximal small intestine and Ile refers to the ileum compartment. The error bars indicate the technical variability between the wells (n = 2).

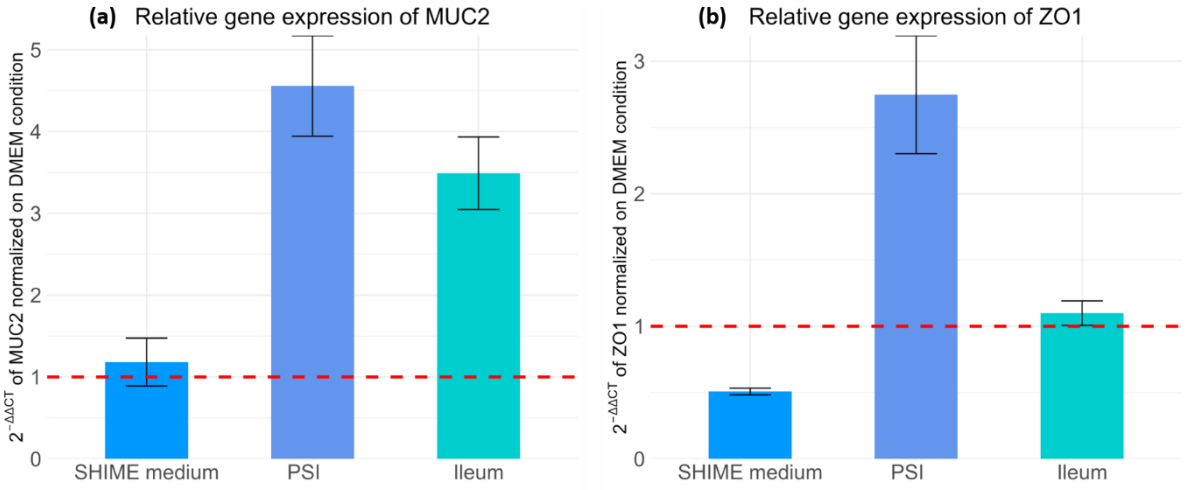

Figure 25: The gene expression level of *MUC2* (a) and *ZO1* (b) in $2^{-\Delta\Delta CT}$ values relative to the non-stimulated condition. SHIME medium refers to the medium used during the SHIME run. PSI refers to the proximal small intestine and Ile refers to the ileum compartment. The error bars indicate the technical variability of the qPCR wells (n = 3).

3.3.2. Stimulation of small intestinal epithelium with bile acids

The complex microbial community tested in section 3.3.1 includes multiple microbial metabolites, probably including secondary bile acids (BAs) produced by the microbiota. To shed light on the importance of this bacterial-derived mediators of host-bacteria dialogue, the effect of two specific **secondary bile acids** was investigated on the **small intestinal model** with either LS174T or HT29-MTX-E12 as goblet-like cells (Caco-2:Goblet:NCI-H716 with ratio 89:10:1) and THP-1 differentiated macrophages at the basal side of the Transwell insert. In particular, the effect of Tauroursodeoxycholic acid (TUDCA, Figure 26) and Lithocholic acid (LCA, Figure 27) was studied on the barrier integrity, the permeability, the apical secretion of IL-8 cytokine, and the basal secretion of IL-8 cytokine.

Upon **TUDCA** stimulation, the barrier integrity (Figure 26a) increased for both models, with a larger increase of (30.98 ± 17.48)% for the HT29-MTX-E12 model, compared to (11.85 ± 4.81)% for the LS174T model. Coherently, a higher decrease in permeability (Figure 26b) of (54.13 ± 16.40)% was observed for the HT29-MTX-E12 model compared to (20.43 ± 4.97)% for the LS174T model.

The secretion of IL-8 cytokine decreased both in the apical (Figure 26c) and the basal (Figure 26d) compartment of the Transwell with a larger decrease for the model with LS174T. The apical secretion of IL-8 cytokine decreased (48.89 ± 10.23)% for the model with HT29-MTX-E12 and (64.37 ± 4.08)% for the model including LS174T. The basal secretion of IL-8 cytokine decreased even more for both models with (54.27 ± 17.19)% and (84.48 ± 2.30)%, respectively for the model with HT29-MTX-E12 and LS174T.

Upon **LCA** stimulation, the barrier integrity (Figure 27a) remains similar for both models with only a decrease of (4.43 ± 51.06)% and (8.29 ± 1.35)% for respectively the model with HT29-MTX-E12 and LS174T, but the former shows a high technical variability. In contrast, the permeability (Figure 27b) increased upon LCA stimulation with (66.69 ± 61.90)% for the model with LS174T and even a higher increase of (821.25 ± 648.93)% for the model with HT29-MTX-E12. The latter exhibits a substantial increase, and both model types demonstrate considerable technical variability, suggesting potential issues with the measurements.

The secretion of IL-8 cytokine at the apical compartment (Figure 27c) upon LCA stimulation increased with (31.15 ± 22.36)% for the model with HT29-MTX-E12 and decreased with (21.71 ± 5.94)% for the model with LS174T. The basal secretion of IL-8 cytokine (Figure 27d) increased with (75.56 ± 81.12)% and (37.30 ± 34.85)% for respectively the HT29-MTX-E12 and LS174T models.

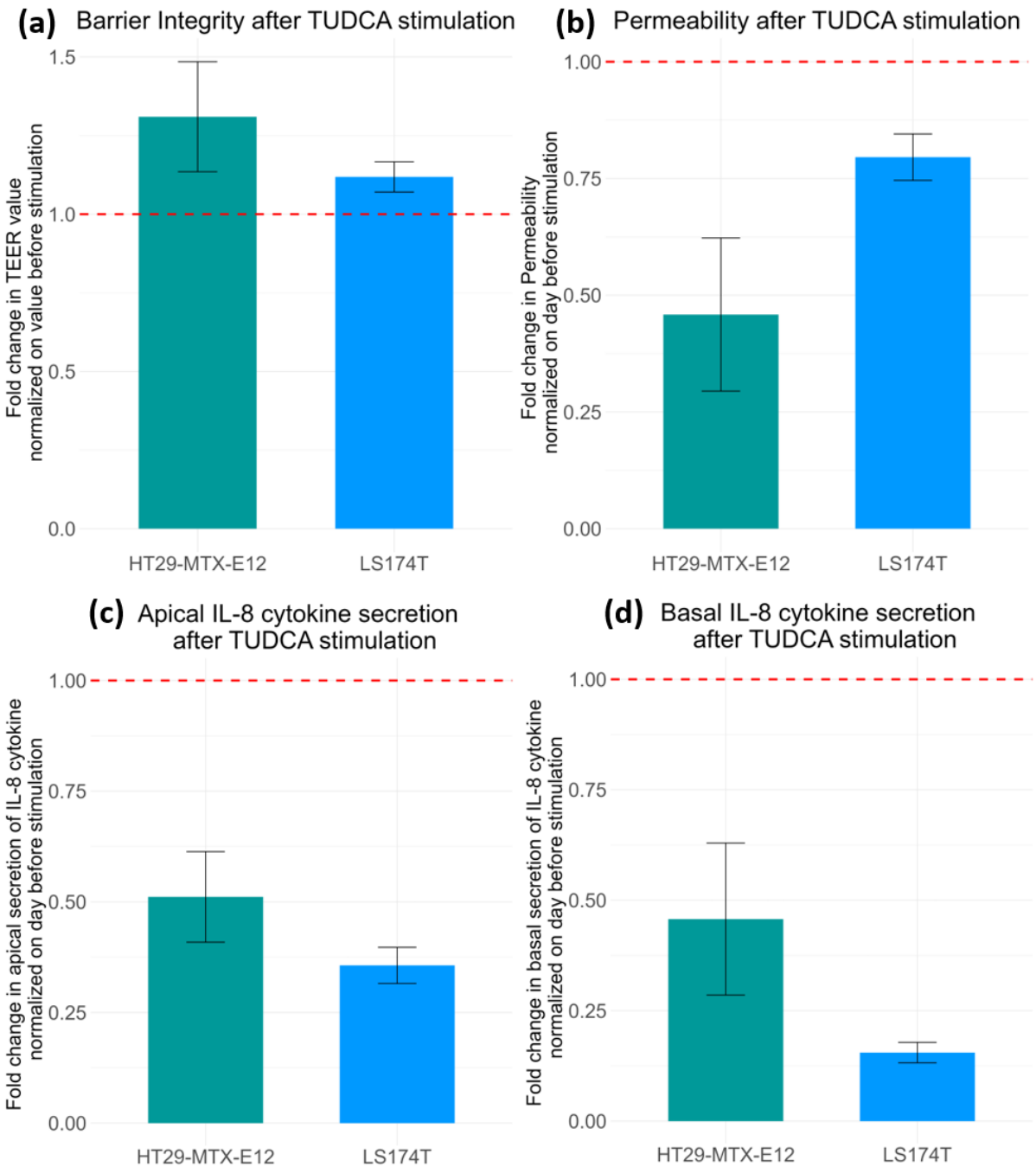

Figure 26: The difference in effect of a triple cell model with either HT29-MTX-E12 cells or LS174T upon **TUDCA** stimulation. The (a) barrier integrity, (b) permeability, (c) apical secretion of IL-8 cytokine, and (d) basal secretion of IL-8 cytokine are normalized on the measurements of the day before stimulation. The error bars represent the technical variability (n = 2).

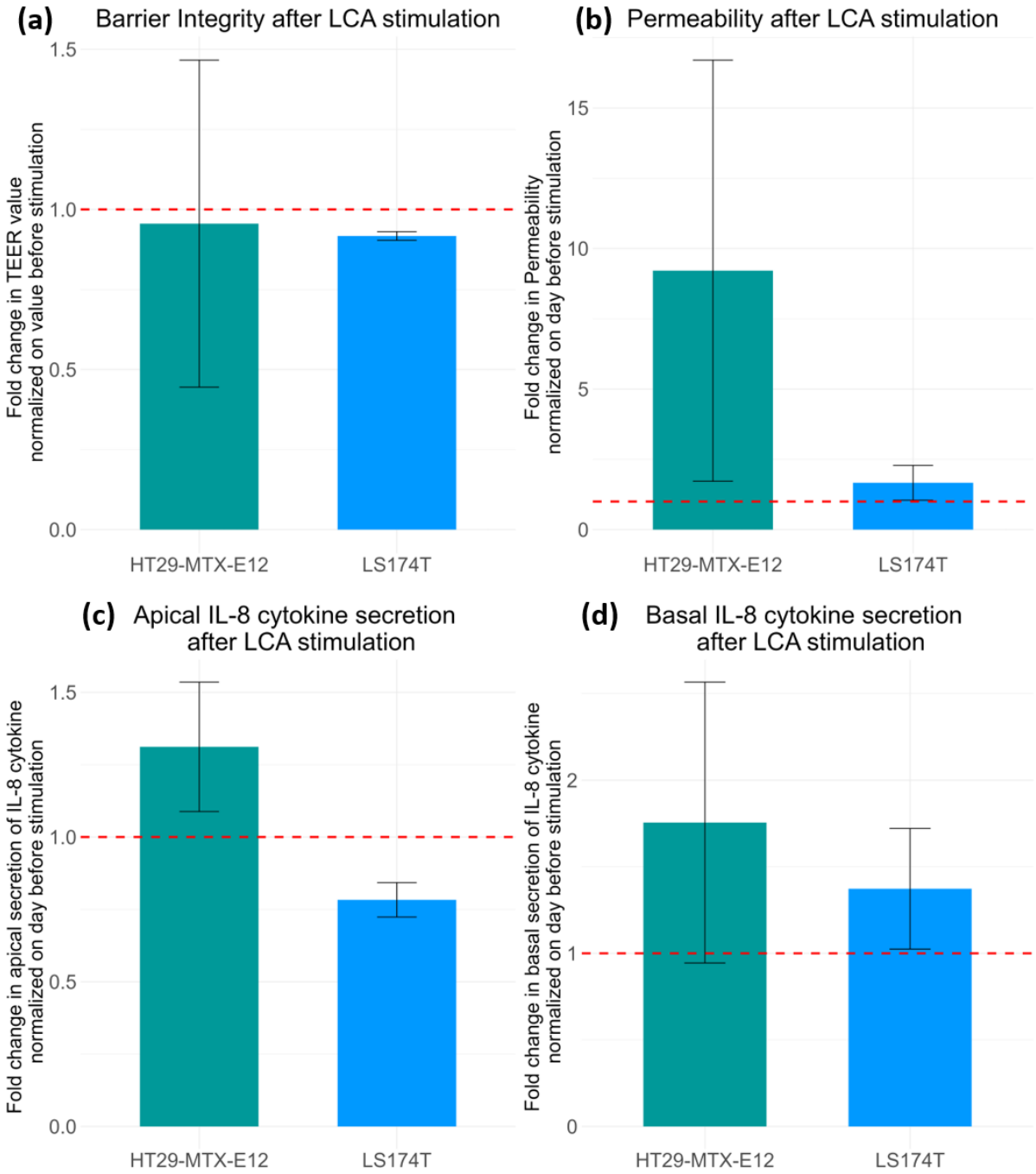

Figure 27: The difference in effect of a triple cell model with either HT29-MTX-E12 cells or LS174T upon **LCA** stimulation. The (a) barrier integrity, (b) permeability, (c) apical secretion of IL-8 cytokine, and (d) basal secretion of IL-8 cytokine are normalized on the measurements of the day before stimulation. The error bars represent the technical variability (n = 2).

3.3.3. Stimulation of small intestinal epithelium with *Clostridium leptum*

After testing the effect of pure secondary bile acids TUDCA and LCA on the small intestinal epithelium, the host-bile-bacteria interaction induced by *Clostridium leptum*, a well-described human gut bacterium, is investigated. It has been reported that this bacterium has 12α-Hydroxysteroid Dehydrogenase (12α-HSDH) activity [167, 168]. This enzyme is involved in the transformation of bile acids, specifically, it reduces 12-oxolithocholic acid to deoxycholic acid. Moreover, previous research already described 7α-dehydroxylation activity of *C. leptum* [169]. By dihydroxylation at the α-oriented hydroxyl group on C-7 of the primary bile acid CDCA (Chenodeoxycholic acid), can be transformed by gut bacteria into the secondary bile acid, lithocholic acid (LCA) [170].

For this aim, the effect of stimulation with **living bacterium *C. leptum*** on the epithelial barrier integrity, permeability, *ZO1* gene expression and *MUC2* gene expression was tested, along with multiple control conditions, on a **triple small intestinal model** (Caco-2:HT29-MTX-E12:NCI-H716).

The barrier integrity is shown in Figure 28. DMSO, used to dissolve the bile acids, did not had an effect on the barrier integrity, neither did the stimulation with CDCA. In contrast, the bacterial medium of *C. leptum* showed an increase in barrier integrity of (15.21 ± 0.04)% compared to cell model without any stimulation.

The *C. leptum* as well as the *C. leptum* with CDCA stimulation increased the barrier integrity for (4.88 ± 0.59)% and (4.40 ± 0.01)% respectively. Since the stimulation of CDCA did not affect the barrier integrity, this (4.88 ± 0.59)% and (4.40 ± 0.01)% increase can be assigned to the stimulation of the bacterium. However, considering that the bacterial medium already increased the barrier integrity for approximately 15% the stimulation of *C. leptum* has a decreasing effect on the barrier integrity.

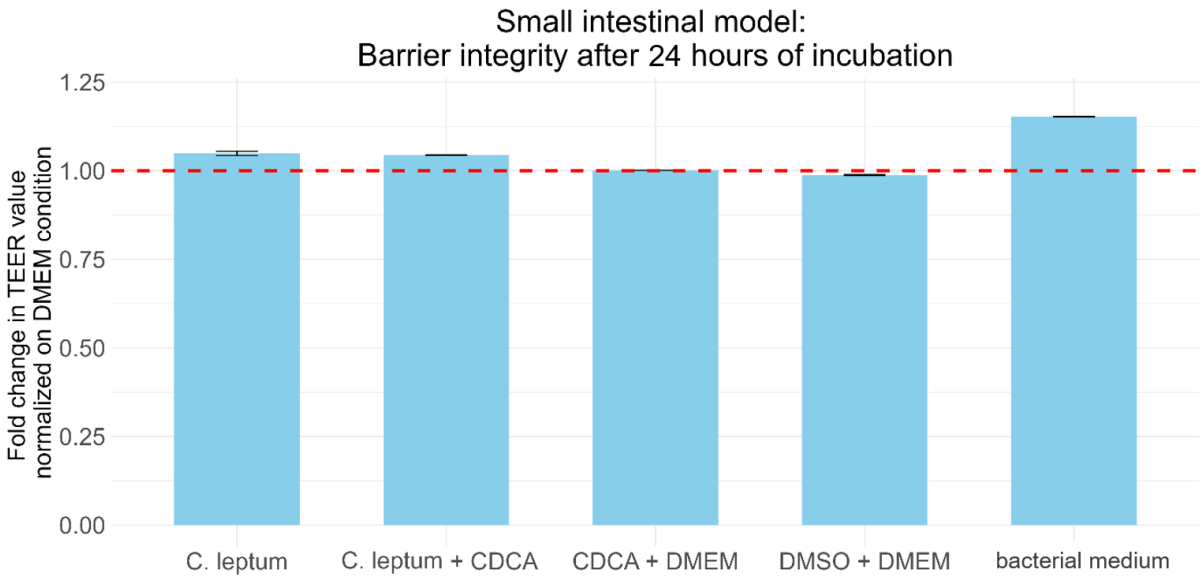

Figure 28: The effect upon the barrier integrity after stimulation of a small intestinal model with *Clostridium leptum*; *Clostridium leptum* with addition of CDCA; CDCA in culture medium (DMEM); DMSO in culture medium (DMEM); and bacterial medium for culturing *Clostridium leptum*. The error bars represent the technical variability (n = 2).

Multiple samples did not reach the detection limit of the lucifer yellow assay, thus no permeability data about the stimulation of this model is available (scatterplot with missing values in appendix Figure **32**). Neither the gene expression of *ZO1* can give additional information about the tight junctions, due to the high technical variability and missing measurements (Figure 29b). Likewise, the *MUC2* gene expression data could not be analysed (Figure 29a).

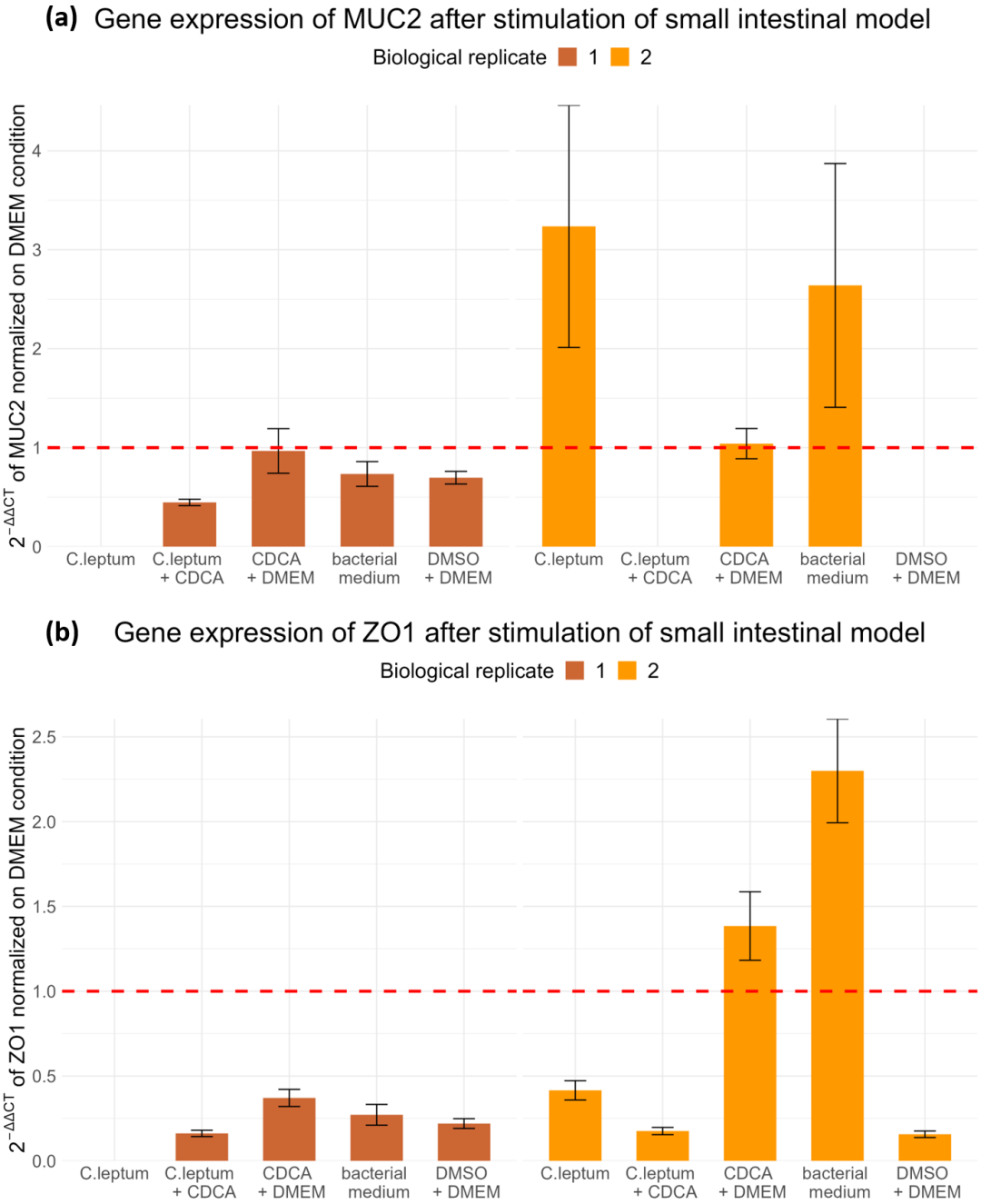

Figure 29: The gene expression level of (a) *MUC2* and (b) *ZO1* in $2^{-\Delta\Delta CT}$ values relative to the non-stimulated condition (DMEM). Small intestinal model was stimulated for 24 hours according to the conditions indicated on the x-axis labels. The error bars indicate the technical variability of the qPCR (n = 3).

3.3.4. Disease: Colon epithelium SBS versus non-SBS

Transverse colon (TC) samples from different time points of a SHIME were used to stimulate the colon models. Filtered samples from a resected and non-resected SHIME were used, to compare effect of the bacterial supernatant for health versus disease in the context of Short Bowel Syndrome (SBS). Three biological replicates of colon models were stimulated.

The effect of the 16 hours stimulation on the barrier integrity and the permeability is seen in Figure **30**. It can be observed that the change in barrier integrity and permeability differs for the three biological replicates.

In some cases, the SHIME medium might induce the change in barrier integrity and permeability (Figure **30**). To illustrate, a similar change is seen for the SHIME sample, the TC non-SBS sample and the TC SBS sample for the barrier integrity of biological replicate one and the permeability of biological replicate three. However, also the microbial supernatant might change the epithelial barrier characteristics. For example, in Figure 30a the barrier integrity increases more for the “TC SBS” sample than for the “SHIME” sample, both in biological replicate two and three. Nevertheless, overall, there is too much biological variability between the three biological replicates to make conclusions about the effect induced by the microbial supernatants of a resected and non-resected SHIME.

Due to missing values and technical variability, the gene expression data for both *MUC2* as *ZO1* could not be analysed (Figure 31) and needs to be repeated.

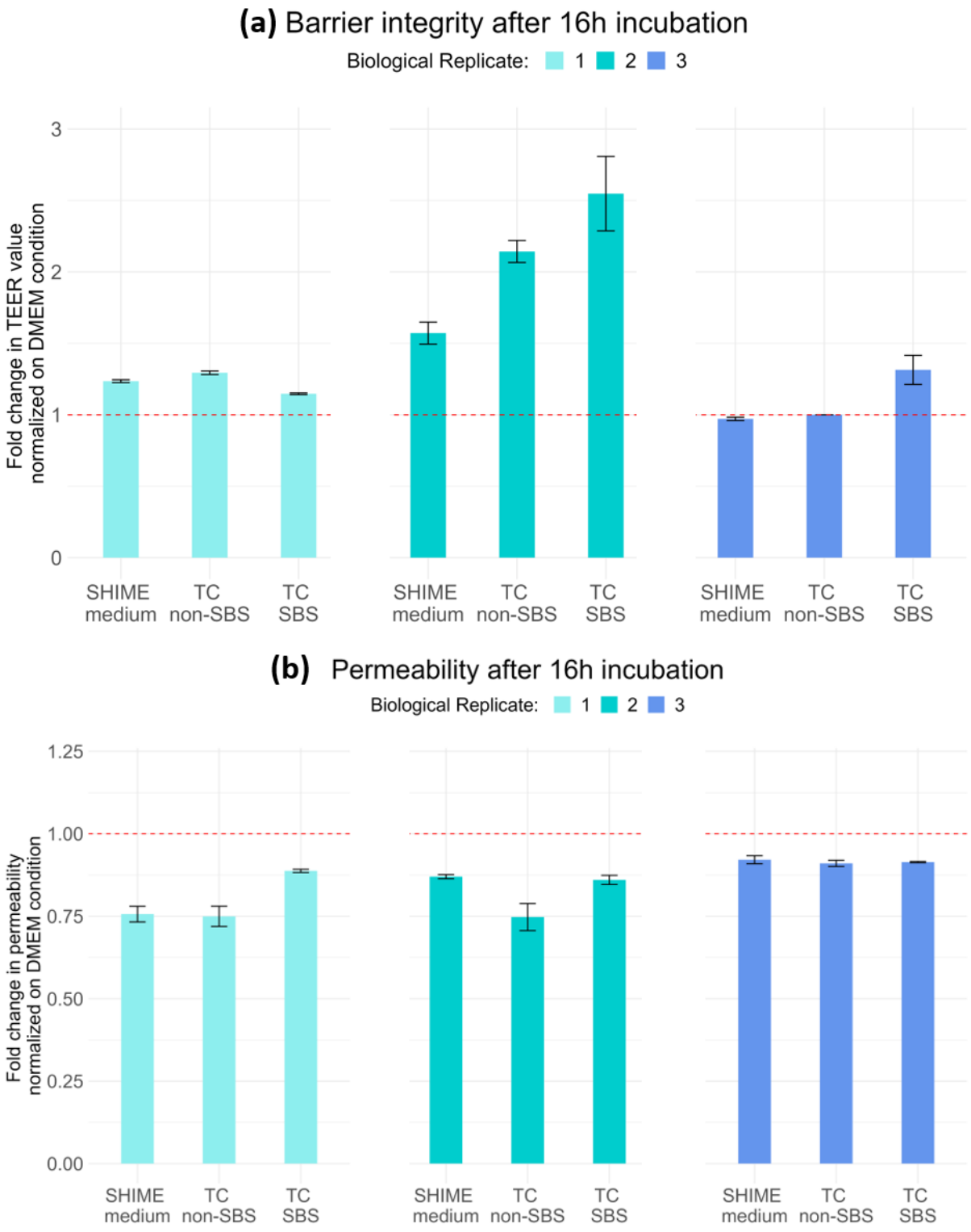

Figure 30: The barrier integrity (a) and the permeability (b) of differentiated colon models after 16 hours of stimulation with SHIME samples. TC non-SBS is the transverse colon before resection and TC SBS is the transverse colon after resection of the SHIME. The conditions are normalized on the control model without any stimulation (DMEM). The effect on three biological replicates is shown and the error bars represent the technical variability (n = 2).

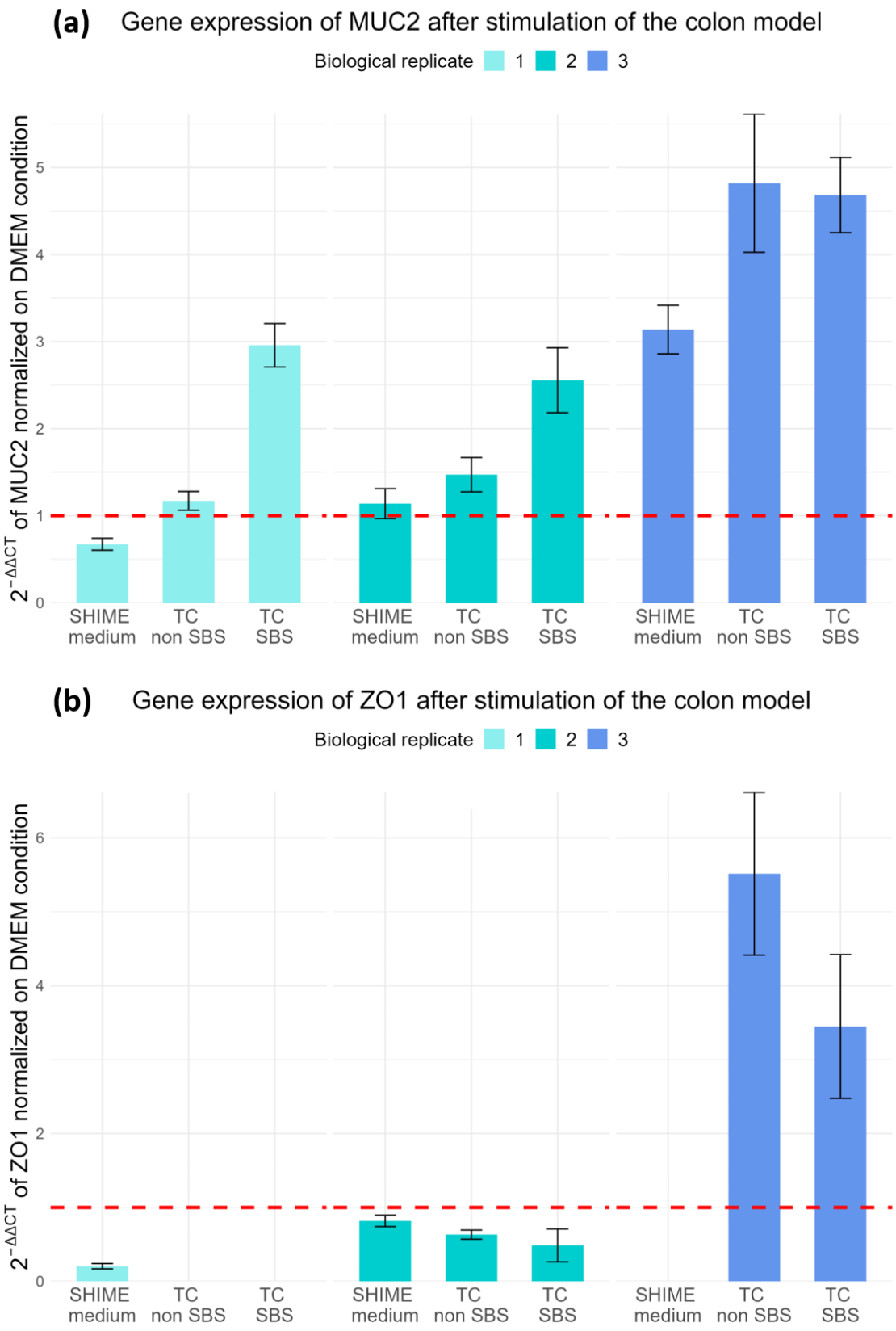

Figure 31: The gene expression level of (a) *MUC2* and (b) *ZO1* in $2^{-\Delta\Delta CT}$ values relative to the non-stimulated condition. SHIME medium refers to the medium used during the SHIME run. TC non SBS and TC SBS, respectively, refer to the transverse colon of the non-resected and resected SHIME. The error bars indicate the technical variability of the qPCR (n = 3).

CHAPTER 4.
DISCUSSION

4.1. Extracellular matrix proteins supporting the epithelial cells

The extracellular matrix (ECM) is the structural support network for epithelial cells, providing essential functions such as cell adhesion, migration, differentiation, and signalling [171]. To replicate the ECM in studies, collagen, one of the key structural proteins in humans, is often used [172]. Collagen plays a crucial role in maintaining the integrity and functionality of epithelial tissues, thereby facilitating various cellular processes. Consequently, to better mimic the *in vivo* environment collagen coating of the Transwell *in vitro* model, before seeding the cells, is commonly used.

When testing different incubation conditions for collagen coating, either overnight at 4°C or overnight at room temperature with a concentration of 6 µg/cm^2, the barrier integrity and permeability of the cell layers showed a high technical variability. Therefore, incubation of collagen for 2 hours at 37°C with concentration of 6 µg/cm² was opted for a more controlled condition in subsequent experiments. Previous studies have employed different protocols for **collagen** coating of Transwells. For instance, *Beterams et al. (2022)* incubated the collagen overnight at 4°C with a concentration of 5.5 µg/cm^2 [145]. A study of *Moysidou et al. (2022)* incubated at 37°C for 30 minutes with a concentration of 3 mg/mL, while a study of *Slyker et al. (2021)* incubated at 37°C for 2 hours at the same concentration [173, 174]. According to Corning's protocol for collagen coating of Transwell inserts, the coating time and temperature impact cell attachment and spreading [175, 176].

An alternative coating agent in several cell models is **Matrigel**, which is derived from mouse tumour, the EHS tumour, and therefore exhibits significant batch-to-batch variation [154, 177-179]. Matrigel contains multiple tissue basement membrane components, such as ECM proteins, growth factors and fibres, whereas collagen type I is a well-defined protein with known composition [180]. Different values for the barrier integrity and permeability were observed when coating with either collagen or Matrigel. This suggests that the choice of coating material impacts the barrier properties and permeability dynamics of the *in vitro* model. Literature confirms that collagen facilitates the differentiation of some cells, while Matrigel, containing diverse growth and differentiation factors, enhances the attachment and differentiation of a broader range of cells [181-183].

Furthermore, the choice of coating agent influences the **adherence of NCI-H716 cells**, with improved adherence observed for Matrigel (illustrated in Figure 21). In future studies, the differentiation of this cell line upon Matrigel or collagen coating could further be assessed by analysing the GLP-1 expression and secretion.

4.2. Mucus production and barrier characteristics of intestinal goblet cells

The mucus layer of the intestine serves as a barrier for bacteria, limiting microbial contact with the epithelium [184]. MUC2, secreted by the goblet cells, is the most abundant mucin of the small intestine [185]. To simulate the mucus-producing characteristics of goblet cells *in vitro*, different cell lines can be used, among which LS174T and HT29-MTX-E12. For a **double model** of Caco-2 cells along with either one of the mentioned goblet-like cell lines, higher *MUC2* gene expression for the LS174T model was observed compared to the HT29-MTX-E12 model. This aligns with *Bu et al. (2011)* who reported higher *MUC2* mRNA expression in the LS174T cell line compared to the HT29 cell line [134]. Although no complete comparison can be made because HT29-MTX is a subclone of HT29 selected to produce more mucins.

When studying the expression of tight junctions and, specifically the zona occludens 1 (*ZO1*), the double cell model with HT29-MTX-E12 exhibited higher *ZO1* gene expression than the model including LS174T. Indeed, HT29-MTX-E12 cells are described to form a tight cell layer and grow in confluent monolayers [186]. *Hoffman et al. (2021)* used the same setup for a double model with Caco-2 and HT29-MTX (ratio 90:10) and demonstrated, through *ZO1* expression analysis, that this model is functional for studying physiological intestinal functions [187].

In contrast, LS174T cells do not grow as an organized cell layer but instead grow in dome-like structures [134]. *Navabi et al. (2013)* even found that the LS174T cell line, cultured in glucose free media supplemented with galactose, is not capable of forming an organized cell layer with functional tight junctions [188]. Similar morphology characteristics of both cell lines can be observed in the triple cell models of this work (Figure 12), namely the dome-like structures for the model including LS174T cells and the organized cell layer for the model including HT29-MTX-E12.

For the **triple models** with either LS174T or HT29-MTX-E12 goblet-like cells, the barrier integrity, the permeability and the *ZO1* gene expression will be discussed simultaneously, because they all provide insight into the barrier properties of the epithelial layer. Comparing the barrier integrity values during differentiation, the HT29-MTX-E12 triple model ranged between 350-1400 Ω·cm² (Figure 14a), whilst the LS174T model ranged between 10-110 Ω·cm² (Figure 14c). For gastrointestinal epithelia, the TEER values for the HT29-MTX-E12 model are considered “tight” and those of the LS174T model are considered “leaky” [162]. TEER values of the small intestinal epithelium range between 50 – 100 Ω·cm² according to *ex vivo* experiments using the Ussing Chambers [162]. Therefore, the triple model including LS174T cells best corresponds to this *ex vivo* range.

Several factors affect the TEER measurements, contributing to the observed variation at different timepoints and between biological replicates. A first factor is the cell passage number, studied by *Briske-Anderson et al. (1997)* [189]. They emphasized that monitoring the culture characteristics during growth and differentiation under specific experimental conditions is needed, since they observed higher TEER values for Caco-2 cells with a higher passage number, than Caco-2 cultures with a lower passage number. This variability complicates comparison of results between different research laboratories. A second factor is the temperature. Ideally, the measurements are conducted at 37°C [162, 190]. The TEER experiments presented in this work were conducted immediately after taking the cell models out of the incubator. However, experiment-to-experiment variability in temperature could have affected the measurements, explaining the variability observed in TEER values. Thirdly, the cell culture period is considered as an important factor for the formation of tight junctions between cells [189, 191]. Figure 14 shows that the barrier integrity changes over time during the culturing period. For example, at the middle of the differentiation period (DIV13-15) TEER values for the model with HT29-MTX-E12 cells are higher than at the end of the 21-22 days differentiation period. This suggests

that approximately 21 days are needed to reach TEER values that are representative for the *in vivo* situation. Similarly, the LS174T model requires a differentiation period to decrease the TEER values, although this decrease can result in very low TEER values at the end of the differentiation period, which is not ideal.

The second readout used for the barrier functions of the epithelial layer is the permeability, more specifically the paracellular permeability of Lucifer Yellow across the cell layer. Comparing the triple small intestinal models of this thesis with *Xiaojun et al. (2018)*, who validated a Transwell model of Caco-2 cells, differences in permeability are observed [192]. *Xiaojun et al. (2018)* reported an apparent permeability (apical to basal) for Lucifer Yellow of $3.57 \cdot 10^{-7}$ cm/s after 21 days of culturing. This value comparable to the triple small intestinal model with HT29-MTX-E12 cells ($3.09 \cdot 10^{-7}$ cm/s) but lower than the LS174T triple model ($179.89 \cdot 10^{-7}$ cm/s) after 21 culturing days. According to protocols described by *Tavelin et al. (2002)* and *Hubatsch et al. (2007)*, the model including LS174T cells is considered *high* permeable and the HT29-MTX-E12 *low* permeable [193-195]. Unfortunately, data regarding cell passage number, seeding density and the specific culture conditions utilized by *Xiaojun et al. (2018)* are not shared, precluding a possible explanation of the observed differences. However, the integration of the goblet-like cell lines and their characteristics may explain the higher permeability observed in the model including LS174T and lower permeability for the model including HT29-MTX-E12, compared to the mono-culture model of Caco-2 cells by *Xiaojun et al. (2018)*.

As a third read-out for the barrier function, the *ZO-1* gene expression was analysed. For triple small intestinal models, including either LS174T or HT29-MTX-E12, more *ZO1* gene expression is observed in the models including HT29-MTX-E12. This is in line with the observations of the double models, previously discussed.

The three readouts for the barrier function of the epithelium at the end of the differentiation period are complementing each other. For the model including HT29-MTX-E12 the barrier integrity is higher, the permeability is lower and the *ZO1* gene expression is higher than the model including LS174T cells.

Lastly, at the end of the differentiation period (DIV20) for triple models with either one of the goblet-like cells, the IL-8 cytokine secretion was higher at the apical compartment for the model including LS174T and higher at the basal compartment for the model including HT29-MTX-E12. This might be due to polarization of IL-8 cytokine secretion by the epithelial cells. For example, Tataru et al. (2023) reported the polarized IL-8 cytokine secretion of Caco-2 cells upon different stimulations [196]. However, this model included macrophages, thus also the differentiated THP-1 cells might contribute to the observed cytokine IL-8 secretion levels [197, 198].

4.3. Evaluation of the barrier integrity in association with the permeability

Examining the evolution of barrier integrity and permeability during differentiation (Figure 14c and Figure 14d), the **LS174T** model shows a decrease in barrier integrity accompanied by an increase in permeability. A decrease in barrier integrity, measured by TEER, indicates a reduction in resistance across the cell layer and thus an increase in the ionic conductance of the paracellular pathway [162]. Similarly, the Lucifer Yellow assay is an indicator of the paracellular transport from apical to basal compartment, and also provides information about the size of the pores through which the transport occurs [199]. When barrier integrity is compromised, the paracellular permeability is expected to be higher, as observed in the model including LS174T, allowing the Lucifer Yellow molecule to pass more

easily paracellularly. However, other paracellular-transport markers like 4-dextran and 10-dextran, or transcellular-transport marker transferrin can also be used to assess the permeability and providing additional insights into the permeability characteristics of the epithelium [200].

Epithelial integrity is expected to increase during differentiation, as for example studied by *Marziano et al. (2019)* who assessed the integrity of Caco-2 cells using impedance-based sensors (instead of TEER) [201]. Contrary to this, a decrease in barrier integrity is observed for the triple model including LS174T for both biological replicates. The morphology and the way LS174T cells grow is characterized by regions, resembling domes, rather than a uniformly flat monolayer (also indicated on Figure 12) [134]. During the formation of epithelial membranes in the triple model including LS174T this growth patterns of LS174T may result in discontinuities, meaning regions with better and regions with lower barrier integrity. Consequently, this growth pattern could impact the overall integrity of the epithelial barrier, contributing to the observed decrease in barrier integrity compared to models with other cell lines.

In contrast, **HT29-MTX-E12** cells grow as a confluent monolayer. Next to this morphological difference, the trend in **barrier integrity and permeability** during the differentiation period (Figure 14) also differs. The model including HT29-MTX-E12 first shows an increase and then a decrease, in both barrier integrity and permeability. A decrease in barrier integrity measured by TEER does not necessarily mean an increase in apparent permeability measured by the Lucifer Yellow assay. Changes in barrier integrity reflect alterations in specific tight junction components that affect ionic conductance [162]. This does not necessarily affect the paracellular passage of certain molecules, such as Lucifer Yellow. For example, changes in tight junction pore sizes might restrict the passage of LY, while still allowing smaller molecules and ions to pass paracellularly. If for smaller pores, still a lot of ions can pass through (low barrier integrity) but the LY molecule cannot pass (lower permeability), this can lead to both the decrease in barrier integrity and permeability measurements. Thus, this might explain the similar evolution of permeability and barrier integrity observed in the small intestinal model including HT29-MTX-E12 cells.

Moreover, this increasing and decreasing trend for the **barrier integrity** during differentiation of the small intestinal model including **HT29-MTX-E12** cells is in line with the research of *Felix et al. (2021)* and *Hofmann et al. (2021*) [187, 202]. The former analysed epithelial cell monolayers of Caco-2 cells and observed that the TEER increases until confluency, then decreases before it is increasing again until the state of a full epithelial barrier. They concluded that changes in cell numbers and the maturation of tight junctions during proliferation and differentiation impact TEER values. Although these observations were made for Caco-2 monolayers, Caco-2 and HT29-MTX E12 cells share the same origin (human Caucasian colon adenocarcinoma) and both grow in structured monolayers. Additionally, *Hofmann et al. (2021)* demonstrated that a double model including Caco-2 and HT29-MTX cells seeded in a 90:10 ratio on Snapwells® showed similar TEER values over a 24-day cultivation period as a monoculture model with only Caco-2 cells. Therefore, the evolution of barrier integrity in the triple model with HT29-MTX E12 cells aligns with existing literature.

4.4. Differences between colon and small intestinal *in vitro* model

The distribution of the goblet cells in the intestinal epithelium gradually increases from 4% to 16% from the duodenum to the terminal colon. Consequently, the colon models presented in this work have a higher seeding ratio for the goblet-like cells. Thus, it is expected that the colon models would secrete more mucus, also mimicking the *in vivo* situation where the small intestine is composed of one mucus layer whereas the colon has two mucus layers. However, upon comparing the small intestinal *in vitro* model and colon model, most small intestinal models showed higher gene expression of *MUC2*. The cell ratio after differentiation of those models was not studied, thus it might be that the goblet cells of the small intestinal model proliferated more and were present at a higher ratio upon differentiation. Additionally, biological variability and a difference in passage number could also be involved in the gene expression levels. Moreover, the expression of other mucin genes was not examined, so maybe the overall mucin expression might provide further indications. Neither the *MUC2* protein synthesis nor secretion was studied. Therefore, no description of the actual mucus layer is provided by the executed experiments. In future studies obtaining more complementary data would give an added value, such as examining gene expression of other mucin genes, analysing mucin protein expression and secretion, and making epithelial cross-sections with histochemical staining of the mucus layer.

Another difference between the small intestinal models and the colon models characterized in this thesis is the use of Caco-2 cell line for the former and T84 cell line as colonocytes for the latter. It is known that Caco-2 cells also express *MUC2* [203]. However, a comparison of *MUC2* gene expression between Caco-2 and T84 cells has up to now not been conducted, but could be interesting to explore. Moreover, different cellular mechanisms can influence the *MUC2* gene expression in cell lines. For example, exposure of T84 cells to PMA (phorbol 12-myristate 13-acetate) stimulates mucin gene expression, as reported by *Hong et al. (1999)* [204]. A similar analysis for Caco-2 cells could be insightful, especially considering our models involving macrophages where PMA is used to stimulate THP-1 cells. If the THP-1 are in co-culture with the epithelial layer, PMA stimulation might impact the epithelial layer and the cells' gene expression.

In vivo the small intestinal epithelium is generally considered more permeable than the colon due to the distinct physiological roles and structural differences. ZO1 is a tight junction protein, and a higher gene expression level might indicate more ZO1 protein expression and thus more tight junctions between the epithelial cells [205]. Increased tight junctions typically indicate a tighter barrier and a less permeable epithelium. However, the *ZO1* gene expression was higher for the small intestinal models than the colon models. Nonetheless, this *contradictory* finding regarding *ZO1* gene expression between the small intestinal and colon models cannot be confirmed without protein expression data, or proper visualization techniques to detect the tight junction reorganization, or information on the expression levels of other tight junction proteins. Thus, further investigations can give better insights.

4.5. Including the immune barrier adds value to the *in vitro* model

The intestinal epithelial cells form a physical barrier and interact closely with the immune cells of the *lamina propria*. Together, they maintain gut homeostasis by preventing the translocation of pathogens and regulating immune responses [206-208]. The cells sense changes in microenvironment and release immune regulators to signal the underlying immune cells. This interaction between epithelial and immune cells is crucial for maintaining the gut functions, thus including immune cells in *in vitro* models mimics better the *in vivo* environment. Immune cells have already been incorporated in Transwell models to study the intestinal immune response by differentiating THP-1 cells into macrophage populations [209, 210].

Initially, **macrophages** were seeded at the **basal side of the Transwell insert** to simulate closer proximity between immune and epithelial cells (illustrated in Figure 9A). As shown in Figure 16a, the barrier integrity changed upon **PMA** differentiation of the THP-1 cells into macrophages. In research of *Calatayud et al. (2019)* a similar Transwell setup was used, seeding Caco-2 cells along with HT29-MTX cells at the apical side of the insert and THP-1 cells at the basal side of the insert [165]. They observed a reduction in barrier integrity of 50% upon PMA differentiation of THP-1 cells. The heterogeneity in phenotype and function of macrophages has been documented in the literature and might be the underlying cause of the observed variations in barrier integrity [211, 212]. However, this setup did not allow for monitoring macrophage heterogeneity, which could have provided more information about the macrophage morphology, size and granularity [213]. Thus, there is no confirmation about the altered barrier integrity being attributed to macrophage heterogeneity.

Additionally, in this setup, the polarization of the macrophages by 24 hours **LPS** stimulation decreased the barrier integrity (Figure 16b). *Kämpfer et al. (2017)* observed a reduction in TEER of 20% after 4 hours LPS stimulation for a co-culture of Caco-2 and THP-1, but a the barrier integrity was reestablished after 24 hours [209]. To further verify the LPS activation of macrophages, the cytokine secretion of TNF-α, IL-1 or IL-6 could be assessed, since LPS stimulates the immune response by interacting with membrane receptor CD14 which induced the production of those cytokines [214]. Moreover, the gene expression kinetics of those inflammation-related cytokines and their transcription factors can be analysed by qPCR, as described in *Chanput et al. (2010)* [215].

In an attempt to limit variability in barrier integrity, the **THP-1 cells** were **seeded at the bottom of the well** (illustrated in Figure 9B). The differentiated THP-1 cells were added to the cell model after 21 days of differentiation. This approach did not result in a change in barrier integrity of the epithelial cell layer before and after adding the macrophages to the Transwell models (Figure 18a). Since the macrophages were seeded at the bottom of the well-plate, imaging was possible. Over the following 10 days the phenotype of the macrophages was monitored (Figure 19) using the incucyte as a live-cell imaging and analysis platform enabling automated quantification of cell behaviour over time. The morphology of macrophages depends on their activity [165]. So, further research can investigate how macrophage morphology affects the epithelial cell layer of the triple *in vitro* model.

For the model with macrophages at the bottom of the well, the detection limit of the Lucifer Yellow assay was not always reached. A possible explanation is that macrophages take up Lucifer Yellow molecules that paracellularly pass through the epithelial layer and reach the basal compartment of the Transwell where the macrophages reside. It has been reported that macrophages take up Lucifer Yellow by macropinocytosis [216, 217].

4.6. Health: complex mechanisms regulating the intestinal barrier upon exposure of bile acids, bacterial metabolites and live bacterium

After differentiation of the *in vitro* epithelial model, stimulation with bacterial supernatant samples, bile acids and a live bacterium was studied, in the context of a healthy intestinal environment.

The approach of using supernatant samples of the SHIME allowed a focused investigation of the impact of **bacterial metabolites** on the intestinal epithelium. Upon stimulation with bacterial supernatant from the proximal small intestine and ileum, the barrier integrity decreased, but not to a biologically relevant extent. However, permeability increased with approximately 30-40%. This suggests that the microbial metabolites of the samples influence the intestinal epithelium, making it more permeable. However, the results of the permeability and *ZO1* gene expression do not confirm the same effect, as the *ZO1* gene expression increases. Thus, additional readouts, such as the gene expression of other tight junction proteins or the visualization of the reorganisation of the tight junctions, are needed to interpret these results. Nevertheless, it is known that microbial metabolites, such as SCFA, indoles, purines, bile acids and polyamides can alter the epithelial barrier [218, 219].

Secondary bile acids can have an effect on the epithelial barrier. *Song et al. (2022)* found that Tauroursodeoxycholic acid (TUDCA) improves the intestinal barrier function [220]. Moreover, *Yang and Hou et al. (2017)* reported that TUDCA enhances the intestinal barrier function by increasing levels of tight junction molecules [221]. Coherently, TUDCA stimulation of the triple *in vitro* models studied in this thesis increased barrier integrity and decreased permeability in models with HT29-MTX-E12 and LS174T as goblet-like cells (Figure 26a and Figure 26b).

Another secondary bile acid studied in this work is lithocholic acid (LCA), which is known to have an anti-inflammatory effect [222]. LCA is mainly produced by 7α-dehydroxylase-producing bacteria such as *Clostridium* and *Eubacterium* in human [223]. Therefore, stimulation with **living *C. leptum* bacterium**, which produces LCA, was also studied during this thesis. The role of LCA on the epithelial cells needs further analysis, since the triple model including LS174T or HT29-MTX-E12 responded differently on the LCA polarization and there was no biological relevant change in barrier integrity upon *C. leptum* stimulation (< 15%). Notably, for future experiments, the bacterial medium needs to be used as a control because it increased barrier integrity. This is expected, as the bacterial medium contains more nutrients than the cell culture medium (Table 4 in appendix).

4.7. Disease: effect of microbial metabolites from resected and non-resected SHIME in the context of Short Bowel Syndrome

Short Bowel Syndrome (SBS) is a condition defined by extensive loss in small intestinal mass. Due to the shortened length of the intestine, the intestinal luminal environment of SBS patients is altered. For example, oxygen levels are higher leading to different microbial communities in the gut [110, 111]. At physiological level of the patient's epithelium, three phases are recognized post-surgery: the acute intestinal failure phase, the adaptation phase, and the chronic SBS phase [103]. During the adaptation phase, spontaneous morphological modifications of the epithelium occur, characterized by intestinal dilatation, increased area and length of the villi, expanded number of goblet cells, and elevated intestinal epithelial sodium permeability [2].

To investigate this adaptation of the epithelium after surgery, microbial supernatant samples from a resected and non-resected SHIME (transverse colon compartment) were used to stimulate the *in vitro* colon models. The aim was to check the epithelial functions upon stimulation, even though the adaptation phase takes place after weeks to months. Overall, the three biological replicates showed variability upon stimulation. Therefore, the impact on the epithelium by microbial metabolites from a resected and non-resected intestine needs to be further investigated. This can be achieved by including more biological replicates and/or assessing additional readouts to analyse the epithelial barrier, such as visualizing cross-sections of the epithelium by histochemical staining. However, the exact composition of the metabolites in the samples might explain some of the observed differences. For example, *Peng et al. (2009)* showed that butyrate enhances the intestinal barrier of Caco-2 monolayers by facilitating thigh junction assembly. *Wang et al. (2012)* reported that butyrate enhances the barrier integrity by increasing the transcription of tight junction protein Claudin-1 [224].

Similar to the bacterial medium in the *C. leptum* model, the SHIME medium could be causing some of the changes in barrier integrity and permeability (Figure 30). This can again be explained by the composition of the SHIME medium, which contains more nutrients than the cell culture medium (Table 5 in appendix).

CHAPTER 5.
CONCLUSIONS & FUTURE PERSPECTIVES

This thesis contributed to optimize and characterize a Transwell *in vitro* model to study the small intestinal epithelium and the host-microbe interactions. The *in vitro* model offers an alternative to *in vivo* studies, providing a controlled environment and allowing detailed examination of cellular mechanisms.

Overall, this work contributed to the development of *in vitro* models mimicking the small intestinal epithelium and the intestinal functions. The models are characterized by assessing the barrier integrity, permeability, *MUC2* gene expression, *ZO1* gene expression and IL-8 cytokine secretion. These readouts are also applied to study the host-microbiota interaction by stimulating models with bacterial metabolites from a complex microbial community, well-defined bile acids, or a live *C. leptum* bacterium.

Key findings include the importance of extracellular matrix proteins such as collagen and Matrigel in supporting epithelial cells. Next, the choice of goblet cell lines (LS174T or HT29-MTX-E12) within the triple model has an impact on the barrier integrity, permeability, *MUC2* gene expression, tight junction expression (*ZO1*), morphology, and IL-8 cytokine secretion of the triple cell models. Furthermore, the addition of an immune compartment to the model by seeding macrophages at the bottom of the well-plate allowed monitoring of the macrophages' morphology. Subsequently, this work examined the effect of microbial metabolites, bile acids, and live bacteria on the intestinal barrier. The results suggest that diverse microbial metabolites can influence the barrier properties, although further studies are needed to elucidate the specific roles on a molecular level of various metabolites.

Although this work includes complementary readouts for the epithelial barrier, future research should include additional methods and expand the number of biological replicates to confirm the results. Additional studies on the expression of other mucin genes or other tight junction genes can be assessed. An even more comprehensive understanding of the intestinal barrier would be obtained by analysing mucin and tight junction protein expression, along with visualizing the mucus layer and the functional organization of tight junctions. Additionally, profiling the effect of the microbial metabolites will enhance the utility of these models in studying gut physiology and pathology. Nevertheless, the results obtained in this work highlight the importance of the development of *in vitro* models for the small intestinal and to study HMI. The intestinal model described in this thesis was a proof-of-concept for a versatile model, allowing various readouts to characterize the intestinal barrier, and allowing the investigation of Host-Microbiota interactions.

BIBLIOGRAPHY

[1] S.M. Jung, S. Kim, In vitro Models of the Small Intestine for Studying Intestinal Diseases, Front Microbiol 12 (2021) 767038.
[2] K. Delbaere, I. Roegiers, A. Bron, C. Durif, T. Van de Wiele, S. Blanquet-Diot, L. Marinelli, The small intestine: dining table of host–microbiota meetings, FEMS Microbiology Reviews 47(3) (2023).
[3] J. Creff, L. Malaquin, A. Besson, In vitro models of intestinal epithelium: Toward bioengineered systems, J Tissue Eng 12 (2021) 2041731420985202.
[4] S. Kong, Y.H. Zhang, W. Zhang, Regulation of Intestinal Epithelial Cells Properties and Functions by Amino Acids, Biomed Res Int 2018 (2018) 2819154.
[5] V. Mahadevan, Anatomy of the small intestine, Surgery (Oxford) 38(6) (2020) 283-288.
[6] S.N. Steinway, J. Saleh, B.K. Koo, D. Delacour, D.H. Kim, Human Microphysiological Models of Intestinal Tissue and Gut Microbiome, Front Bioeng Biotechnol 8 (2020) 725.
[7] A.L. Planchette, C. Schmidt, O. Burri, M. Gomez de Aguero, A. Radenovic, A. Mylonas, J. Extermann, Optical imaging of the small intestine immune compartment across scales, Commun Biol 6(1) (2023) 352.
[8] J. Costa, A. Ahluwalia, Advances and Current Challenges in Intestinal in vitro Model Engineering: A Digest, Front Bioeng Biotechnol 7 (2019) 144.
[9] J.T. Collins, N. A., M. Badireddy, Anatomy, Abdomen and Pelvis, Small Intestine, StatPearls Treasure Island (FL), 2023.
[10] S. Yates, Practical bodywork in the postpartum, in: S. Yates (Ed.), Pregnancy and Childbirth, Churchill Livingstone, Edinburgh, 2010, pp. 313-338.
[11] C.A. Picut, G.D. Coleman, Gastrointestinal Tract, Atlas of Histology of the Juvenile Rat2016, pp. 127-171.
[12] R. Yamamura, K.Y. Inoue, K. Nishino, S. Yamasaki, Intestinal and fecal pH in human health, Frontiers in Microbiomes 2 (2023).
[13] J.D. Wood, Autonomic/Enteric Reflexes, in: M.D. Binder, N. Hirokawa, U. Windhorst (Eds.), Encyclopedia of Neuroscience, Springer Berlin Heidelberg, Berlin, Heidelberg, 2009, pp. 284-292.
[14] H.M. Becker, U.E. Seidler, Bicarbonate secretion and acid/base sensing by the intestine, Pflugers Arch 476(4) (2024) 593-610.
[15] R.E. Cormier, Abdominal Gas. In: Walker HK, Hall WD, Hurst JW, editors. Clinical Methods: The History, Physical, and Laboratory Examinations. , 3rd edition ed., Butterworths, Boston, 1990.
[16] W.G. Sheridan, R.H. Lowndes, H.L. Young, Intraoperative tissue oximetry in the human gastrointestinal tract, The American Journal of Surgery 159(3) (1990) 314-319.
[17] B.A.H. Jensen, M. Heyndrickx, D. Jonkers, A. Mackie, S. Millet, M. Naghibi, S.I. Paerregaard, B. Pot, D. Saulnier, C. Sina, L.G.W. Sterkman, P. Van den Abbeele, N.V. Venlet, E.G. Zoetendal, A.C. Ouwehand, Small intestine vs. colon ecology and physiology: Why it matters in probiotic administration, Cell Rep Med 4(9) (2023) 101190.
[18] A.J. Kastl, Jr., N.A. Terry, G.D. Wu, L.G. Albenberg, The Structure and Function of the Human Small Intestinal Microbiota: Current Understanding and Future Directions, Cell Mol Gastroenterol Hepatol 9(1) (2020) 33-45.
[19] P.R. Kiela, F.K. Ghishan, Physiology of Intestinal Absorption and Secretion, Best Pract Res Clin Gastroenterol 30(2) (2016) 145-59.
[20] E.M. Fish, B. Burns, Physiology, Small Bowel, 2022. https://www.ncbi.nlm.nih.gov/books/NBK532263/. (Accessed 2023/12/22.
[21] M. Boland, Human digestion – a processing perspective, Journal of the Science of Food and Agriculture 96(7) (2016) 2275-2283.
[22] R. Heda, F. Toro, C.R. Tombazzi, Physiology, Pepsin Treasure Island (FL): StatPearls Publishing2023.

[23] D.C. Whitcomb, M.E. Lowe, Human pancreatic digestive enzymes, Dig Dis Sci 52(1) (2007) 1-17.
[24] J. Iqbal, M.M. Hussain, Intestinal lipid absorption, Am J Physiol Endocrinol Metab 296(6) (2009) E1183-94.
[25] B. Staels, V.A. Fonseca, Bile acids and metabolic regulation: mechanisms and clinical responses to bile acid sequestration, Diabetes Care 32 Suppl 2(Suppl 2) (2009) S237-45.
[26] A. Di Ciaula, G. Garruti, R. Lunardi Baccetto, E. Molina-Molina, L. Bonfrate, D.Q.H. Wang, P. Portincasa, Bile Acid Physiology, Annals of Hepatology 16 (2017) S4-S14.
[27] F. Deng, Y.H. Bae, Bile acid transporter-mediated oral drug delivery, J Control Release 327 (2020) 100-116.
[28] Y. Qi, C. Jiang, J. Cheng, K.W. Krausz, T. Li, J.M. Ferrell, F.J. Gonzalez, J.Y. Chiang, Bile acid signaling in lipid metabolism: metabolomic and lipidomic analysis of lipid and bile acid markers linked to anti-obesity and anti-diabetes in mice, Biochim Biophys Acta 1851(1) (2015) 19-29.
[29] P.A. Dawson, S.J. Karpen, Intestinal transport and metabolism of bile acids, J Lipid Res 56(6) (2015) 1085-99.
[30] M.D. Sinnott, P.W. Cleary, S.M. Harrison, Peristaltic transport of a particulate suspension in the small intestine, Applied Mathematical Modelling 44 (2017) 143-159.
[31] J.D. Wood, Peristalsis, in: L.R. Johnson (Ed.), Encyclopedia of Gastroenterology, Elsevier, New York, 2004, pp. 164-165.
[32] M. Antfolk, K.B. Jensen, A bioengineering perspective on modelling the intestinal epithelial physiology in vitro, Nat Commun 11(1) (2020) 6244.
[33] S.A. Hewes, R.L. Wilson, M.K. Estes, N.F. Shroyer, S.E. Blutt, K.J. Grande-Allen, In Vitro Models of the Small Intestine: Engineering Challenges and Engineering Solutions, Tissue Eng Part B Rev 26(4) (2020) 313-326.
[34] T. Ayabe, D.P. Satchell, C.L. Wilson, W.C. Parks, M.E. Selsted, A.J. Ouellette, Secretion of microbicidal α-defensins by intestinal Paneth cells in response to bacteria, Nature Immunology 1(2) (2000) 113-118.
[35] C. Wallaeys, N. Garcia-Gonzalez, C. Libert, Paneth cells as the cornerstones of intestinal and organismal health: a primer, EMBO Mol Med 15(2) (2023) e16427.
[36] J.M. Allaire, S.M. Crowley, H.T. Law, S.Y. Chang, H.J. Ko, B.A. Vallance, The Intestinal Epithelium: Central Coordinator of Mucosal Immunity, Trends Immunol 39(9) (2018) 677-696.
[37] V. Bonis, C. Rossell, H. Gehart, The Intestinal Epithelium - Fluid Fate and Rigid Structure From Crypt Bottom to Villus Tip, Front Cell Dev Biol 9 (2021) 661931.
[38] Y. Xu, N. Shrestha, V. Preat, A. Beloqui, An overview of in vitro, ex vivo and in vivo models for studying the transport of drugs across intestinal barriers, Adv Drug Deliv Rev 175 (2021) 113795.
[39] J.I. Gordon, Understanding gastrointestinal epithelial cell biology: lessons from mice with help from worms and flies, Gastroenterology 105(2) (1993) 315-324.
[40] E. Tumer, A. Broer, S. Balkrishna, T. Julich, S. Broer, Enterocyte-specific regulation of the apical nutrient transporter SLC6A19 (B(0)AT1) by transcriptional and epigenetic networks, J Biol Chem 288(47) (2013) 33813-33823.
[41] H.F. Helander, L. Fändriks, Surface area of the digestive tract – revisited, Scandinavian Journal of Gastroenterology 49(6) (2014) 681-689.
[42] N. Miron, V. Cristea, Enterocytes: active cells in tolerance to food and microbial antigens in the gut, Clin Exp Immunol 167(3) (2012) 405-12.
[43] Y.S. Kim, S.B. Ho, Intestinal goblet cells and mucins in health and disease: recent insights and progress, Curr Gastroenterol Rep 12(5) (2010) 319-30.
[44] R.D. Specian, M.G. Oliver, Functional biology of intestinal goblet cells, (1991).
[45] A. Macierzanka, A.R. Mackie, L. Krupa, Permeability of the small intestinal mucus for physiologically relevant studies: Impact of mucus location and ex vivo treatment, Sci Rep 9(1) (2019) 17516.

[46] G.C. Hansson, Mucus and mucins in diseases of the intestinal and respiratory tracts, J Intern Med 285(5) (2019) 479-490.
[47] G.C. Hansson, Role of mucus layers in gut infection and inflammation, Curr Opin Microbiol 15(1) (2012) 57-62.
[48] M. Herath, S. Hosie, J.C. Bornstein, A.E. Franks, E.L. Hill-Yardin, The Role of the Gastrointestinal Mucus System in Intestinal Homeostasis: Implications for Neurological Disorders, Front Cell Infect Microbiol 10 (2020) 248.
[49] H. Schneider, T. Pelaseyed, F. Svensson, M.E.V. Johansson, Study of mucin turnover in the small intestine by in vivo labeling, Sci Rep 8(1) (2018) 5760.
[50] C. Taylor Nordgard, K.I. Draget, Dynamic responses in small intestinal mucus: Relevance for the maintenance of an intact barrier, Eur J Pharm Biopharm 95(Pt A) (2015) 144-50.
[51] L.V. Hooper, Epithelial cell contributions to intestinal immunity, Adv Immunol 126 (2015) 129-72.
[52] A.A. Lee, C. Owyang, Sugars, sweet taste receptors, and brain responses, Molecular Nutrition: Carbohydrates2019, pp. 265-283.
[53] C.A. Houghton, The gut microbiome: its role in brain health Nutraceuticals in Brain Health and Beyond2021, pp. 193-212.
[54] L.-I. Larsson, Developmental biology of gastrin and somatostatin cells in the antropyloric mucosa of the stomach, Microscopy Research and Technique 48(5) (2000) 272-281.
[55] X. Guan, X. Shi, X. Li, B. Chang, Y. Wang, D. Li, L. Chan, GLP-2 receptor in POMC neurons suppresses feeding behavior and gastric motility, Am J Physiol Endocrinol Metab 303(7) (2012) E853-64.
[56] I.M. Modvig, D.B. Andersen, K.V. Grunddal, R.E. Kuhre, C. Martinussen, C.B. Christiansen, C. Orskov, P. Larraufie, R.G. Kay, F. Reimann, F.M. Gribble, B. Hartmann, K.N. Bojsen-Moller, S. Madsbad, N.J. Wewer Albrechtsen, J.J. Holst, Secretin release after Roux-en-Y gastric bypass reveals a population of glucose-sensitive S cells in distal small intestine, Int J Obes (Lond) 44(9) (2020) 1859-1871.
[57] M. Kanova, P. Kohout, Serotonin-Its Synthesis and Roles in the Healthy and the Critically Ill, Int J Mol Sci 22(9) (2021).
[58] J. Bas, P. Jay, F. Gerbe, Intestinal tuft cells: Sentinels, what else?, Semin Cell Dev Biol 150-151 (2023) 35-42.
[59] Y. Du, H. Gao, C. He, S. Xin, B. Wang, S. Zhang, F. Gong, X. Yu, L. Pan, F. Sun, W. Wang, J. Xu, An update on the biological characteristics and functions of tuft cells in the gut, Front Cell Dev Biol 10 (2022) 1102978.
[60] J.M. Williams, C.A. Duckworth, M.D. Burkitt, A.J. Watson, B.J. Campbell, D.M. Pritchard, Epithelial cell shedding and barrier function: a matter of life and death at the small intestinal villus tip, Vet Pathol 52(3) (2015) 445-55.
[61] A. Buckley, J.R. Turner, Cell Biology of Tight Junction Barrier Regulation and Mucosal Disease, Cold Spring Harb Perspect Biol 10(1) (2018).
[62] A. Horowitz, S.D. Chanez-Paredes, X. Haest, J.R. Turner, Paracellular permeability and tight junction regulation in gut health and disease, Nat Rev Gastroenterol Hepatol 20(7) (2023) 417-432.
[63] S.J. Shemtov, R. Emani, O. Bielska, A.J. Covarrubias, E. Verdin, J.K. Andersen, D.A. Winer, The intestinal immune system and gut barrier function in obesity and ageing, FEBS J 290(17) (2023) 4163-4186.
[64] K. Palucka, J. Banchereau, Dendritic Cells: A Link Between Innate and Adaptive Immunity, Journal of Clinical Immunology Vol. 19, No. 1 (1999).
[65] A. Geremia, P. Biancheri, P. Allan, G.R. Corazza, A. Di Sabatino, Innate and adaptive immunity in inflammatory bowel disease, Autoimmunity Reviews 13(1) (2014) 3-10.
[66] H. Kumar, T. Kawai, S. Akira, Pathogen Recognition by the Innate Immune System, International Reviews of Immunology 30(1) (2011) 16-34.

[67] W. Zhang, B. Tan, J. Deng, Q. Yang, S. Chi, A. Pang, Y. Xin, Y. Liu, H. Zhang, PRR-Mediated Immune Response and Intestinal Flora Profile in Soybean Meal-Induced Enteritis of Pearl Gentian Groupers, Epinephelus fuscoguttatusfemale symbol x Epinephelus lanceolatusmale symbol, Front Immunol 13 (2022) 814479.
[68] M.R. Neutra, N.J. Mantis, J.-P. Kraehenbuhl, Collaboration of epithelial cells with organized mucosal lymphoid tissues, Nature Immunology 2(11) (2001) 1004-1009.
[69] F. Hoentje, Proinflammatory cytokines and signaling pathways in intestinal innate immune cells, Vrije Universiteit Amsterdam, 2005.
[70] T.L. Bonfield, M.W. Konstan, P. Burfeind, J.R. Panuska, J.B. Hilliard, M. Berger, Normal Bronchial Epithelial Cells Constitutively Produce the Anti-inflammatory Cytokine Interleukin-10, Which Is Downregulated in Cystic Fibrosis, American Journal of Respiratory Cell and Molecular Biology Vol. 13 (1995).
[71] G.P. Donaldson, S.M. Lee, S.K. Mazmanian, Gut biogeography of the bacterial microbiota, Nat Rev Microbiol 14(1) (2016) 20-32.
[72] L.M. Sompayrac, How The Immune System Works, Seventh Edition ed., John Wiley & Sons Ltd, The Atrium, Southern Gate, Chichester, West Sussecc, PO19 8SQ, UK, 2023.
[73] A.M. Mowat, W.W. Agace, Regional specialization within the intestinal immune system, Nat Rev Immunol 14(10) (2014) 667-85.
[74] P.I. Costea, F. Hildebrand, M. Arumugam, F. Backhed, M.J. Blaser, F.D. Bushman, W.M. de Vos, S.D. Ehrlich, C.M. Fraser, M. Hattori, C. Huttenhower, I.B. Jeffery, D. Knights, J.D. Lewis, R.E. Ley, H. Ochman, P.W. O'Toole, C. Quince, D.A. Relman, F. Shanahan, S. Sunagawa, J. Wang, G.M. Weinstock, G.D. Wu, G. Zeller, L. Zhao, J. Raes, R. Knight, P. Bork, Enterotypes in the landscape of gut microbial community composition, Nat Microbiol 3(1) (2018) 8-16.
[75] M. Arumugam, J. Raes, E. Pelletier, D. Le Paslier, T. Yamada, D.R. Mende, G.R. Fernandes, J. Tap, T. Bruls, J.M. Batto, M. Bertalan, N. Borruel, F. Casellas, L. Fernandez, L. Gautier, T. Hansen, M. Hattori, T. Hayashi, M. Kleerebezem, K. Kurokawa, M. Leclerc, F. Levenez, C. Manichanh, H.B. Nielsen, T. Nielsen, N. Pons, J. Poulain, J. Qin, T. Sicheritz-Ponten, S. Tims, D. Torrents, E. Ugarte, E.G. Zoetendal, J. Wang, F. Guarner, O. Pedersen, W.M. de Vos, S. Brunak, J. Dore, H.I.T.C. Meta, M. Antolin, F. Artiguenave, H.M. Blottiere, M. Almeida, C. Brechot, C. Cara, C. Chervaux, A. Cultrone, C. Delorme, G. Denariaz, R. Dervyn, K.U. Foerstner, C. Friss, M. van de Guchte, E. Guedon, F. Haimet, W. Huber, J. van Hylckama-Vlieg, A. Jamet, C. Juste, G. Kaci, J. Knol, O. Lakhdari, S. Layec, K. Le Roux, E. Maguin, A. Merieux, R. Melo Minardi, C. M'Rini, J. Muller, R. Oozeer, J. Parkhill, P. Renault, M. Rescigno, N. Sanchez, S. Sunagawa, A. Torrejon, K. Turner, G. Vandemeulebrouck, E. Varela, Y. Winogradsky, G. Zeller, J. Weissenbach, S.D. Ehrlich, P. Bork, Enterotypes of the human gut microbiome, Nature 473(7346) (2011) 174-80.
[76] F. Mobeen, V. Sharma, P. Tulika, Enterotype Variations of the Healthy Human Gut Microbiome in Different Geographical Regions, Bioinformation 14(9) (2018) 560-573.
[77] Y. Fan, O. Pedersen, Gut microbiota in human metabolic health and disease, Nat Rev Microbiol 19(1) (2021) 55-71.
[78] G. Leite, M. Pimentel, G.M. Barlow, C. Chang, A. Hosseini, J. Wang, G. Parodi, R. Sedighi, A. Rezaie, R. Mathur, Age and the aging process significantly alter the small bowel microbiome, Cell Rep 36(13) (2021) 109765.
[79] C.J. Stewart, N.J. Ajami, J.L. O'Brien, D.S. Hutchinson, D.P. Smith, M.C. Wong, M.C. Ross, R.E. Lloyd, H. Doddapaneni, G.A. Metcalf, D. Muzny, R.A. Gibbs, T. Vatanen, C. Huttenhower, R.J. Xavier, M. Rewers, W. Hagopian, J. Toppari, A.G. Ziegler, J.X. She, B. Akolkar, A. Lernmark, H. Hyoty, K. Vehik, J.P. Krischer, J.F. Petrosino, Temporal development of the gut microbiome in early childhood from the TEDDY study, Nature 562(7728) (2018) 583-588.

[80] D. Rothschild, O. Weissbrod, E. Barkan, A. Kurilshikov, T. Korem, D. Zeevi, P.I. Costea, A. Godneva, I.N. Kalka, N. Bar, S. Shilo, D. Lador, A.V. Vila, N. Zmora, M. Pevsner-Fischer, D. Israeli, N. Kosower, G. Malka, B.C. Wolf, T. Avnit-Sagi, M. Lotan-Pompan, A. Weinberger, Z. Halpern, S. Carmi, J. Fu, C. Wijmenga, A. Zhernakova, E. Elinav, E. Segal, Environment dominates over host genetics in shaping human gut microbiota, Nature 555(7695) (2018) 210-215.
[81] Erica D. Sonnenburg, Justin L. Sonnenburg, Starving our Microbial Self: The Deleterious Consequences of a Diet Deficient in Microbiota-Accessible Carbohydrates, Cell Metabolism 20(5) (2014) 779-786.
[82] E.D. Sonnenburg, S.A. Smits, M. Tikhonov, S.K. Higginbottom, N.S. Wingreen, J.L. Sonnenburg, Diet-induced extinctions in the gut microbiota compound over generations, Nature 529(7585) (2016) 212-5.
[83] R. Jumpertz, D.S. Le, P.J. Turnbaugh, C. Trinidad, C. Bogardus, J.I. Gordon, J. Krakoff, Energy-balance studies reveal associations between gut microbes, caloric load, and nutrient absorption in humans, Am J Clin Nutr 94(1) (2011) 58-65.
[84] M.A. Vinolo, H.G. Rodrigues, R.T. Nachbar, R. Curi, Regulation of inflammation by short chain fatty acids, Nutrients 3(10) (2011) 858-76.
[85] A. Nogal, A.M. Valdes, C. Menni, The role of short-chain fatty acids in the interplay between gut microbiota and diet in cardio-metabolic health, Gut Microbes 13(1) (2021) 1-24.
[86] D. Parada Venegas, M.K. De la Fuente, G. Landskron, M.J. Gonzalez, R. Quera, G. Dijkstra, H.J.M. Harmsen, K.N. Faber, M.A. Hermoso, Short Chain Fatty Acids (SCFAs)-Mediated Gut Epithelial and Immune Regulation and Its Relevance for Inflammatory Bowel Diseases, Front Immunol 10 (2019) 277.
[87] W. Fusco, M.B. Lorenzo, M. Cintoni, S. Porcari, E. Rinninella, F. Kaitsas, E. Lener, M.C. Mele, A. Gasbarrini, M.C. Collado, G. Cammarota, G. Ianiro, Short-Chain Fatty-Acid-Producing Bacteria: Key Components of the Human Gut Microbiota, Nutrients 15(9) (2023).
[88] J.H. Cummings, E.W. Pomare, W.J. Branch, C.P. Naylor, G.T. Macfarlane, Short chain fatty acids in human large intestine, portal, hepatic and venous blood, Gut 28(10) (1987) 1221.
[89] D.L. Topping, P.M. Clifton, Short-Chain Fatty Acids and Human Colonic Function: Roles of Resistant Starch and Nonstarch Polysaccharides, Physiological Reviews 81(3) (2001) 1031-1064.
[90] I.A. Finnie, A.D. Dwarakanath, B.A. Taylor, J.M. Rhodes, Colonic mucin synthesis is increased by sodium butyrate, Gut 36(1) (1995) 93.
[91] A.J. Bilotta, Y. Cong, Gut microbiota metabolite regulation of host defenses at mucosal surfaces: implication in precision medicine, Precis Clin Med 2(2) (2019) 110-119.
[92] D. Bolognini, A.B. Tobin, G. Milligan, C.E. Moss, The Pharmacology and Function of Receptors for Short-Chain Fatty Acids, Mol Pharmacol 89(3) (2016) 388-98.
[93] J.K. Nicholson, E. Holmes, J. Kinross, R. Burcelin, G. Gibson, W. Jia, S. Pettersson, Host-gut microbiota metabolic interactions, Science 336(6086) (2012) 1262-7.
[94] P. Liu, Y. Wang, G. Yang, Q. Zhang, L. Meng, Y. Xin, X. Jiang, The role of short-chain fatty acids in intestinal barrier function, inflammation, oxidative stress, and colonic carcinogenesis, Pharmacol Res 165 (2021) 105420.
[95] A. Hofmann, L. Hagey, M. Krasowski, Bile salts of vertebrates: Structural variation and possible evolutionary significance, Journal of lipid research 51 (2009) 226-46.
[96] A.L. Ticho, P. Malhotra, P.K. Dudeja, R.K. Gill, W.A. Alrefai, Intestinal Absorption of Bile Acids in Health and Disease, Compr Physiol 10(1) (2019) 21-56.
[97] H. Zeng, S. Umar, B. Rust, D. Lazarova, M. Bordonaro, Secondary Bile Acids and Short Chain Fatty Acids in the Colon: A Focus on Colonic Microbiome, Cell Proliferation, Inflammation, and Cancer, Int J Mol Sci 20(5) (2019).
[98] J.M. Ridlon, S.C. Harris, S. Bhowmik, D.J. Kang, P.B. Hylemon, Consequences of bile salt biotransformations by intestinal bacteria, Gut Microbes 7(1) (2016) 22-39.

[99] C. Human Microbiome Project, Structure, function and diversity of the healthy human microbiome, Nature 486(7402) (2012) 207-14.
[100] W. Strober, I. Fuss, P. Mannon, The fundamental basis of inflammatory bowel disease, J Clin Invest 117(3) (2007) 514-21.
[101] Y. Zhao, D.W. Zou, Gut microbiota and irritable bowel syndrome, Journal of Digestive Diseases 24(5) (2023) 312-320.
[102] A.D. Kostic, R.J. Xavier, D. Gevers, The Microbiome in Inflammatory Bowel Disease: Current Status and the Future Ahead, Gastroenterology 146(6) (2014) 1489-1499.
[103] S. Massironi, F. Cavalcoli, E. Rausa, P. Invernizzi, M. Braga, M. Vecchi, Understanding short bowel syndrome: Current status and future perspectives, Dig Liver Dis 52(3) (2020) 253-261.
[104] Orphanet: Short bowel syndrome. . https://www.orpha.net/en/disease/detail/104008?name=Short%20bowel%20syndrome&mode=name#menu. 2024).
[105] R. Silva, P. Guerra, A. Rocha, M. Correia, R. Ferreira, J. Fonseca, E. Lima, A. Oliveira, M. Vargas Gomes, D. Ramos, V. Andreozzi, M.D. Santos, Clinical, Economic, and Humanistic Impact of Short-Bowel Syndrome/Chronic Intestinal Failure in Portugal (PARENTERAL Study), GE Port J Gastroenterol 30(4) (2023) 293-304.
[106] S. Lakkasani, D. Seth, I. Khokhar, M. Touza, T.J. Dacosta, Concise review on short bowel syndrome: Etiology, pathophysiology, and management, World J Clin Cases 10(31) (2022) 11273-11282.
[107] L. Pironi, Definition, classification, and causes of short bowel syndrome, Nutr Clin Pract 38 Suppl 1 (2023) S9-S16.
[108] L. Pironi, Definitions of intestinal failure and the short bowel syndrome, Best Practice & Research Clinical Gastroenterology 30(2) (2016) 173-185.
[109] T. Zuvarox, C. Belletieri, Malabsorption Syndromes, Treasure Island (FL): StatPearls Publishing, 2023.
[110] J. Le Beyec, L. Billiauws, A. Bado, F. Joly, M. Le Gall, Short Bowel Syndrome: A Paradigm for Intestinal Adaptation to Nutrition?, Annu Rev Nutr 40 (2020) 299-321.
[111] S. Lapthorne, P.M. Pereira-Fantini, F. Fouhy, G. Wilson, S.L. Thomas, N.L. Dellios, M. Scurr, O. O'Sullivan, R.P. Ross, C. Stanton, G.F. Fitzgerald, P.D. Cotter, J.E. Bines, Gut microbial diversity is reduced and is associated with colonic inflammation in a piglet model of short bowel syndrome, Gut Microbes 4(3) (2013) 212-221.
[112] M.S. Frolova, I.A. Suvorova, S.N. Iablokov, S.N. Petrov, D.A. Rodionov, Genomic reconstruction of short-chain fatty acid production by the human gut microbiota, Front Mol Biosci 9 (2022) 949563.
[113] B. Remund, B. Yilmaz, C. Sokollik, D-Lactate: Implications for Gastrointestinal Diseases, Children (Basel) 10(6) (2023).
[114] F. Benavides, T. Rulicke, J.B. Prins, J. Bussell, F. Scavizzi, P. Cinelli, Y. Herault, D. Wedekind, Genetic quality assurance and genetic monitoring of laboratory mice and rats: FELASA Working Group Report, Lab Anim 54(2) (2020) 135-148.
[115] J. Enriquez, B.M.D. Mims, S. Trasti, K.L. Furr, M.B. Grisham, Genomic, microbial and environmental standardization in animal experimentation limiting immunological discovery, BMC Immunol 21(1) (2020) 50.
[116] F. Hugenholtz, W.M. de Vos, Mouse models for human intestinal microbiota research: a critical evaluation, Cell Mol Life Sci 75(1) (2018) 149-160.
[117] R.E. Ley, M. Hamady, C. Lozupone, P.J. Turnbaugh, R.R. Ramey, J.S. Bircher, M.L. Schlegel, T.A. Tucker, M.D. Schrenzel, R. Knight, J.I. Gordon, Evolution of Mammals and Their Gut Microbes, Science 320(5883) (2008) 1647-1651.
[118] C. Casteleyn, A. Rekecki, A. Van der Aa, P. Simoens, W. Van den Broeck, Surface area assessment of the murine intestinal tract as a prerequisite for oral dose translation from mouse to man, Lab Anim 44(3) (2010) 176-83.

[119] S.C. Pearce, H.G. Coia, J.P. Karl, I.G. Pantoja-Feliciano, N.C. Zachos, K. Racicot, Intestinal in vitro and ex vivo Models to Study Host-Microbiome Interactions and Acute Stressors, Front Physiol 9 (2018) 1584.
[120] J. Iske, A. Schroeter, S. Knoedler, T.Z. Nazari-Shafti, L. Wert, M.J. Roesel, F. Hennig, A. Niehaus, C. Kuehn, F. Ius, V. Falk, M. Schmelzle, A. Ruhparwar, A. Haverich, C. Knosalla, S.G. Tullius, F.W.R. Vondran, B. Wiegmann, Pushing the boundaries of innovation: the potential of ex vivo organ perfusion from an interdisciplinary point of view, Front Cardiovasc Med 10 (2023) 1272945.
[121] R. Nunes, C. Silva, L. Chaves, Tissue-based in vitro and ex vivo models for intestinal permeability studies, Concepts and Models for Drug Permeability Studies2016, pp. 203-236.
[122] G. Hecht, J.A. Marrero, A. Danilkovich, K.A. Matkowskyj, S.D. Savkovic, A. Koutsouris, R.V. Benya, Pathogenic Escherichia coli increase Cl- secretion from intestinal epithelia by upregulating galanin-1 receptor expression, J Clin Invest 104(3) (1999) 253-62.
[123] T.A. Yawitz, N. Barts, K.D. Kohl, Comparative digestive morphology and physiology of five species of Peromyscus under controlled environment and diet, Comp Biochem Physiol A Mol Integr Physiol 271 (2022) 111265.
[124] C. Nowicki, L. Ray, P. Engen, A. Madrigrano, T. Witt, T. Lad, M. Cobleigh, E.A. Mutlu, Comparison of gut microbiome composition in colonic biopsies, endoscopically-collected and at-home-collected stool samples, Front Microbiol 14 (2023) 1148097.
[125] O. Levitan, L. Ma, D. Giovannelli, D.B. Burleson, P. McCaffrey, A. Vala, D.A. Johnson, The gut microbiome-Does stool represent right?, Heliyon 9(3) (2023) e13602.
[126] R. Negoro, K. Takayama, K. Kawai, K. Harada, F. Sakurai, K. Hirata, H. Mizuguchi, Efficient Generation of Small Intestinal Epithelial-like Cells from Human iPSCs for Drug Absorption and Metabolism Studies, Stem Cell Reports 11(6) (2018) 1539-1550.
[127] A. Beloqui, A. des Rieux, V. Preat, Mechanisms of transport of polymeric and lipidic nanoparticles across the intestinal barrier, Adv Drug Deliv Rev 106(Pt B) (2016) 242-255.
[128] P. Lundquist, P. Artursson, Oral absorption of peptides and nanoparticles across the human intestine: Opportunities, limitations and studies in human tissues, Adv Drug Deliv Rev 106(Pt B) (2016) 256-276.
[129] S. Devriese, L. Van den Bossche, S. Van Welden, T. Holvoet, I. Pinheiro, P. Hindryckx, M. De Vos, D. Laukens, T84 monolayers are superior to Caco-2 as a model system of colonocytes, Histochem Cell Biol 148(1) (2017) 85-93.
[130] A. Beterams, K. De Paepe, L. Maes, I.J. Wise, H. De Keersmaecker, A. Rajkovic, D. Laukens, T. Van de Wiele, M. Calatayud Arroyo, Versatile human in vitro triple coculture model coincubated with adhered gut microbes reproducibly mimics pro-inflammatory host-microbe interactions in the colon, FASEB J 35(12) (2021) e21992.
[131] A. Zweibaum, M. Laburthe, E. Grasset, D. Louvard, Use of Cultured Cell Lines in Studies of Intestinal Cell Differentiation and Function, Comprehensive Physiology2011, pp. 223-255.
[132] A. Beduneau, C. Tempesta, S. Fimbel, Y. Pellequer, V. Jannin, F. Demarne, A. Lamprecht, A tunable Caco-2/HT29-MTX co-culture model mimicking variable permeabilities of the human intestine obtained by an original seeding procedure, Eur J Pharm Biopharm 87(2) (2014) 290-8.
[133] T. Lesuffleur, A. Barbat, E. Dussaulx, A. Zweibaum, Growth Adaptation to Methotrexate of HT-29 Human Colon Carcinoma Cells Is Associated with Their Ability to Differentiate into Columnar Absorptive and Mucus-secreting Cells1, Cancer Research 50(19) (1990) 6334-6343.
[134] X.D. Bu, N. Li, X.Q. Tian, P.L. Huang, Caco-2 and LS174T cell lines provide different models for studying mucin expression in colon cancer, Tissue Cell 43(3) (2011) 201-6.
[135] A.P. de Bruïne, W.N.M. Dinjens, M.M.J. Pijls, E.P.M. v. d. Linden, M.J.M. Rousch, P.T. Moerkerk, A.F.P.M. de Goeij, F.T. Bosnian, NCI-H716 cells as a model for endocrine differentiation in colorectal cancer, Virchows Archiv B 62(1) (1992) 311-320.
[136] P. Phuangbubpha, S. Thara, P. Sriboonaied, P. Saetan, W. Tumnoi, A. Charoenpanich, Optimizing THP-1 Macrophage Culture for an Immune-Responsive Human Intestinal Model, Cells 12(10) (2023).

[137] M.V. Plikus, X. Wang, S. Sinha, E. Forte, S.M. Thompson, E.L. Herzog, R.R. Driskell, N. Rosenthal, J. Biernaskie, V. Horsley, Fibroblasts: Origins, definitions, and functions in health and disease, Cell 184(15) (2021) 3852-3872.
[138] M. Raymond, T. Marchbank, M.P. Moyer, R.J. Playford, I.R. Sanderson, L. Kruidenier, IL-1beta stimulation of CCD-18co myofibroblasts enhances repair of epithelial monolayers through Wnt-5a, Am J Physiol Gastrointest Liver Physiol 303(11) (2012) G1270-8.
[139] O. Cameron, J.F. Neves, E. Gentleman, Listen to Your Gut: Key Concepts for Bioengineering Advanced Models of the Intestine, Adv Sci (Weinh) (2023) e2302165.
[140] Y. Liu, Y.G. Chen, 2D- and 3D-Based Intestinal Stem Cell Cultures for Personalized Medicine, Cells 7(12) (2018).
[141] M. Delos, Cell culture models as an in vitro alternative to study the absorption and biotransformation of drugs and mycotoxins in humans and animals, in: G. University (Ed.) 2020-2021.
[142] A. Fedi, C. Vitale, G. Ponschin, S. Ayehunie, M. Fato, S. Scaglione, In vitro models replicating the human intestinal epithelium for absorption and metabolism studies: A systematic review, J Control Release 335 (2021) 247-268.
[143] Guidelines for Use: Transwell® Permeable Supports Including Snapwell™ and Netwell ™ Inserts. https://www.corning.com/worldwide/en/products/life-sciences/products/permeable-supports/transwell-guidelines.html. (Accessed 2023/12/20.
[144] F. Antunes, F. Andrade, F. Araujo, D. Ferreira, B. Sarmento, Establishment of a triple co-culture in vitro cell models to study intestinal absorption of peptide drugs, Eur J Pharm Biopharm 83(3) (2013) 427-35.
[145] A. Beterams, M. Calatayud Arroyo, K. De Paepe, A.S. De Craemer, D. Elewaut, K. Venken, T. Van de Wiele, In vitro triple coculture with gut microbiota from spondyloarthritis patients is characterized by inter-individual differences in inflammatory responses, Sci Rep 12(1) (2022) 10475.
[146] T. Gautier, N. Fahet, Z. Tamanai-Shacoori, N. Oliviero, M. Blot, A. Sauvager, A. Burel, S.D. Gall, S. Tomasi, S. Blat, L. Bousarghin, Roseburia intestinalis Modulates PYY Expression in a New a Multicellular Model including Enteroendocrine Cells, Microorganisms 10(11) (2022).
[147] C.M. Costello, J. Hongpeng, S. Shaffiey, J. Yu, N.K. Jain, D. Hackam, J.C. March, Synthetic small intestinal scaffolds for improved studies of intestinal differentiation, Biotechnol Bioeng 111(6) (2014) 1222-32.
[148] S. Ahn, D. Kim, K. Cho, W.-G. Koh, Microfabrication methods for 3D spheroids formation and their application in biomedical engineering, Korean Journal of Chemical Engineering 40(2) (2023) 311-324.
[149] S. Gunti, A.T.K. Hoke, K.P. Vu, N.R. London, Jr., Organoid and Spheroid Tumor Models: Techniques and Applications, Cancers (Basel) 13(4) (2021).
[150] Organoid vs. Spheroid: What's the Difference? https://www.corning.com/emea/en/products/life-sciences/resources/stories/at-the-bench/organoid-vs-spheroid-what-is-the-difference.html.
[151] S. Lukovac, C. Belzer, L. Pellis, B.J. Keijser, W.M. de Vos, R.C. Montijn, G. Roeselers, Differential modulation by Akkermansia muciniphila and Faecalibacterium prausnitzii of host peripheral lipid metabolism and histone acetylation in mouse gut organoids, mBio 5(4) (2014).
[152] K. Baumann, Stem cells: Colonic organoids for drug testing and colorectal disease modelling, Nat Rev Mol Cell Biol 18(8) (2017) 467.
[153] T. Roodsant, M. Navis, I. Aknouch, I.B. Renes, R.M. van Elburg, D. Pajkrt, K.C. Wolthers, C. Schultsz, K.C.H. van der Ark, A. Sridhar, V. Muncan, A Human 2D Primary Organoid-Derived Epithelial Monolayer Model to Study Host-Pathogen Interaction in the Small Intestine, Front Cell Infect Microbiol 10 (2020) 272.
[154] C.W. Wright, N. Li, L. Shaffer, A. Hill, N. Boyer, S.E. Alves, S. Venkataraman, K. Biswas, L.A. Lieberman, S. Mohammadi, Establishment of a 96-well transwell system using primary human gut organoids to capture multiple quantitative pathway readouts, Sci Rep 13(1) (2023) 16357.

[155] T. Van de Wiele, P. Van den Abbeele, W. Ossieur, S. Possemiers, M. Marzorati, The Simulator of the Human Intestinal Microbial Ecosystem (SHIME((R))), in: K. Verhoeckx, P. Cotter, I. Lopez-Exposito, C. Kleiveland, T. Lea, A. Mackie, T. Requena, D. Swiatecka, H. Wichers (Eds.), The Impact of Food Bioactives on Health: in vitro and ex vivo models, Cham (CH), 2015, pp. 305-17.
[156] D. Marrero, F. Pujol-Vila, D. Vera, G. Gabriel, X. Illa, A. Elizalde-Torrent, M. Alvarez, R. Villa, Gut-on-a-chip: Mimicking and monitoring the human intestine, Biosens Bioelectron 181 (2021) 113156.
[157] H.J. Kim, D. Huh, G. Hamilton, D.E. Ingber, Human gut-on-a-chip inhabited by microbial flora that experiences intestinal peristalsis-like motions and flow, Lab Chip 12(12) (2012) 2165-74.
[158] P. Shah, J.V. Fritz, E. Glaab, M.S. Desai, K. Greenhalgh, A. Frachet, M. Niegowska, M. Estes, C. Jager, C. Seguin-Devaux, F. Zenhausern, P. Wilmes, A microfluidics-based in vitro model of the gastrointestinal human-microbe interface, Nat Commun 7 (2016) 11535.
[159] M. Marzorati, B. Vanhoecke, T. De Ryck, M. Sadaghian Sadabad, I. Pinheiro, S. Possemiers, P. Van den Abbeele, L. Derycke, M. Bracke, J. Pieters, T. Hennebel, H.J. Harmsen, W. Verstraete, T. Van de Wiele, The HMI module: a new tool to study the Host-Microbiota Interaction in the human gastrointestinal tract in vitro, BMC Microbiol 14 (2014) 133.
[160] R.B. Colquitt, D.A. Colquhoun, R.H. Thiele, In silico modelling of physiologic systems, Best Pract Res Clin Anaesthesiol 25(4) (2011) 499-510.
[161] P. Du, N. Paskaranandavadivel, T.R. Angeli, L.K. Cheng, G. O'Grady, The virtual intestine: in silico modeling of small intestinal electrophysiology and motility and the applications, Wiley Interdiscip Rev Syst Biol Med 8(1) (2016) 69-85.
[162] B. Srinivasan, A.R. Kolli, M.B. Esch, H.E. Abaci, M.L. Shuler, J.J. Hickman, TEER measurement techniques for in vitro barrier model systems, J Lab Autom 20(2) (2015) 107-26.
[163] O. Vincentini, V. Prota, S. Cecchetti, L. Bertuccini, A. Tinari, F. Iosi, I. De Angelis, Towards the Standardization of Intestinal In Vitro Advanced Barrier Model for Nanoparticles Uptake and Crossing: The SiO(2) Case Study, Cells 11(21) (2022).
[164] K.J. Livak, T.D. Schmittgen, Analysis of relative gene expression data using real-time quantitative PCR and the 2(-Delta Delta C(T)) Method, Methods 25(4) (2001) 402-8.
[165] M. Calatayud, O. Dezutter, E. Hernandez-Sanabria, S. Hidalgo-Martinez, F.J.R. Meysman, T. Van de Wiele, Development of a host-microbiome model of the small intestine, FASEB J 33(3) (2019) 3985-3996.
[166] N.J. Darling, C.L. Mobbs, A.L. Gonzalez-Hau, M. Freer, S. Przyborski, Bioengineering Novel in vitro Co-culture Models That Represent the Human Intestinal Mucosa With Improved Caco-2 Structure and Barrier Function, Front Bioeng Biotechnol 8 (2020) 992.
[167] J.N. Harris, P.B. Hylemon, Partial purification and characterization of NADP-dependent 12α-hydroxysteroid dehydrogenase from clostridium leptum, Biochimica et Biophysica Acta (BBA) - Lipids and Lipid Metabolism 528(1) (1978) 148-157.
[168] H. Doden, A. Sallam Lina, S. Devendran, L. Ly, G. Doden, L. Daniel Steven, M.P. Alves João, M. Ridlon Jason, Metabolism of Oxo-Bile Acids and Characterization of Recombinant 12α-Hydroxysteroid Dehydrogenases from Bile Acid 7α-Dehydroxylating Human Gut Bacteria, Applied and Environmental Microbiology 84(10) (2018) e00235-18.
[169] E.J. Stellwag, P.B. Hylemon, 7alpha-Dehydroxylation of cholic acid and chenodeoxycholic acid by Clostridium leptum, Journal of Lipid Research 20(3) (1979) 325-333.
[170] L.N. Lucas, K. Barrett, R.L. Kerby, Q. Zhang, L.E. Cattaneo, D. Stevenson, F.E. Rey, D. Amador-Noguez, Dominant Bacterial Phyla from the Human Gut Show Widespread Ability To Transform and Conjugate Bile Acids, mSystems 6(4) (2021) 10.1128/msystems.00805-21.
[171] T. Rozario, D.W. DeSimone, The extracellular matrix in development and morphogenesis: a dynamic view, Dev Biol 341(1) (2010) 126-40.
[172] J.K. Kular, S. Basu, R.I. Sharma, The extracellular matrix: Structure, composition, age-related differences, tools for analysis and applications for tissue engineering, J Tissue Eng 5 (2014) 2041731414557112.

[173] C.M. Moysidou, A.M. Withers, A.J. Nisbet, D.R.G. Price, C.E. Bryant, C. Cantacessi, R.M. Owens, Investigation of Host-Microbe-Parasite Interactions in an In Vitro 3D Model of the Vertebrate Gut, Adv Biol (Weinh) 6(8) (2022) e2200015.
[174] L. Slyker, N. Diamantides, J. Kim, L.J. Bonassar, Mechanical performance of collagen gels is dependent on purity, alpha1/alpha2 ratio, and telopeptides, J Biomed Mater Res A 110(1) (2022) 11-20.
[175] Collagen Coating Transwell® Inserts from Corning, Tewksbury, Massachusetts, 2009, p. 2.
[176] H. Sherman, M. Rothenberg, T. Upton, Considerations When Optimizing Coating Protocols for Corning® Transwell® Permeable Supports, Lowell, Massachusetts, 2010, p. 4.
[177] L. Vincent, A.J. Engler, 5.5 Effect of Substrate Modulus on Cell Function and Differentiation, in: P. Ducheyne (Ed.), Comprehensive Biomaterials II, Elsevier, Oxford, 2017, pp. 88-101.
[178] S. Kim, S. Min, Y.S. Choi, S.H. Jo, J.H. Jung, K. Han, J. Kim, S. An, Y.W. Ji, Y.G. Kim, S.W. Cho, Tissue extracellular matrix hydrogels as alternatives to Matrigel for culturing gastrointestinal organoids, Nat Commun 13(1) (2022) 1692.
[179] C.R. Justus, M.A. Marie, E.J. Sanderlin, L.V. Yang, Transwell In Vitro Cell Migration and Invasion Assays, Methods Mol Biol 2644 (2023) 349-359.
[180] S.R. Caliari, J.A. Burdick, A practical guide to hydrogels for cell culture, Nat Methods 13(5) (2016) 405-14.
[181] H.K. Kleinman, K. Kim, H. Kang, Matrigel uses in cell biology and for the identification of thymosin β4, a mediator of tissue regeneration, Applied Biological Chemistry 61(6) (2018) 703-708.
[182] S. Grefte, S. Vullinghs, A.M. Kuijpers-Jagtman, R. Torensma, J.W. Von den Hoff, Matrigel, but not collagen I, maintains the differentiation capacity of muscle derived cells in vitro, Biomed Mater 7(5) (2012) 055004.
[183] A. Passaniti, H.K. Kleinman, G.R. Martin, Matrigel: history/background, uses, and future applications, J Cell Commun Signal 16(4) (2022) 621-626.
[184] T. Pelaseyed, J.H. Bergstrom, J.K. Gustafsson, A. Ermund, G.M. Birchenough, A. Schutte, S. van der Post, F. Svensson, A.M. Rodriguez-Pineiro, E.E. Nystrom, C. Wising, M.E. Johansson, G.C. Hansson, The mucus and mucins of the goblet cells and enterocytes provide the first defense line of the gastrointestinal tract and interact with the immune system, Immunol Rev 260(1) (2014) 8-20.
[185] A.M. Rodríguez-Piñeiro, J.H. Bergström, A. Ermund, J.K. Gustafsson, A. Schütte, M.E.V. Johansson, G.C. Hansson, Studies of mucus in mouse stomach, small intestine, and colon. II. Gastrointestinal mucus proteome reveals Muc2 and Muc5ac accompanied by a set of core proteins, American Journal of Physiology-Gastrointestinal and Liver Physiology 305(5) (2013) G348-G356.
[186] I. Behrens, P. Stenberg, P. Artursson, T. Kissel, Transport of Lipophilic Drug Molecules in a New Mucus-Secreting Cell Culture Model Based on HT29-MTX Cells, Pharmaceutical Research 18(8) (2001) 1138-1145.
[187] P. Hoffmann, M. Burmester, M. Langeheine, R. Brehm, M.T. Empl, B. Seeger, G. Breves, Caco-2/HT29-MTX co-cultured cells as a model for studying physiological properties and toxin-induced effects on intestinal cells, PLoS One 16(10) (2021) e0257824.
[188] N. Navabi, M.A. McGuckin, S.K. Linden, Gastrointestinal cell lines form polarized epithelia with an adherent mucus layer when cultured in semi-wet interfaces with mechanical stimulation, PLoS One 8(7) (2013) e68761.
[189] M.J. Briske-Anderson, J.W. Finley, S.M. Newman, The Influence of Culture Time and Passage Number on the Morphological and Physiological Development of Caco-2 Cells, Proceedings of the Society for Experimental Biology and Medicine 214(3) (1997) 248-257.
[190] L.F. Blume, M. Denker, F. Gieseler, T. Kunze, Temperature corrected transepithelial electrical resistance (TEER) measurement to quantify rapid changes in paracellular permeability, Die Pharmazie - An International Journal of Pharmaceutical Sciences 65(1) (2010) 19-24.

[191] Y. Sambuy, I. De Angelis, G. Ranaldi, M.L. Scarino, A. Stammati, F. Zucco, The Caco-2 cell line as a model of the intestinal barrier: influence of cell and culture-related factors on Caco-2 cell functional characteristics, Cell Biology and Toxicology 21(1) (2005) 1-26.
[192] L.Y.U. Xiaojun, C.A.O. Yidan, H.E. Kaiyong, Establishment and Validation of Caco-2 Cell in Vitro Absorption Model, Herald of Medicine (2018).
[193] S. Tavelin, J. Gråsjö, J. Taipalensuu, G. Ocklind, P. Artursson, Applications of Epithelial Cell Culture in Studies of Drug Transport, in: C. Wise (Ed.), Epithelial Cell Culture Protocols, Humana Press, Totowa, NJ, 2002, pp. 233-272.
[194] M. Kus, I. Ibragimow, H. Piotrowska-Kempisty, Caco-2 Cell Line Standardization with Pharmaceutical Requirements and In Vitro Model Suitability for Permeability Assays, Pharmaceutics 15(11) (2023).
[195] I. Hubatsch, E.G. Ragnarsson, P. Artursson, Determination of drug permeability and prediction of drug absorption in Caco-2 monolayers, Nat Protoc 2(9) (2007) 2111-9.
[196] C. Tataru, M. Livni, C. Marean-Reardon, M.C. Franco, M. David, Cytokine induced inflammatory bowel disease model using organ-on-a-chip technology, PLoS One 18(12) (2023) e0289314.
[197] X. Liu, S. Yin, Y. Chen, Y. Wu, W. Zheng, H. Dong, Y. Bai, Y. Qin, J. Li, S. Feng, P. Zhao, LPS-induced proinflammatory cytokine expression in human airway epithelial cells and macrophages via NF-kappaB, STAT3 or AP-1 activation, Mol Med Rep 17(4) (2018) 5484-5491.
[198] Z. Jakopin, E. Corsini, THP-1 Cells and Pro-inflammatory Cytokine Production: An in Vitro Tool for Functional Characterization of NOD1/NOD2 Antagonists, Int J Mol Sci 20(17) (2019).
[199] Barrier Formation and Permeability Assays using Millicell® Hanging Cell Culture Inserts. https://www.sigmaaldrich.com/BE/en/technical-documents/technical-article/cell-culture-and-cell-culture-analysis/cell-based-assays/barrier-formation-permeability-assays. 2024).
[200] T.S. Frost, L. Jiang, R.M. Lynch, Y. Zohar, Permeability of Epithelial/Endothelial Barriers in Transwells and Microfluidic Bilayer Devices, Micromachines (Basel) 10(8) (2019).
[201] M. Marziano, S. Tonello, E. Cantu, G. Abate, M. Vezzoli, W. Rungratanawanich, M. Serpelloni, N.F. Lopomo, M. Memo, E. Sardini, D. Uberti, Monitoring Caco-2 to enterocyte-like cells differentiation by means of electric impedance analysis on printed sensors, Biochim Biophys Acta Gen Subj 1863(5) (2019) 893-902.
[202] K. Felix, S. Tobias, H. Jan, S. Nicolas, M. Michael, Measurements of transepithelial electrical resistance (TEER) are affected by junctional length in immature epithelial monolayers, Histochem Cell Biol 156(6) (2021) 609-616.
[203] A.F. Mattar, D.H. Teitelbaum, R.A. Drongowski, F. Yongyi, C.M. Harmon, A.G. Coran, Probiotics up-regulate MUC-2 mucin gene expression in a Caco-2 cell-culture model, Pediatr Surg Int 18(7) (2002) 586-90.
[204] D.H. Hong, G. Petrovics, W.B. Anderson, J. Forstner, G. Forstner, Induction of mucin gene expression in human colonic cell lines by PMA is dependent on PKC-ε, American Journal of Physiology-Gastrointestinal and Liver Physiology 277(5) (1999) G1041-G1047.
[205] U. Heinemann, A. Schuetz, Structural Features of Tight-Junction Proteins, Int J Mol Sci 20(23) (2019).
[206] T. Takiishi, C.I.M. Fenero, N.O.S. Camara, Intestinal barrier and gut microbiota: Shaping our immune responses throughout life, Tissue Barriers 5(4) (2017) e1373208.
[207] M.A. Odenwald, J.R. Turner, The intestinal epithelial barrier: a therapeutic target?, Nat Rev Gastroenterol Hepatol 14(1) (2017) 9-21.
[208] G. Noel, N.W. Baetz, J.F. Staab, M. Donowitz, O. Kovbasnjuk, M.F. Pasetti, N.C. Zachos, A primary human macrophage-enteroid co-culture model to investigate mucosal gut physiology and host-pathogen interactions, Sci Rep 7 (2017) 45270.
[209] A.A.M. Kampfer, P. Urban, S. Gioria, N. Kanase, V. Stone, A. Kinsner-Ovaskainen, Development of an in vitro co-culture model to mimic the human intestine in healthy and diseased state, Toxicol In Vitro 45(Pt 1) (2017) 31-43.

[210] M. Busch, A.A.M. Kämpfer, R.P.F. Schins, An inverted in vitro triple culture model of the healthy and inflamed intestine: Adverse effects of polyethylene particles, Chemosphere 284 (2021) 131345.
[211] S. Gordon, P.R. Taylor, Monocyte and macrophage heterogeneity, Nature Reviews Immunology 5(12) (2005) 953-964.
[212] S. Gordon, A. Pluddemann, Tissue macrophages: heterogeneity and functions, BMC Biol 15(1) (2017) 53.
[213] B. Weber, L. Saurer, C. Mueller, Intestinal macrophages: differentiation and involvement in intestinal immunopathologies, Semin Immunopathol 31(2) (2009) 171-84.
[214] F. Meng, C.A. Lowell, Lipopolysaccharide (LPS)-induced Macrophage Activation and Signal Transduction in the Absence of Src-Family Kinases Hck, Fgr, and Lyn, Journal of Experimental Medicine 185(9) (1997) 1661-1670.
[215] W. Chanput, J. Mes, R.A. Vreeburg, H.F. Savelkoul, H.J. Wichers, Transcription profiles of LPS-stimulated THP-1 monocytes and macrophages: a tool to study inflammation modulating effects of food-derived compounds, Food Funct 1(3) (2010) 254-61.
[216] D.V. Krysko, G. Denecker, N. Festjens, S. Gabriels, E. Parthoens, K. D'Herde, P. Vandenabeele, Macrophages use different internalization mechanisms to clear apoptotic and necrotic cells, Cell Death Differ 13(12) (2006) 2011-22.
[217] D.R. Michael, T.S. Davies, L. Laubertova, H. Gallagher, D.P. Ramji, The phosphoinositide 3-kinase signaling pathway is involved in the control of modified low-density lipoprotein uptake by human macrophages, Lipids 50(3) (2015) 253-60.
[218] E. Rath, D. Haller, Intestinal epithelial cell metabolism at the interface of microbial dysbiosis and tissue injury, Mucosal Immunology 15(4) (2022) 595-604.
[219] A. Ornelas, A.S. Dowdell, J.S. Lee, S.P. Colgan, Microbial Metabolite Regulation of Epithelial Cell-Cell Interactions and Barrier Function, Cells 11(6) (2022).
[220] M. Song, F. Zhang, Y. Fu, X. Yi, S. Feng, Z. Liu, D. Deng, Q. Yang, M. Yu, C. Zhu, X. Zhu, L. Wang, P. Gao, G. Shu, X. Ma, Q. Jiang, S. Wang, Tauroursodeoxycholic acid (TUDCA) improves intestinal barrier function associated with TGR5-MLCK pathway and the alteration of serum metabolites and gut bacteria in weaned piglets, J Anim Sci Biotechnol 13(1) (2022) 73.
[221] W. Wang, J. Zhao, W. Gui, D. Sun, H. Dai, L. Xiao, H. Chu, F. Du, Q. Zhu, B. Schnabl, K. Huang, L. Yang, X. Hou, Tauroursodeoxycholic acid inhibits intestinal inflammation and barrier disruption in mice with non-alcoholic fatty liver disease, Br J Pharmacol 175(3) (2018) 469-484.
[222] H. Duboc, S. Rajca, D. Rainteau, D. Benarous, M.A. Maubert, E. Quervain, G. Thomas, V. Barbu, L. Humbert, G. Despras, C. Bridonneau, F. Dumetz, J.P. Grill, J. Masliah, L. Beaugerie, J. Cosnes, O. Chazouilleres, R. Poupon, C. Wolf, J.M. Mallet, P. Langella, G. Trugnan, H. Sokol, P. Seksik, Connecting dysbiosis, bile-acid dysmetabolism and gut inflammation in inflammatory bowel diseases, Gut 62(4) (2013) 531-9.
[223] S. Fiorucci, M. Biagioli, A. Zampella, E. Distrutti, Bile Acids Activated Receptors Regulate Innate Immunity, Front Immunol 9 (2018) 1853.
[224] H.-B. Wang, P.-Y. Wang, X. Wang, Y.-L. Wan, Y.-C. Liu, Butyrate Enhances Intestinal Epithelial Barrier Function via Up-Regulation of Tight Junction Protein Claudin-1 Transcription, Digestive Diseases and Sciences 57(12) (2012) 3126-3135.

APPENDIX

Table 4: Medium composition for the *C.leptum* culture.

Medium:

Trypticase peptone	5g	Fisher scientific
Meat peptone	5g	Sigma Aldrich
Sodium resazurin (0.1% w/v)	0.5 ml	Merck Life science
L-cysteine HCL x H2O	0.5 g	Merck Life science
Na2CO3	1g	Sigma Aldrich
D-glucose	5 g	Sigma Aldrich
Distilled water	960 ml	
Salt solution	40ml	

Salt solution:

CaCl2 x 2 H2O	0.25g	Carl Roth
MgSO4 x 7 H2O	0.5g	Carl Roth
K2HPO4	1g	Sigma Aldrich
KH2PO4	1g	VWR
NaHCO3	10g	Carl Roth
NaCl	2g	Carl Roth
Distilled water	1000ml	

Table 5: Composition of the SHIME medium.

SI M-SHIME medium	**g/L**
M-SHIME*	10.2
Starch	6.0
Glucose	0.8
Fructose	0.8
Galactose	0.4
Mannose	0.4
Maltose	0.8
Sucrose	0.8
Lactose	0.8
* Contains (g/L): Arabic gum (1.2), pectin (2), xylan (0.5), glucose (0.4), yeast extract (3), special peptone (1), mucin (2), L-cysteine-HCl (0.5)	

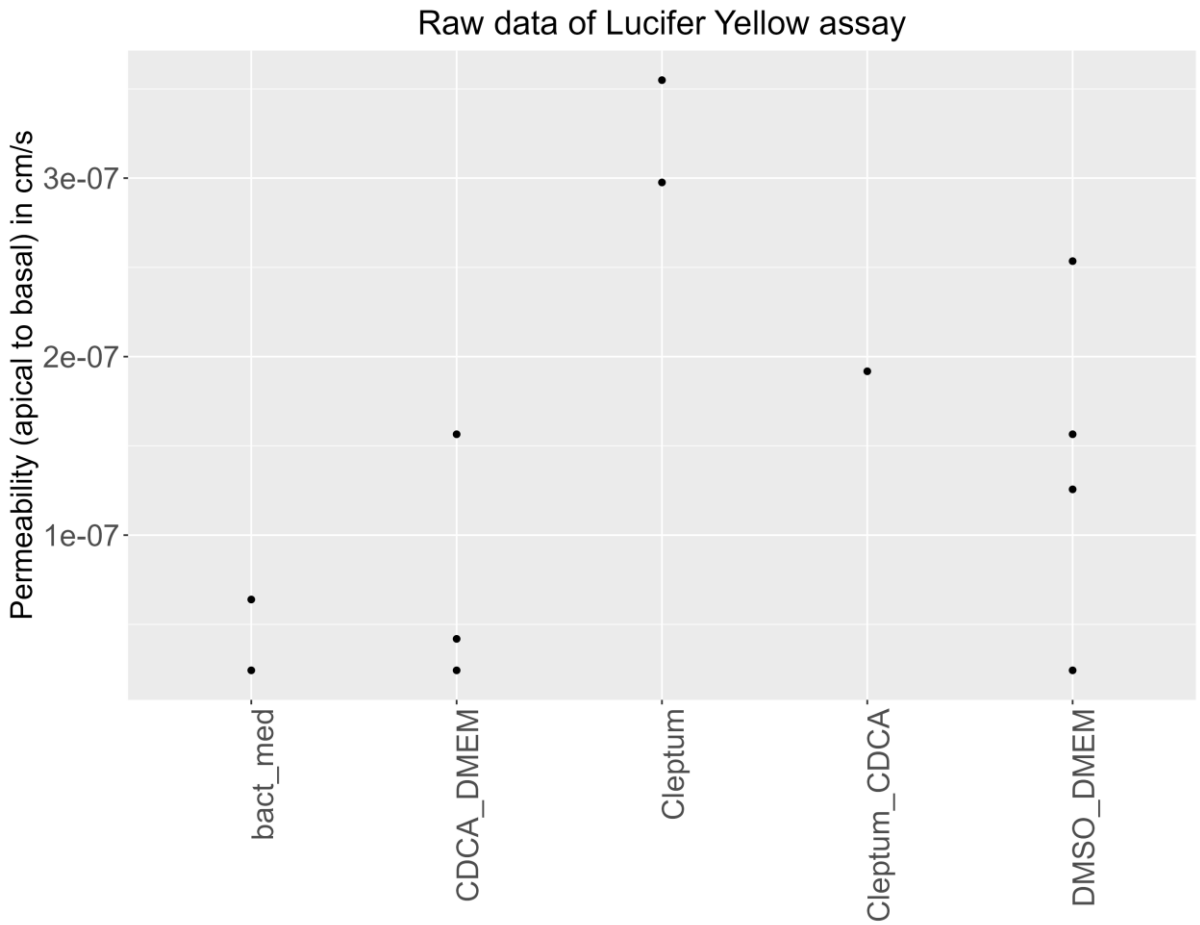

Figure 32: Scatterplot of the raw data of the Lucifer Yellow assay at day 31 (after live bacterial stimulation of small intestinal model). Due to various missing values, it was not possible to make the permeability plot.